STABILITY OF GOLD NANOPARTICLES AND THEIR INHIBITORY EFFECT ON

AMYLOID-$\beta_{1\text{-}42}$ PROTEIN AGGREGATION

Miss Chutima Kongsuwan

A Thesis Submitted in Partial Fulfillment of the Requirements

for the Degree of Master of Science Program in Pharmaceutical Technology

Department of Pharmaceutics and Industrial Pharmacy

Faculty of Pharmaceutical Sciences

Chulalongkorn University

Academic Year 2014

ความคงตัวของนาโนพาร์ทิเคิลทองคำและผลยับยั้งต่อการรวมกลุ่มของโปรตีนแอมีลอยด์บีตา
ชนิด 1-42

นางสาวชุติมา กองสุวรรณ

Thesis Title	STABILITY OF GOLD NANOPARTICLES AND THEIR INHIBITORY EFFECT ON AMYLOID-$\beta_{1\text{-}42}$ PROTEIN AGGREGATION
By	Miss Chutima Kongsuwan
Field of Study	Pharmaceutical Technology
Thesis Advisor	Associate Professor Warangkana Warisnoicharoen, Ph.D.
Thesis Co-Advisor	Professor Suwabun Chirachanchai, Ph.D.

Accepted by the Faculty of Pharmaceutical Sciences, Chulalongkorn University in Partial Fulfillment of the Requirements for the Master's Degree

....Dean of the Faculty of Pharmaceutical Sciences

(Assistant Professor Rungpetch Sakulbumrungsil, Ph.D.)

THESIS COMMITTEE

....Chairman

(Assistant Professor Nontima Vardhanabhuti, Ph.D.)

....Thesis Advisor

(Associate Professor Warangkana Warisnoicharoen, Ph.D.)

....Thesis Co-Advisor

(Professor Suwabun Chirachanchai, Ph.D.)

....Examiner

(Associate Professor Pornpen Werawatganone, Ph.D.)

....External Examiner

(Associate Professor Ubonthip Nimmanit, Ph.D.)

ชุติมา กองสุวรรณ์ : ความคงตัวของนาโนพาร์ทิเคิลทองคำและผลยับยั้งต่อการรวมกลุ่มของโปรตีนแอมี ลอยด์บีตาชนิด 1-42 (STABILITY OF GOLD NANOPARTICLES AND THEIR INHIBITORY EFFECT ON AMYLOID-β_{1-42} PROTEIN AGGREGATION) อ.ที่ปรึกษาวิทยานิพนธ์หลัก: รศ. ภญ. ดร. วรางคณา วารีสน้อยเจริญ, อ.ที่ปรึกษาวิทยานิพนธ์ร่วม: ศ. ดร. สุวบุญ จิรชาญชัย, 94 หน้า.

เป็นที่รู้กันว่าการรวมกลุ่มของโปรตีนแอมีลอยด์บีตามีความเป็นพิษต่อระบบประสาทซึ่งมีความเกี่ยวข้อง กับโรคอัลไซเมอร์ ด้วยเหตุนี้สารที่สามารถป้องกันหรือลดการรวมกลุ่มของแอมีลอยด์บีตาจะเป็นกลยุทธ์สำหรับ รักษาโรคอัลไซเมอร์ นาโนพาร์ทิเคิลทองคำเป็นสารที่ถูกพิจารณาว่าน่าจะนำมาใช้ในการรักษาโรคอัลไซเมอร์ได้ เนื่องจากคุณสมบัติเชิงแสงและมีความเข้ากันได้กับเนื้อเยื่อในร่างกายรวมไปถึงมีความสามารถในการผ่านสิ่งกั้น ระหว่างสมองและเลือด ในการศึกษาครั้งนี้นาโนพาร์ทิเคิลทองคำที่ใช้ซิเตรทเป็นสารเพิ่มเสถียรภาพ (AuCt) และนา โนพาร์ทิเคิลทองคำที่ใช้โพลีแอทาทิลีนอิมีนเป็นสารเพิ่มเสถียรภาพ (AuPEI) ถูกสังเคราะห์และศึกษาความคงตัว ตลอดจนการแสดงลักษณะเฉพาะ ได้แก่ ขนาดของนาโนพาร์ทิเคิลโดยใช้เทคนิคยูวี-วิสิเบิลสเปกโทรสโกปี การ วิเคราะห์ด้วยกล้องจุลทรรศน์อิเลคตรอนแบบส่องผ่าน (TEM) การวิเคราะห์ด้วยเทคนิควัดการกระเจิงแสงพลวัต วัด ขนาดประจุของอนุภาคโดยเทคนิคการเคลื่อนสู่ขั้วไฟฟ้า นอกจากนั้นยังทำการศึกษาผลยับยั้งต่อการรวมกลุ่มของ โปรตีนแอมีลอยด์บีตาชนิด 1-42 ที่ไม่ถูกเหนี่ยวนำและถูกเหนี่ยวนำด้วยสังกะสีของนาโนพาร์ทิเคิลทองคำ โดยใช้วิธี วิเคราะห์จากการเรืองแสงฟลูออเรสเซนซ์ของไธโอฟลาวิน ที และศึกษาลักษณะการรวมกลุ่มของโปรตีนด้วยเทคนิค TEM จากผลจากการศึกษา พบว่า ขนาดเส้นผ่านศูนย์กลางแบบไฮโดรไดนามิกของ AuCt และ AuPEI มีค่าเท่ากับ 18.37 ± 0.34 นาโนเมตร และ 18.59 ± 0.59 นาโนเมตร ตามลำดับ ขนาดประจุของ AuCt และ AuPEI มีค่า เท่ากับ -35.37 ± 2.56 มิลลิโวลต์ และ 38.00 ± 1.68 มิลลิโวลต์ ตามลำดับ นอกจากนั้น ผลจาก TEM สามารถ ระบุได้ว่า AuPEI มีขนาดเล็กว่า AuCt และมีการกระจายของขนาดอนุภาคน้อยกว่า AuCt หลังจากการเก็บรักษาไว้ ที่ระยะเวลาหนึ่ง พบว่า AuPEI มีความคงตัวมากกว่า AuCt และนาโนพาร์ทิเคิลทองคำทั้งสองชนิดแสดงผลยับยั้ง การรวมกลุ่มของแอมีลอยด์บีตาชนิด 1-42 ในแบบที่ถูกเหนี่ยวนำให้รวมกลุ่มโดยสังกะสี และไม่ถูกเหนี่ยวนำให้ รวมกลุ่มโดยสังกะสี อย่างไรก็ตาม AuCt มีผลยับยั้งการรวมกลุ่มของแอมีลอยด์บีตาชนิด 1-42 ที่ถูกเหนี่ยวนำและ ไม่ถูกเหนี่ยวนำโดยสังกะสีน้อยกว่า AuPEI และการเพิ่มขึ้นของความเข้มข้นของนาโนพาร์ทิเคิลทองคำทั้งสองชนิด ยังเพิ่มการยับยั้งการรวมกลุ่มของโปรตีนแอมีลอยด์บีตาได้ด้วย ผลการศึกษาที่ได้มีความสอดคล้องกับผลวิเคราะห์ที่ ได้จาก TEM ดังนั้นจึงอาจสรุปได้ว่าศักยภาพในการยับยั้งการรวมกลุ่มของโปรตีนแอมีลอยด์บีตาชนิด 1-42 ของนา โนพาร์ทิเคิลทองคำ อาจขึ้นกับชนิดประจุและความเข้มข้นของนาโนพาร์ทิเคิล สำหรับกลไกในการยับยั้งการ รวมกลุ่มของโปรตีนแอมีลอยด์บีตาของนาโนพาร์ทิเคิลทองคำนั้นควรมีการศึกษาเพิ่มเติมต่อไป

ภาควิชา	วิทยาการเภสัชกรรมและเภสัชอุตสาหกรรม	ลายมือชื่อนิสิต ....
สาขาวิชา	เทคโนโลยีเภสัชกรรม	ลายมือชื่อ อ.ที่ปรึกษาหลัก ....
ปีการศึกษา	2557	ลายมือชื่อ อ.ที่ปรึกษาร่วม ....

5376858433 : MAJOR PHARMACEUTICAL TECHNOLOGY

KEYWORDS: GOLD NANOPARTICLES / NANOTECHNOLOGY / PROTEIN AGGREGATION / AMYLOID BETA AGGREGATION / ZINC-INDUCED AMYLOID BETA AGGREGATION

CHUTIMA KONGSUWAN: STABILITY OF GOLD NANOPARTICLES AND THEIR INHIBITORY EFFECT ON AMYLOID-β_{1-42} PROTEIN AGGREGATION. ADVISOR: ASSOC. PROF. WARANGKANA WARISNOICHAROEN, Ph.D., CO-ADVISOR: PROF. SUWABUN CHIRACHANCHAI, Ph.D., 94 pp.

Aggregation of amyloid-β (Aβ) protein is known as the neurotoxicity involving in Alzheimer's disease (AD). Thus, prevention or reduction of Aβ aggregation would be a therapeutic strategy for AD. Gold nanoparticles (AuNPs) is considered to be a tool for AD treatment due to optical and biocompatible properties including ability to cross blood-brain barrier. In this study, citrate-stabilized AuNPs (AuCt) and polyethyleneimine-stabilized AuNPs (AuPEI) were synthesized and determined for their stability. Nanoparticle sizes of AuNPs were characterized by UV-vis spectroscopy, transmission electron microscopy (TEM) and dynamic light scattering (DLS). The zeta potentials of AuNPs were determined by laser electrophoresis. The inhibitory effects of AuNPs on amyloid-β_{1-42} (Aβ_{1-42}) aggregation and zinc-induced Aβ_{1-42} aggregation were examined using Thioflavin T fluorescence assay, and the appearance of aggregates were also observed under TEM. From the results, hydrodynamic diameters of AuCt and AuPEI obtained from DLS were 18.37 ± 0.34 nm and 18.59 ± 0.59 nm, respectively. The zeta potentials of AuCt and AuPEI were -35.37 ± 2.56 mV and 38.00 ± 1.68 mV, in orderly. Moreover, TEM analysis showed that AuPEI were smaller and less in size distribution than AuCt. After time storage, AuPEI were found to be more stable than AuCt. Both AuCt and AuPEI exhibited the inhibitory effect on Aβ_{1-42} aggregation and zinc-induced Aβ_{1-42} aggregation. However, AuCt had less inhibitory effect on the aggregation as compared to AuPEI. Increasing concentrations of AuCt and AuPEI AuNPS resulted in higher inhibitory effect on the aggregation. These results were in parallel with TEM images. Hence, the potential of AuNPs on inhibition of Aβ_{1-42} aggregation seemed to depend on the surface charges and concentrations of nanoparticles. The inhibitory mechanism of AuNPs on Aβ_{1-42} aggregates should be further clarified.

Department:	Pharmaceutics and Industrial Pharmacy	Student's Signature	....
		Advisor's Signature	....
Field of Study:	Pharmaceutical Technology	Co-Advisor's Signature	....
Academic Year:	2014		

ACKNOWLEDGEMENTS

CONTENTS

LIST OF TABLES

LIST OF FIGURES

LIST OF ABBREVIATIONS

°C	degree Celsius
ε	dielectric constant
η	absolute zero-shear viscosity of the medium
λ_{max}	maximum absorption peak
µL	microliter (s)
µM	micromolar (s)
AD	Alzheimer's disease
ApoE	apolipoprotein E
ApoE4	apolipoprotein E4
APP	amyloid-β precursor protein
Aß	amyloid-β
AuCt	citrate-stabilized gold nanoparticles
AuNPs	gold nanoparticles
AuPEI	polyethyleneimine-stabilized gold nanoparticles
BACE	beta-site APP cleaving enzyme
BBB	blood brain barrier
cdk5	cyclin-dependent kinase 5
CNS	central nervous system
CT	computed tomography
CTAB	cetyltrimethylammonium bromide
D	diffusion coefficient
DCS	differential centrifugal sedimentation

LIST OF ABBREVIATIONS (CONT.)

d_H	hydrodynamic diameter
DLS	dynamic light scattering
DODAB	dimethyldioctadecylammonium bromide
e.g.	example gratia
et al.	et alii (and others)
f (Ka)	Henry function
FTIR	fourier-transform infrared spectrometry
GSK3	glycogen synthase kinase 3
h	hour (s)
H_2O_2	hydrogen peroxide
IC_{50}	median (50%) inhibitory concentration
IDE	insulin-degrading enzyme
k	Boltsmann constant
LDL	low-density lipoprotein
LDV	laser doppler velocimetry
m	month (s)
M	molar (s)
MAPT	microtubule-associated protein tau
ml	milliliter(s)
mM	millimolar (s)
MRI	magnetic resonance imaging
mV	millivolt (s)

LIST OF ABBREVIATIONS (CONT.)

MW	molecular weight
NFTs	neurofibrillary tangles
nm	nanometers
PAA	polyacrylic acid
PAH	poly (allylamine) hydrochloride
PBS	phosphate buffer solution
PCS	photon correlation spectroscopy
PdI	polydisperse index
PEGDA	polyethylene (glycol) diacrylate
PEI	polyethyleneimine
PET	positron emission tomography
pH	potential of hydrogen
PS-1	presenilin 1
PS-2	presenilin 2
PVA	polyvinyl alcohol
RT	room temperature
SPR	surface plasmon resonance
TEM	transmission electron microscopy
ThT	thioflavin T
U_E	electrophoretic mobility
UV-vis	ultraviolet-visible
w	week (s)

LIST OF ABBREVIATIONS (CONT.)

XPS   X-ray photoelectron spectroscopy

XRD   X-ray diffraction

z zeta potential

CHAPTER I

INTRODUCTION

1. Background and significance of the study

Alzheimer's disease (AD) is a leading cause of dementia in the aging population. Patients with AD exhibit unusual behaviors like memory loss, disorientation, confusion with time or place, impaired judgment, behavioral change and speaking difficulty. There are 20 to 30 million AD patients around the world and a number of patients are expected to increase in triple by 2040 (Minati *et al.*, 2009). AD pathology is related to aggregation and accumulation of amyloid-ß (Aß) proteins which are derived from the proteolysis of Aß precursor protein (APP). The cleavage by enzymes ß-secretase and γ-secretase results in Aß products that are composed of $Aß_{1-40}$ and $Aß_{1-42}$ (Crews and Masliah, 2010). There are multisteps involved in Aß aggregation including Aß conformation change which is initiated by Aß monomer misfolding, association of monomer to form oligomers and, finally, growth in fibrilla aggregation (Kumar and Walter, 2011). The aggregation of $Aß_{1-40}$ and $Aß_{1-42}$ protein is known to be an important cause of AD. It has been found that $Aß_{1-42}$ aggregation seems to be more toxic than $Aß_{1-40}$ aggregation in neuron cell model (Zhang *et al.*, 2002). *In vitro* exposure to the metal ion, zinc, is one of the other risk factors for AD since an excessive zinc can induce aggregation of Aß protein much faster than the self-assembly of Aß aggregation (Noy *et al.*, 2008). The toxicity of zinc-induced Aß aggregation in hypothalamic neuron (GT1-7) cells has been reported (Konoha *et al.*, 2006). The prevention or inhibition of Aß protein aggregation plays as an important key in therapeutic strategy for AD. Unfortunately, there is still no effective treatment for AD. The U.S. Food and Drug Administration has approved some drugs that slow progress in AD symptoms but they are ineffective in some cases (Thies and Bleiler, 2011). Recently, the combination of biomedical science and nanotechnology has been concerned as a new strategy for treatment of AD. Also, development of diagnostic device for AD based on nanotechnology has been reported (Nazem and Mansoori, 2011).

Gold nanoparticles (AuNPs) are metallic nanoparticles that have attracted much attention due to their optical properties, being easily visualized and detected by spectroscopic techniques (Philip, 2008). The particle size and surface modification of AuNPs can be controlled by chemical composition. Due to their biocompatibility, AuNPs have been found to pass through blood brain barrier (Sonavane et al., 2008). The toxicity of AuNPs were not found in murine neural progenitor cells even using with the high concentration of AuNPs (Soenen et al., 2012). Recently, it has been hypothesized that AuNPs may attach to Aß protein, thus reducing the amount of protein available for aggregation (Liao et al., 2012; Lim et al., 2011). Hence, it could be advantageous to use AuNPs for treatment of neurodegenerative disease such as AD.

Some previous studies found that utility of AuNPs combined with microwave or laser irradiation resulted in the disaggregation of Aß protein (Bastus et al., 2007; Triulzi et al., 2008). Irradiation to peptide-conjugated AuNPs (CLPFFD-AuNPs) could cause selective attachment of AuNPs to Aß protein leading to the inhibition of Aß aggregation (Araya et al., 2008). Moreover, AuNPs have been employed as diagnostic tools for AD. AuNPs were used as a biomarker for Alzheimer's tau protein detection by coating the surface of nanoparticles with anti-tau antibody (Neely et al., 2009). The antibody-coated AuNPs presented as a nanosensor for occurrence of tau protein at low concentration as 1 pg/ml. The red-color precipitates were visually observed when antibody (6E10) conjugated AuNPs was incubated with Aß oligomers and Aß fibrils while no precipitate occurred in the presence of Aß monomer (Sakono et al., 2011).

Since AuNPs are promising candidate for Aß AD therapy, the evaluation of AuNPs effects on Aß protein is beneficial for therapeutic use of AuNPs. In this study, two types of AuNPs were prepared as follow Kim et al and Kimling et al (Kim et al., 2011; Kimling et al., 2006). Trisodium citrate or polyethyleneimine were chosen for AuNPs preparation due to their properties as stabilizer and reducer in the preparation without using other reagents. AuNPs were synthesized and characterized by using several techniques. The synthesized AuNPs were determined for their stability after

time storage. Their ability to inhibit the aggregation of Aβ protein was determined using the fluorescent-based assay.

2. Objectives of the study

2.1 To characterize and to test the stability of synthesized AuNPs

2.2 To investigate inhibitory effect of AuNPs on amyloid $\beta_{1\text{-}42}$ protein aggregation.

CHAPTER II

LITERATURE REVIEW

1. Alzheimer's disease

Alzheimer's disease (AD) is a neurodegenerative disease which is progress in brain cell death that happens over a course of time. AD has been known for more than 100 years but the research in symptoms, cause, and therapeutic has only gained in the last 30 years. Nowadays, there are 20 to 30 million AD patients around the world and a number of patients are expected to increase in triple by 2040 (Minati *et al.,* 2009). The incidence and prevalence of AD are also increasing with the age of population and until now there is no cure for AD. Therefore, AD problem is becoming one of the major universal healthcare problems.

1.1 Symptoms and diagnosis of AD

AD can affect different people in different way and progress in AD from mild AD to moderate and severe disease occurs with the different rate which is individual. Mostly, patients with AD exhibit unusual behaviors like memory loss, disorientation, confusion with time or place, impaired judgment, personality changes and difficultly in speaking and writing. Some people have behavioral change until they cannot live in the social anymore. In advance AD, patient will need help with the basic activities of daily living, including bathing, dressing, using the bathroom and eating. Patients can lose their ability to communicate, fail to recognize loved ones and become bed-bound and need around-the-clock care in finally. The progressive AD cannot be stop or reversed. Therefore, an early diagnosis is necessary for AD patients and their families to understand the disease. The benefits of early diagnosis are not only get a better chance from the treatment but also get more time to manage and plan for the future. Generally, patient with AD will be diagnosed by physician which commonly refer to the criteria given (First, 1994). To meet the criteria, the decline in cognitive abilities must be severe enough to interfere with daily life and symptoms and must include decline in memory and decline in at least one of the following cognitive abilities:

1. Ability to generate coherent speech or understand spoken or written language;

2. Ability to recognize or identify objects, assuming intact sensory function;

3. Ability to execute motor activities, assuming intact motor abilities, sensory function, and comprehension of the required task; and

4. Ability to think abstractly, make sound judgments, and plan and carry out complex tasks.

Furthermore, the decline in memory is not accounted for by another disorder like major depressive disorder or schizophrenia. To identify the possible causes of AD, the physician also conducts the physical and neurologic examinations in parallel with the cognitive test. The AD patient may undergo the brain scanning such as positron emission tomography (PET), magnetic resonance imaging (MRI) and computed tomography (CT) scans including autotopsy to examine the abnormal brain changes (Knopman *et al.*, 2001; McGeer *et al.*, 1986). Recently, there were the reports which revealed the biomarkers in cerebrospinal fluid and blood of AD patient including that may be useful for AD diagnosis and AD characteristic but these approaches were still be studied in the small-scale (Georganopoulou *et al.*, 2005; Han *et al.*, 2011). The further study and development is necessary to ensure in the safety, accuracy and reliability.

1.2 Cause of AD

At present, the scientists are not known yet about the causes of AD but mostly of them agree that AD is a complex disease that probably develops as a result of multiple factors rather than a single factor.

1.2.1 Age

The advancing age is one of the important factors for AD. Most AD patient is over 65 years old which called "late-onset" AD (Gurland et al., 1999). However, around 1 in 20 people with AD aged less than 65 years old that means the younger people can also develop the disease condition. This is called "early-onset" AD.

1.2.2 Family history

Another risk factor for AD is family history. People who have close family member with AD condition are more likely to develop the disease than those who do not have a relation with AD. Children having both mother and father with AD had a cumulative risk of 54% to be AD which was 5 times greater than the risk of children having normal parents and was 1.5 times greater than children having affected by mothers or fathers (Lautenschlager *et al.*, 1996). Genetic mutation inheriting from parents can be the cause of the disease relating to the gene mutations on chromosomes 1, 14 and 21. Each of these mutations causes abnormal proteins to be formed. The mutation on chromosome 21 led to the formation of abnormal amyloid precursor protein (APP) gene while mutations on chromosome 1 and 14 led to abnormal presenilin 1 (PS-1) and presenilin 2 (PS-2) gene, respectively (Forsell *et al.*, 1997; Nochlin *et al.*, 1998; St George-Hyslop *et al.*, 1987).

1.2.3 Amyloid beta

In AD, there are various pathologies of AD such as cognitive impairment, brain shrinkage, widespread brain cell dead and dying neuron which the accumulation of amyloid beta (Aß) is believed being the cause by interfering the neuron-to-neuron communication and contributing to cell death. Aß precursor protein (APP) was found in the brain and required for migration of neuron precursor cell in cerebral cortex (Young-Pearse *et al.*, 2007). (Figure 1) APP can be proteolytically cleaved *via* two pathways called non-amyloidogenic and amyloidogenic pathways (Verdile *et al.*, 2004). For non-amyloidogenic pathway, an enzyme, namely α-secretase, cleaves APP to release soluble carboxyl-truncated forms of APP (αAPP). The rest of C-terminal proteolytic products are further cleaved by γ-secretase to yield non-amyloidogenic fragments. For amyloidogenic pathway, beta-site APP cleaving enzyme (BACE) (also known as β-secretase) cleaves APP near N-terminal of Aß. Then, cleavage of C-terminal by γ-secretase was conduct in the final step to create Aß monomer. Normally, the degradation of Aß monomer by neprilysin and insulin-degrading enzyme (IDE) creates the balance between Aß production and Aß clearance (Crews and Masliah, 2010). When the process is disturbed, the level of Aß monomer

production increases over Aß clearance and becomes abnormal accumulation which involves in AD. Therefore, Aß has been used as one of the biomarkers in neurotoxic for AD.
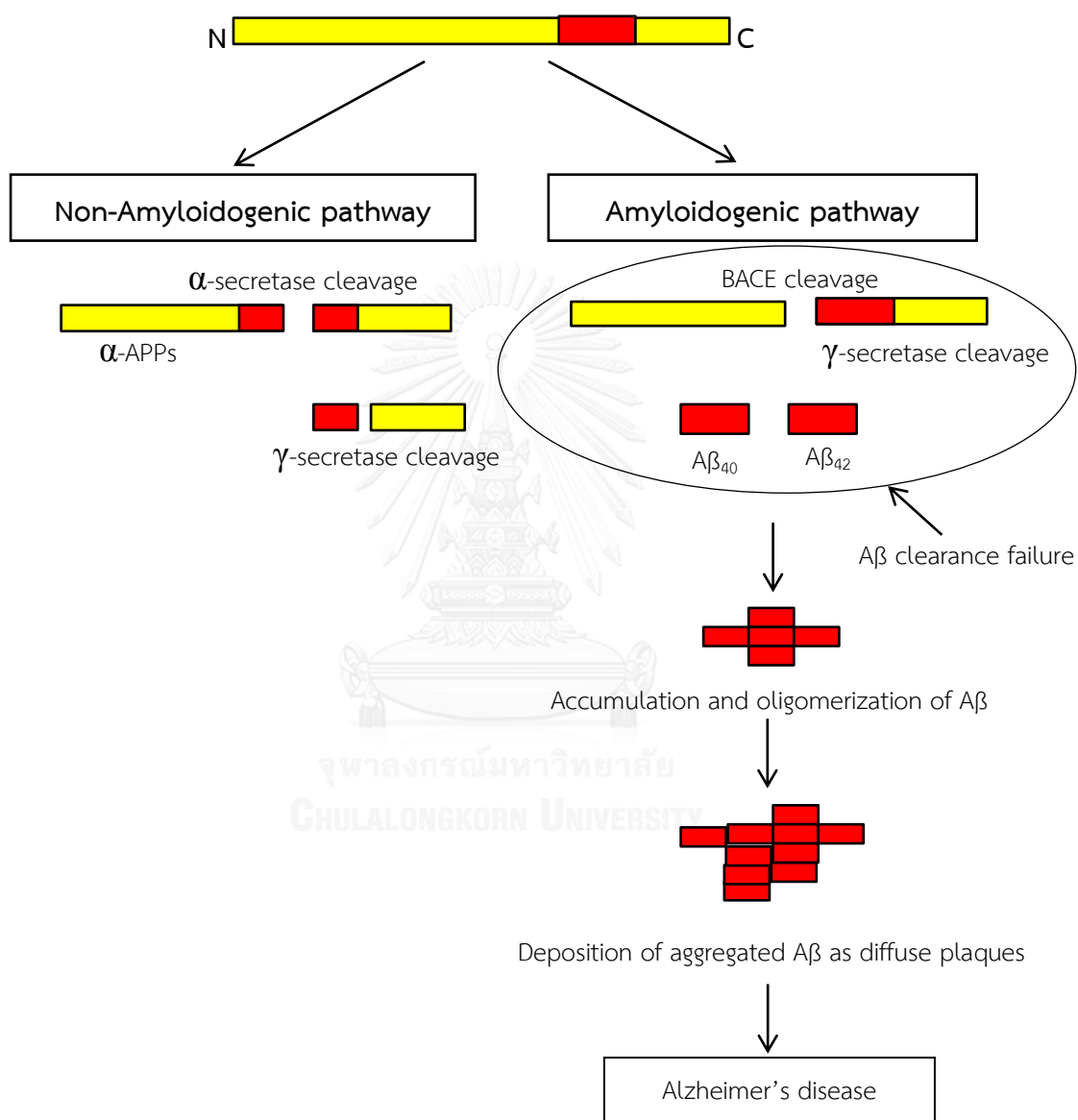
Figure 1. Amylodogenic pathway causing neurodegeneration in AD.
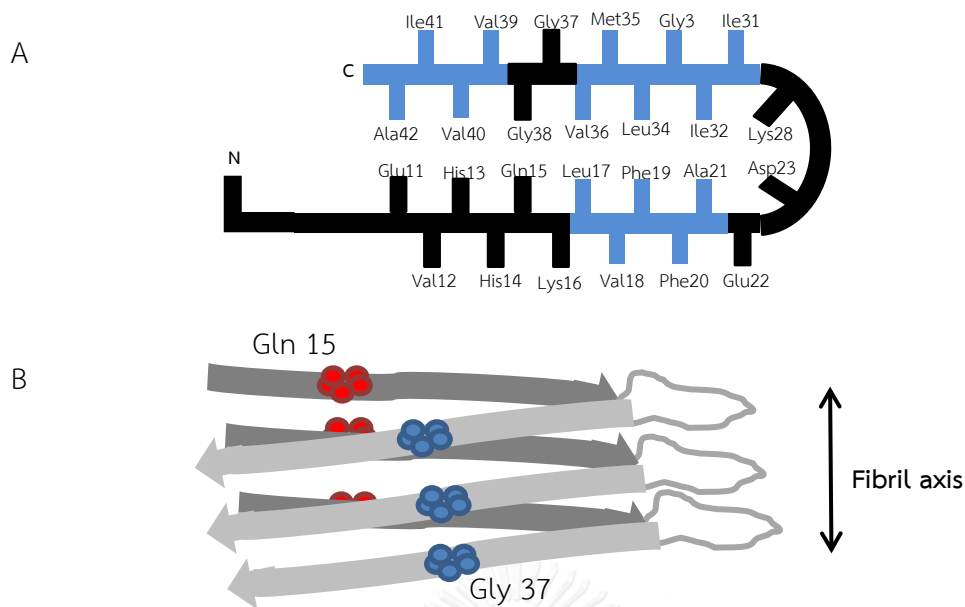
Figure 2. Schematic of Aß1-42 monomer (A) and ß-sheet within Aß1-42 fibrils (B).

Aß monomer consists of 39-43 amino acid residues with 4 kDa in length. Self-aggregation of Aß due to imbalance of amyloidogenic pathway crated Aß fibrils and Aß plaques (Figure 2). There are multisteps involved in the Aß aggregation as following: **i).** Aß monomer misfolding in form in α-helix which driven by intramolecular interaction of side chain observed between Phe19 and Leu34 and between Gln15 and Gly37 **ii).** association of monomers to form oligomers and creation of ß-sheet structure which carried out by intermolecular interaction observed between Gln15 and His13/14 **iii).** growth in fibrilla aggregation and **iv).** deposition as the plaque (Ahmed *et al.*, 2010; Kumar and Walter, 2011). Numerous studies have shown that Aß aggregation causes neurotoxicity in various cell lines, mammalian brain including AD patient cerebral cortex (Arriagada *et al.*, 1992; Guela *et al.*, 1998; Lorenzo and Yankner, 1994; Tomiyama *et al.*, 1997). Aß associated free radical was concerned as a cause of neurotoxicity (Butterfield, 1997). Moreover, the physiological effects of Aß were found to defend upon the concentration, neurotrophic effect was demonstrated at low doses (10^{-10} M – 10^{-8} M) while the neurotoxic effect was shown at higher doses ($> 10^{-7}$ M) (Yankner *et al.*, 1990).

1.2.4 Apolipoprotein E4

Apolipoprotein E4 (ApoE4) is another genetic risk factor for development of AD (Klaver et al., 1998). Apolipoprotein E (ApoE) gene has three isoforms (E2, E3 and E4) which provide the blueprint for a protein involving in lipid transport in the plasma and central nervous system including maintenance and repair of neurons (Mahley, 1988; Nathan et al., 1994). Normally, people inherit one form of the ApoE gene from each parent but who inheriting E4 form have an increased risk for developing AD higher than who inheriting E2 or E3 forms. The rate of ApoE4 allele founding in AD patients was 3 times higher than the general people (Kobayashi et al., 2011). There is the evidence that ApoE can bind to Aß peptide which this binding enhances the clearance of Aß prior to its aggregation into insoluble deposits. APPV717F Ftransgenic mice that absented in ApoE expressing gene demonstrated the enhancement of APP, Aß1-40 and Aß1-42 levels (Dodart et al., 2002). However, the exact mechanism by which ApoE enhances clearance of beta-amyloid plaque is unclear. It has been proposed that ApoE can bind to beta-amyloid and undergo endocytosis via astrocytes by low-density lipoprotein (LDL) receptor (Sagare et al., 2013). In in vitro, the binding affinity of ApoE4-Aß complex was less than ApoE2-Aß and ApoE3-Aß complex while the proteolysis cleavage of ApoE4 is greater than other isoforms (Jolivalt et al., 2000; LaDu et al., 1994). The proteolysis of ApoE4 in central nervous system (CNS) leads to a loss of normal function of ApoE4 like cholesterol transport which is essential for synaptogenesis and neuron growth. The digestion products of ApoE proteolysis conduce to Aß plaque formation and AD pathology evidencing from the detection of ApoE4 fragments in AD brain (Wisniewski et al., 1995). Thus, the expression of ApoE4 allele plays as an important role in developing AD which relates to the loss of the function in cholesterol transportation including Aß elimination.

1.2.5 Tau protein

Another hallmark of AD pathology is neurofibrillary tangles (NFTs) of tau protein which found in AD patient's brain. Tau protein is abundant found in the nerve cell due to the function as a structure providing stability and flexibility of microtubule axon. The diminish of normal tau protein demonstrated in the

cerebellum of AD patients (Čaušević et al., 2010). Six isoforms of tau protein exist in the brain which the difference between each isoform bases on the binding domain at the C-terminal. Three of the tau protein isoforms have three binding domains while another three of the proteins have four of these domains (Adams et al., 2010). The tau protein isoforms are produced through alternative splicing of a single gene called microtubule-associated protein tau (MAPT). Mutation in MAPT led to the NFT production in the brain evidencing from the transgenic mice that was expressed P301L mutation human tau protein in neurons produced the abnormal filaments (straight or helical structure) including phosphorylated tau filaments (Götz et al., 2001). Since protein kinases are capable of phosphorylating tau at many sites, the abnormally phosphorylation such as cyclin-dependent kinase 5 (cdk5) and glycogen synthase kinase 3 (GSK3) of tau can also be the cause of unstable microtubules. The loss of tau function by impairment in binding to tubulin was reported in Evan et al. experiment in which human tau protein was phosphorylated with cdk5 at serine 396 and serine 404 phosphorylated sites (Evans et al., 2000). The hyperphosphorylation of tau protein by cdk5 was detected in pyramidals neurons of AD brains while it was scarcely detected in normal brains (Takahashi et al., 2000). In neuroblastoma N18 cells, GSK3 induced conformational change of tau and reducing in tau's ability to promote tubulin. Thus, these reports revealed that mutation and hyperphosphorylation of tau protein may play an important role in abnormal function of tau protein involving in pathology of AD (Lin et al., 2007).

Beyond the causes of AD mentioned above, numerous researches also suggest that host factors may play a role in the development and course of AD. There is a great deal of interest, for example, in associations between cognitive decline and vascular and metabolic conditions such as heart disease, stroke, high blood pressure, diabetes, and obesity. These diseases are increasing in risk of being AD. However, to understand these relationships, the testing in clinical trials is required to clarify whether reducing risk factors for these conditions may help in improvement of AD pathology.

1.3 Zinc and neurotoxicity

The biological functions of zinc in the body have been known that involves in DNA synthesis, cell growth and development including being a co-factor of more than 300 enzymes. Maylor *et al.* have also found that zinc was relevant to the cognitive formation in the healthy people (Maylor *et al.*, 2006). Approximately 2-2.5 g of zinc is found in the body in which 130 µg/g was found in cerebral cortex (Harrison *et al.*, 1968). The deficiency of zinc promoted lipids and proteins peroxidation in weanling male rats including lingual and esophageal tumors in p53-deficient mice (Fong *et al.*, 2006; Oteliza *et al.*, 1995). Nevertheless, the elevation of zinc level in AD brains was found more than two-fold comparing with the normal brains and the increasing was correlate with tissue amyloid levels and plaque levels (Religa *et al.*, 2006). Consistently with a role of Aß-metal interaction, deficient zinc transporter 3 transgenic mice produced less Aß plaques and less insoluble Aß due to lacking of overexpression of synaptic zinc in the neurological system (Lee *et al.*, 2002). Aggregation of Aß (e.g. in the forms of Aß plaques and NFTs) has been implicated as the neurotoxic form of the peptide (Arriagada *et al.*, 1992; Lorenzo and Yankner, 1994; Tomiyama *et al.*, 1997). Thus, physiological factor like zinc may be involved in the promotion of Aß and progression of AD pathology. Aß was found to rapidly bind to zinc in *in vitro* (Noy *et al.*, 2008). The metal binding sites of Aß peptide were located at histidine sites (Dong et al., 2006) and the formation of Aß in the presence of zinc is different from Aß-self aggregation which is normally aggregated in fibril form (Tõugu *et al.*, 2009). A few concentration of zinc is enough to precipitate Aß and an excess concentration can be harmful to the rat pheochromocytoma (PC12) cells (Garai *et al.*, 2007; Moreira *et al.*, 2000). Also high dose of zinc in APP/PS1 transgenic mice also caused the overexpression of APP and enhanced Aß deposit (Wang *et al.*, 2010). Some reported that neurotoxicity of Aß in the presence of zinc was correlated with oxidative injury in AD through metal reduction and the cell-free generation of hydrogen peroxide (H_2O_2) and human $Aß_{1-42}$ promoted H_2O_2 more than human $Aß_{1-40}$ and rat $Aß_{1-40}$ (Cuajungco *et al.*, 2000). However, it still remains unclear how Aß aggregation in the presence of zinc leads to neurotoxic and dementia in AD.

1.4 Therapeutical strategies in AD

At present, there is no drug treatment that can slow or stop the deterioration of brain cells in AD. The focus in past years for AD treatment was the improvement of memory by activating cholinergic neurotransmission, antioxidants and blocking chemical release (Geldmacher, 2004; McNeill *et al.*, 2011; Motawaj *et al.*, 2011). However, the medicines that developed using these mechanisms can only improve symptoms, or temporarily slow down their progression in some people. The effectiveness of the medicines in AD patients is less than 50%. Now, the scientists have been focused on reducing Aß and tau protein depositions including increasing the rate of Aß clearance through ApoE. Many researches focus using the new approaches such as vaccination, gene therapy and hormonal therapy in order to find the new strategy for treating AD. In addition, the useful of early detection of AD by using Aß and tau protein as the hallmarks also play attention to many scientists.

2. Nanotechnology

Nanotechnology is science, engineering, and technology conducted at the nanoscale. Nanotechnology is utilized in most of the science fields, such as chemistry, biology, physics, material science, engineering and especially medicine. Due to a variety of the nanostructures such as nanotubes, nanorods, nanowires, nanocages, nanoshells and nanodisks, the modification and functionalization of nanostructures can be targeted to the specific objective which is able to develop for imaging, detecting, diagnostic, including healing for the disease. The nanotechnology has opened up the world beyond microscale which will be provided many useful in sciences.

3. Gold nanoparticles

Gold nanoparticles (AuNPs) are the metallic nanoparticles that have mainly been studied because of their unique optical properties (scattering and absorption) compared to bulk material. The absorption of AuNPs falls in the visible range which is able to detect by the routine instrument like spectroscopic techniques (Philip, 2008). The surface plasmon resonance (SPR) is occurred depending on the size,

shape and environmental surrounding AuNPs (Murphy *et al.*, 2008). These properties are very attractive to the scientists to apply AuNPs in many fields of pharmaceutical science.

3.1 Preparation of AuNPs

Size, shape and chemical compositions of AuNPs are controllable during the synthesis process. Both physical and chemical approaches are allowed to use in AuNPs preparation (Gutiérrez-Wing *et al.*, 2012) but the popular approach is chemical method which can prepare in aqueous and nonaqueous solutions. Turkevich method (Kimling *et al.*, 2006) is the simple chemical reduction method for AuNPs preparation by boiling a solution of tetrachloroauric acid with citrate solution. The process is performed until all of Au^{3+} are reduced to be neutral gold atoms and the citrate acts as reducing and anionic stabilizing agents. The particle size of AuNPs prepared from this method is in the range between 9-100 nm depending on stabilizer/gold ratio. As the same procedure described, the combination of tannic acid and citrate solution was report to be used as a reducing agent in order to prepare spherical AuNPs (Philip, 2008). Gold nanoparticles is not only produces at the high temperature but they can also be produced at the room temperature by seed-mediated growth approach (Murphy *et al.*, 2005). The seed particles (with diameter 3.5-4 nm) was initially occurred by reducing gold salts with sodium borohydride and the further growth was then carried out through the addition of ascorbic acid mixture solution. The final particle size of AuNPs can grow out up to 60 nm (Dong *et al.*, 2004; Murphy *et al.*, 2005). For the smaller AuNPs (1-3 nm), the synthesis protocol followed Brust-Schiffrin method in that they were produced in organic phase solution. The tetrachloroauric solution was transferred into toluene phase after that sodium borohydride was added to reduce gold ions to be AuNPs (Perala and Kumar, 2013).

However, it is not only small molecular chemicals like citrate and sodium borohydride that are used for AuNPs synthesis but the bigger molecule chemicals like polymers, lipids and surfactants can be used for AuNPs preparation. Due to the physicochemical properties of polymer such as biocompatible, biodegradable and water-soluble, polymers like polyethyleneimine (PEI), poly (acrylic acid) (PAA) and

chitosan can be fulfilled for AuNPs synthesis in many purposes (Bhumkar *et al.*, 2007; Popovtzer *et al.*, 2008; Thomas and Klibanov, 2003). PEI$_2$-GNPs conjugates as vectors for the delivery of plasmid DNA into monkey kidney (COS-7) cells were prepared by using a reduction method. The transfection efficiency of PEI2-GNPs conjugates was around 25 – 50% (Thomas and Klibanov, 2003). PAA-coated gold nanorods synthesized using seed mediated growth method was utilized for larynx and oral cancer diagnostic. By conjugation PAA-coated gold nanorods with UM-A9 antibody, the contrast in X-ray based CT images were increased leading to the accuracy for cancer detection (Popovtzer *et al.*, 2008). In chitosan capped AuNPs, use of chitosan serves dual purposes by acting as a reducing agent in synthesis of AuNPs and also promoting the penetration and uptake of peptide hormone insulin across the mucosa (Bhumkar *et al.*, 2007). Besides, cetyltrimethylammonium bromide (CTAB) and dimethyldioctadecylammonium bromide (DODAB) were used in preparation of AuNPs for the purposes of DNA and drug delivery (Li *et al.*, 2008; Urban *et al.*, 2011).

AuNPs can be synthesized using various methods. The suface of AuNPs can be modified and functionalized with various stabilizers to target to the specific selector including optical properties of AuNPs. Therefore, AuNPs are very attractive for various applications, nevertheless, the physico-chemical properties of AuNPs should be proved before the applications.

3.2 Physico-chemical characterization of AuNPs

The basic physico-chemical properties of AuNPs such as e.g. size, surface charge, mono- or polydispersity, UV-vis and morphology should be determined before AuNPs will be applied in any sciences.

3.2.1 UV-vis spectrophotometry

One of the important properties of AuNPs is optical properties. Therefore, UV-vis spectrophotometry is the common method utilized in AuNPs analysis. When the light is irradiated to AuNPs, free electrons at the nanoparticles surface will be excited, move into electromagnetic field and become oscillating. The collective oscillation of the elections is known as surface plasmon resonance (SPR). This phenomenon occurs

at particular wavelength which is able to manifest as surface plasmon resonance band (SPR band). The SPR band is not only used in characterization of AuNPs but also related to the particle size of AuNPs by the following equation (Khlebtsov, 2008):

$$d \quad = \quad 3 + 7.5 * 10^{-5} X^4 \qquad \text{for} \quad X < 23 \qquad (1)$$

$$d \quad = \quad \frac{(\sqrt{X\text{-}17} - 1)}{0.06} \qquad \text{for} \quad X \geq 23 \qquad (2)$$

where ; d =   diameter of the nanoparticle (nm), when $5 \leq d \leq 100$

            X =   maximum absorbance wavelength (λ_{max}) - 500

Normally, UV spectra of AuNPs was in the range between 500 and 540 nm with particle size varing form 9 – 120 nm (Kim et al., 2011; Kimling et al., 2006). The maximum absorbance wavelength of SPR band depends on particle size, thus, the shift of SPR peak can be caused particle size or particle shape change (Keene and Tyner, 2011; Kim et al., 2008; Kuo et al., 2005).

3.2.2 Dynamic light scattering

The size of metallic nanoparticles is important in most of the research regardless of emulsions, micelles, polymers, protein, nanoparticles or colloid due to their sizes can influence the physical and biological properties. For example, AuNPs with less than 90 nm in diameter were taken up higher than the larger nanoparticles in prostate cancer cell (PC-3) (Malugin and Ghandehari, 2010). In in vivo experiment, AuNPs with 10 nm diameter showed the higher concentration in rat's heart tissue than 50 nm gold nanoparticles (Mohamed and Halim, 2012). Therefore, the particle size affected the effectiveness of nanoparticles in different way. Generally, Dynamic light scattering (DLS) method or referred as photon correlation spectroscopy (PCS) technique or quasi-elastic light scattering (QELS) is widely applied for size determination and size distribution of particles in solution as a routine laboratory

analysis. DLS method can produce the accurate and reliable results by using small amount of a sample and the experiment can be completed within a short time period. DLS method relies on the Brownian motion of particles which particles diffuse randomly in the liquid medium. As the moving particles can be scattered the light after they are illuminated by laser beam, the detector captures and modifies the scattered light intensity as a function of time. The fluctuations of scattered light intensity are occurred due to the particles are moving with different rates of diffusion (the larger particles diffuse slower than smaller particles). By measuring the time dependence of light intensity fluctuations, DLS instrument computes them into the intensity correlation function. The analyzing of intensity correlation function provides the diffusion coefficient of the particles (known as diffusion constant) as follows (Hackley and Clogston, 2011):

$$\Gamma = q^2 D \tag{3}$$

Γ : the exponential decay rate

q : the modulus of the scattering vector (defined by scattering angle and wavelength of light)

D : diffusion coefficient

In order to obtain the hydrodynamic diameter (d_H) of particles, the diffusion coefficient (D) can be related to the Stokes-Einstein equation:

$$d_H = \frac{kT}{3\P\eta D} \tag{4}$$

d_H : hydrodynamic diameter

k : Boltsmann's constant (1.38×10^{-23} JK^{-1})

T : absolute temperature

η : absolute zero-shear viscosity of the medium

D : diffusion coefficient

The nanoparticle samples are normally not monodispersion due to the defection of synthesis. There is particle size variation in the samples. If the variation is too much, the average particle size obtained from DLS method might not be reliable. Polydisperse index (PdI), defined as a measurement of the width of the particle size distribution, is a parameter that can be related to the quality of the result. The range of PdI is from 0 to 1. The PdI value greater than 0.7 indicates that the sample has a broad size distribution and is probably not suitable for DLS technique (Nidhin *et al.*, 2008). Therefore, the combination of particle size determination is preferred in most of the research in order to compare and confirm the data from any methods.

3.2.3 Zeta potential

Zeta potential is related to the surface charge which is exhibited by nanoparticle dispersed in solution. Generally, the nanoparticles consist of two layer of ion charge, called electrical double layers. The first layer, referred as a stern layer, occurs due to the surface charge of particle attracts a thin layer of the opposite ion charge and binds tightly to the nanoparticle surface. A second outer layer is a diffuse layer which is consisted of loosely associated ions. The amount of ions in this layer is less firmly than a stern layer. The nanoparticles normally stay with the two ion layers as a stable form. When nanoparticles move or diffuse through the solution (due to Brownian motion or applied force), slipping plan boundary is created in the diffuse layer in which ions within the boundary move alongside the particle while ions beyond boundary stay with bulk solution. The potential at the slipping plane boundary is called zeta potential.

In zeta potential measurement, an electrical field is applied to the nanoparticles resulting in the movement of charged nanoparticles. The velocity of nanoparticles detected by laser doppler velocimetry (LDV) is referred to electrophoretic mobility (U_E). According to Henry's equation, zeta potential was obtained as following (Clogston and Patri, 2011) :

$$U_E = \frac{2\,\varepsilon\,z\,f\,(\text{Ka})}{3\,\eta} \tag{5}$$

z :   zeta potential

U_E :   electrophoretic mobility

ε :   dielectric constant

η :   absolute zero-shear viscosity of the medium

$f\,(\text{Ka})$:   Henry function

The magnitude of zeta potential can be used in predictive of colloidal or nanoparticle stability. By dividing zeta potential value in two ranges, more positive than +30 mV and more negative than -30 mV, nanoparticles with zeta potential greater than +30 mV or less than -30 mV are considered to be stable colloid system. On the other hand, nanoparticles will trend to be sedimental and unstable, if nanoparticles have lower zeta potential than the defined range.

3.2.4 Transmission electron microscopy

Transmission electron microscopy (TEM) is a microscopy technique for characterization of particle within a nanometer scale. The high energy electron beam is provided to transmit through a sample to create the image of particles. The size (including size distribution), shape, uniformity and dispersity of particles can be directly observed which is advantages of the TEM technique. However, TEM technique allows only dehydrated form of sample to be detected. Therefore, the particle size obtained by TEM may yield the different diameter from other techniques that need interaction with water or solvent molecules. Kim et al have shown the two different average diameters of AuNPs from TEM analysis and DLS analysis while the smaller size was found from TEM analysis (Kim et al., 2011).

3.2.5 Other analytical methods

There are many analytical methods that can be used for AuNPs characterization. Some methods have been used for long time ago and some methods have been developed for more convenient use such as X-ray diffraction (XRD), differential centrifugal sedimentation (DCS), X-ray photoelectron spectroscopy (XPS) and Fourier-transform infrared spectrometry (FTIR). Since gold can form crystals, the POME-capped AuNPs powder and AuNPs in PVA film were characterized using XRD method resulting in atomic and molecular structure of AuNPs (Gan *et al.*, 2012; Khanna *et al.*, 2005). DCS is another technique that used for gold particle analysis in the fluid under centrifugal force. The particle size and size distribution of AuNPs determined by DCS analysis was 13±3 nm which was in the same range with TEM analysis (Mahl *et al.*, 2011). By using XPS technique, the surface chemical composition of polyacrylic acid and poly (allylamine) hydrochloride-coated AuNPs (Au-APP/PAH) was analyzed which gave both quality and quantity information. In the same way, polyethylene (glycol) diacrylate (PEGDA) coating on the surface of AuNPs was confirmed by XPS spectra (Amici *et al.*, 2011; Minati *et al.*, 2011). The surface functional group of polyvinyl alcohol (PVA) stabilized AuNPs was also studied with FTIR. FTIR spectra of PVA-capped AuNPs showed a different frequency and bandwidth from pure PVA, especially at O-H stretching region at around 3,390 cm^{-1} (Pimpang and Choopun, 2011). Although, these methods are very potential technique and give very specific information in AuNPs characterization but somehow some methods are used rarely due to requirement of special technique and special equipment.

In summary, UV-vis spectrophotometry, DLS and TEM are very useful, easy to use and are often applied for AuNPs analysis. The other analytical techniques (e.g. XRD, DCS, XPS, FTIR) are more complex and infrequent in use, nevertheless they give the very efficient data for AuNPs characterization.

3.3 Toxicity of gold nanoparticles

Along with the number of potential applications for AuNPs especially in biomedicine and scientific purposes, the interest in toxic effects have been risen up as a new concerns for the environmental and human health status. There are many researches demonstrated that the toxicity of AuNPs is dependent on the size, shape and surface modification of AuNPs including the cell-type dependent uptake. Connor *et al* found that citrate capped AuNPs with particle size about 18 nm could penetrate the human leukemia cells without cell injury and toxicity (Connor *et al.*, 2005). Likewise, a study by Vijayakumar and Ganesan also demonstrated that citrate stabilized AuNPs with diameter of 17 nm were non-toxic in prostate cancer cell (PC-3) and human breast cancer cell (MCF-7) even using the concentration higher than 100 µg/ml while the smaller particle size had cytotoxic effect (Vijayakumar and Ganesan, 2013). That might be due to the large surface area to volume ratio provide platforms for increasing surface particle activity (Van Doren *et al.*, 2011). Moreover, AuNPs toxicity is varied due to the particle shape of AuNPs. Gold nanorods have been reported to be more toxic than gold spherical nanoparticles as demonstrated in human keratinocyte cells (HaCaT) and human breast cancer cells (MCF-7) (Chithrani *et al.*, 2006; Qiu *et al.*, 2010). The mechanisms of higher toxicity of rod AuNPs compared to spherical AuNPs have not been yet demonstrated. Using of cetyltrimethylammonium bromide (CTAB) as a surface stabilizer can also be the cause of cytotoxic because it is a surfactant that can break and open cell membranes (Connor *et al.*, 2005). AuNPs prepared with free-CTAB is expected to be non-toxic to the cells. Polymer like polyethyleneimine (PEI) has been widely used for AuNPs preparation because PEI can be both a stabilizer and a reducer without using other reagents. PEI has been reported to be cytotoxic (Hunter, 2006); however, the cytotoxic effects of PEI can be diminished when it is in particulate form as PEI-AuNPs seen from viability of human fibroblast cells (Kim *et al.*, 2011). In addition, the different cell lines can be different sensitive to AuNPs effect in which fibroblast cell was more sensitive to AuNPs than kidney cell (Chueh *et al.*, 2014). Therefore, many factors of AuNPs (such as sizes, shapes and surface modifications) in toxicity test

should be considered because they might exhibit the different properties both *in vitro and in vivo.*

4. Gold nanoparticles for Alzheimer's disease

Recently, nanotechnology is considered as a new strategy for diagnosis and treatment of neurodegenerative disease. The useful of nanotechnology over the others strategy is due to a wide variety of potential applications in biomedical, optical and electronic fields. Based on the pathogenesis of AD, AD is occurred in the brain which has blood brain barrier (BBB) protecting unwanted chemical in the blood. This BBB becomes a huge challenge for scientists to develop the molecule that can pass through BBB. Therefore, the nanoparticles like AuNPs become interesting due to the properties that they are able to pass through BBB (15-50 nm) and their biological compatibility (Sonavane *et al.,* 2008). The studies on utility of AuNPs combined with anti-tau antibody demonstrated that AuNPs is a perfect candidate for using as diagnostic tool in AD. By using AuNPs coated with anti-tau antibody, the increasing in two-photon Rayleigh scattering intensity was accurately detected even in the presence of 1 pg/ml tau protein and the intensity was also distinct from the serum albumin protein. Hence, they are useful in diagnostic tau-protein in cerebrospinal fluid (Neely *et al.,* 2009). When antibody (6E100) conjugated with AuNPs was incubated with Aß, the red-color precipitates was visually observed in the presence of Aß oligomers and Aß fibrils but not in the presence of Aß monomer (Sakono *et al.,* 2011). Early preclinical work included the use of AuNPs to detect a marker for AD in the blood which could distinguish between blood serum of healthy volunteers and AD patients.

Many works are on investigation of the potential of AuNPs for inhibition the formation of Aß protein associated with AD or decreasing the progress of the disease. AuNPs combined with microwave or laser irradiation were used for delivering the thermal energy to the selective target like Aß which resulted in the disaggregation of Aß (Bastus *et al.,* 2007; Triulzi *et al.,* 2008). Irradiation to peptide-conjugated AuNPs (CLPFFD-AuNPs) could cause selective attachment of AuNPs to Aß protein leading to the inhibition of Aß aggregation and restoration of Aß aggregation (Araya *et al.,* 2008).

Modification of AuNPs by using poly (n-acryloyl-L-phenylalanyl-L-phenylalanine methyl ester) and copolymer (*N*-isopropylacrylamide : *N*-tert-butylacrylamide) also promoted the inhibitory effect on Aß fibril formation (Cabaleiro-Lago *et al.*, 2008; Skaat *et al.*, 2012). In addition, it has been hypothesized that AuNPs may attach to Aß protein, thus reducing the amount of protein available for aggregation and altering the structure of Aß (Liao *et al.*, 2012; Lim *et al.*, 2011). So, in this study, the AuNPs stabilized by citrate and polyethyleneimine were synthesized and tested for their inhibitory effect on the aggregation of amyloid-β_{1-42}. The data obtained might provide the application of AuNPs as a new tool for treatment of AD.

CHAPTER III

MATERIALS AND METHODS

1. Materials

1.1 Equipment

1. De-ionized water (DI water) system (ELGAStat Option 3B)

   (ELGA, UK)

2. Fluorescence, absorbance and luminescence reader Victor[3] V

   model (PerkinElmer, USA)

Light source	:	Tungsten-halogen lamp (λ = 340-850 nm)
Detection unit	:	Photomultiplier tube
Fluorometry	:	Fluorescein
Optical emission filter :		486/10 nm
Optical excitation filter:		450/10 nm

3. High speed refrigerated microcentrifuge (Tomy, Japan)

4. Micropipettes (Gilson, France)

   : P20 (2-20 µL), P1000 (200-1000 µL)

   Micropipettes (Biohit, Finland)

   : Proline plus (20-200 µL)

5. Multichannel pipettes (Biohit, Finland)

   : Proline plus (8 channels) (10-100 µL)

   Multichannel pipettes (Rainin, USA)

   : L200 (12 channels) (20-200 µL)

6. Multichannel tips (Rainin, USA)

7. Orbital-shaker (Benchmark, USA)

8. Spectrophotometer Evolution 600 (Thermo Scientific, UK)

Light source	:	Xenon lamp (λ = 190-1100 nm)
Bandwidths	:	0.5, 1.0, 1.5, 2.0, 4.0 nm
Detector	:	Silicon photodiode

9. Syringe filter 0.2 µM (Pall, USA)

10. Timer (Gibthai, Thailand)

11. Transmission Electron Microscopy (JEM-2100) (Jeol, Japan)

Magnification	:	50-1,500,000 X
Acceleration voltage	:	80-200 kV
Resolution (HR)	:	0.14 nm (lattice image)

Transmission Electron Microscopy (H-7650) (Hitachi, Japan)

Magnification	:	50-600,000 X
Acceleration voltage	:	40-120 kV
Resolution (HR)	:	0.20 nm (lattice image)

12. Ultra-purifier water system (Maxima UF, UK)

13. Ultracentrifugal filter 3 kDa (Millipore, USA)

14. Vortex mixer (Clay Adams, USA)

15. Zetasizer NanoZS (Malvern, UK)

Laser	:	4mW He-Ne (633 nm)
Laser attenuator	:	Automatic (transmission 100% to 0.0003%)
Detector	:	Avalanche photodiode (Quantum efficiency > 50% at 633 nm)

16. 96-well black plates (Costar, USA)

1.2 Chemicals

1. β-Amyloid (Aβ) [1-42] (Human) (Invitrogen, USA)

2. Hydrochloric acid (HCl, MW=36.45) (Carlo Erba Reagents, Italy)

3. Hydrogen tetrachloroaurate (III) trihydrate ($HAuCl_4.3H_2O$, MW=393.83) (Aldrich, USA)

4. Nitric acid (HNO_3, MW=63.01) (Carlo Erba Reagents, Italy)

5. Phosphate buffer solution (PBS) (10X) (Invitrogen, USA)

6. Polyethyleneimine (PEI) (($CH_2CH_2NH)_n$, MW ~ 750 kDa) (Sigma-Aldrich, USA)

7. Thioflavin T (ThT) ($C_{17}H_{19}ClN_2S$, MW=318.86) (Sigma-Aldrich, USA)

8. Trisodium citrate dihydrate ($Na_3C_6H_5O_7.2H_2O$, MW=294.07) (Sigma-Aldrich, USA)

9. Ultrapure water (18.2 MΩ) (ELGA, UK)

10. Phosphotungstic acid ($H_3[P(W_3O_{10})_4] \cdot H_2O$, MW=2880.05) (Fluka,USA)

11. Zinc chloride ($ZnCl_2$, MW=136.30) (Fluka, Germany)

2. Methods

2.1 Preparation of gold nanoparticles

Gold nanoparticles (AuNPs) at concentration of 1,015 µM (200 ppm) were synthesized by using either trisodium citrate dihydrate or polyethyleneimine as reducing and stabilizing agents. Before AuNPs synthesis, all glassware were cleaned in aqua regia consisting 3 parts of HCl and 1 part of HNO3, rinsed with ultrapure water (18.2 MΩ) and then oven dried prior to use.

2.1.1 Citrate-stabilized gold nanoparticle preparation

Citrate-stabilized gold nanoparticles (AuCt) were synthesized following the classical Turkevich method (Kimling *et al.*, 2006) (Figure 3). AuCt were prepared at three conditions (1, 2, 3) which made the molar ratios of Au to trisodium citrate be 1:4, 1:8 and 1:12, in orderly. Firstly, 35 µl of 30% w/w hydrogen tetrachloroaurate (III) trihydrate ($HAuCl_4.3H_2O$) was added into 49.5 ml (1), 49 ml (2) or 48.5 ml (3) of ultrapure water. The solution was boiled with vigorously stirring. When the temperature of solution raised up to 90°C, 0.5 ml (1), 1 ml (2) or 1.5 ml (3) of 0.4 M trisodium citrate dihydrate ($Na_3C_6H_5O_7.2H_2O$) solution was added and continuously stirred for 15 minutes until the color of solution was changed to ruby red. The solution was then cooled down to room temperature and transferred into a clean screw-cap glass bottle. All of AuCt were kept in light-protected condition before characterization.

30% HAuCl$_4$.3H$_2$O and ultrapure water

↓ Stir and heat to 90°C

Add 0.4 M citrate solution

↓

Stir and heat until the color changes to be dark red solution

↓

Cool down at room temperature

↓

Store in light-protected container
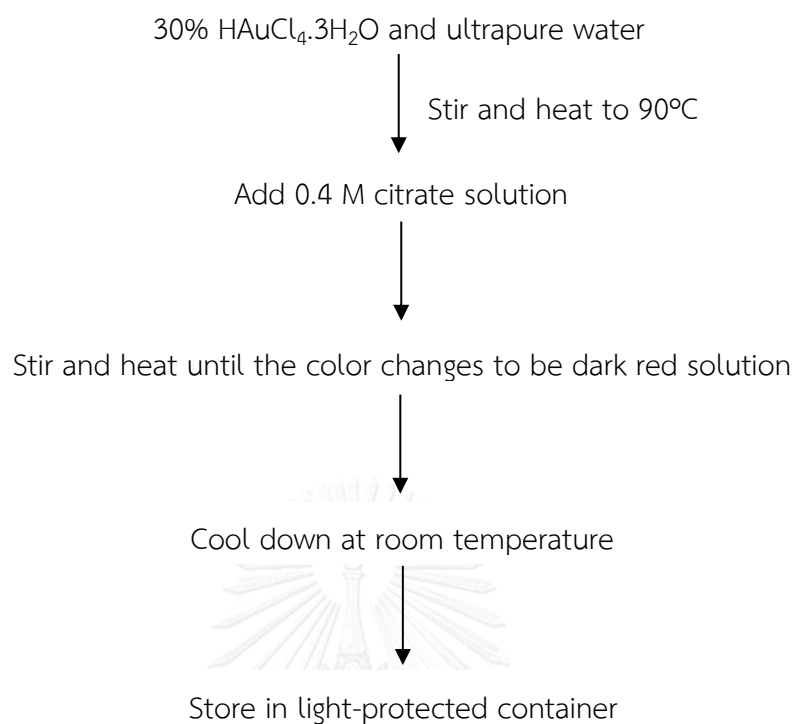
Figure 3. Preparation of citrate-stabilized gold nanoparticles

2.1.2 Polyethyleneimine-tabilized gold nanoparticle preparation

Polyethyleneimine (PEI)-stabilized gold nanoparticles (AuPEI) were prepared at the same Au concentration as AuCts by using PEI as reducing and stabilizing agent (Kim et al., 2011). The procedure of the synthesis was similar to AuCt preparation except for using PEI solution instead of citrate solution (Figure 4) and the molar ratios of Au to PEI were 1:0.36, 1:0.72 and 1:1.08, for condition 1, 2 and 3, respectively. After 49.5 ml (1), 49 ml (2) or 48.5 ml (3) of tetrachloroaurate solution was heated, 0.5 ml (1), 1 ml (2) or 1.5 ml (3) of 0.36 M PEI solution was added to the solution. The mixture was stirred and heated for 15 minutes to complete the reaction. The color of solution was slowly changed from orange color to be dark red color. AuPEI were all cooled down and kept in light protected-container.

30% HAuCl$_4$.3H$_2$O and ultrapure water

↓ Stir and heat to 90℃

Add 0.36 M PEI solution

↓

Stir and heat until the color changes to be dark red solution

↓

Cool down at room temperature

↓

Store in light-protected container
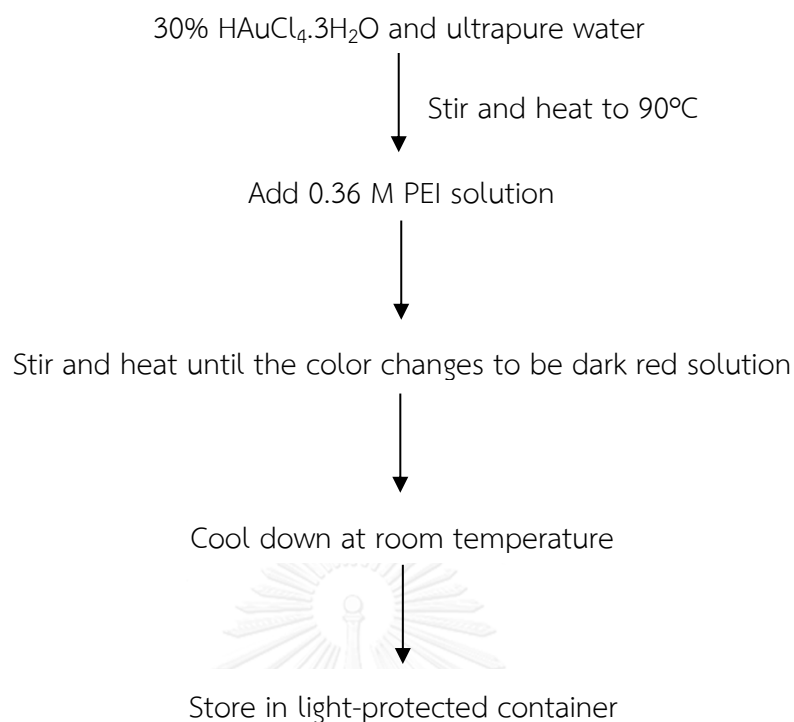
Figure 4. Prepartion of PEI-stabilized gold nanoparticles

2.2 Characterization of gold nanoparticles

2.2.1 UV-vis spectroscopy

AuCt and AuPEI were characterized by using Evolution 600 UV-vis spectrophotometer to obtain optical spectra and maximum absorption peak (λmax). The characterization was performed under wavelengths between 300 to 850 nm. A quartz cuvette with 10-mm optical path length was used for measurement. The ultrapure water was used as a blank for both AuCt and AuPEI.

2.2.2 Particle size analysis

The techniques used for AuCt and AuPEI particle size analysis were transmission electron microscopy (TEM) and dynamic light scattering (DLS). For TEM analysis, the samples were prepared by dropping 10 μL of AuCt or AuPEI on the formvar-coated grid (300 mesh) and drying in the air at room temperature prior to observation under transmission electron microscope. The particle size and size

distribution of AuCt and AuPEI were obtained from SemAfore program version 5.21. The hydrodynamic sizes of AuCt and AuPEI were also measured by using dynamic light scattering (DLS) method. The DLS measurement was performed at room temperature using Zetasizer Nano ZS (Malvern, UK) equipped with He-Ne laser operating at a wavelength of 633 nm and a photon detector. Prior to size measurement, AuCt and AuPEI were diluted with ultrapure water. The data was represented as a mean particle diameter of three measurements.

2.2.3 Zeta potential measurement

The zeta potential of AuCt and AuPEI was measured by using Zetasizer Nano ZS (Malvern, UK). AuCt and AuPEI were diluted with ultrapure water and 750 µl of dilute sample was transferred to disposable folded capillary cell for measurement of zeta potential. All measurements were performed at room temperature and reported as an average value of three determinations.

2.3 Stability test of gold nanoparticles

The prepared AuCt and AuPEI were stored at refrigerator (3°C-5°C) and room temperature (RT) in light- protecting container for 1 week, 1 month, 3 and 6 months. The stability of AuNPs was visually observed and the changes in size, zeta potential and UV-vis spectra after time storage were measured by the previously described methods. The stable formulations were selected to be used in further experiments.

2.4 Thioflavin T binding assay

Thioflavin T (ThT) is a fluorescent dye used to quantify the misfolding amyloid protein (Aß) aggregation. ThT can bind to the long axis β-sheet structure of amyloid aggregates but not a random coil monomer (Levine, 1993). The change in fluorescent property of ThT-bound Aß is exhibited as enhanced emission fluorescence spectrum (Groenning, 2010; Levine, 1993). The experimental procedure for ThT binding assay was performed as follow previous report (Hatters and Griffin, 2011)

2.4.1 Thioflavin T solution preparation

For ThT solution preparation, the dye was diluted with PBS to yield 1 mM ThT stock solution. ThT solution was filtrated through 0.2 µm filter and kept in light-protected container until use.

2.4.2 Aß$_{1-42}$ solution preparation

Human Aß1-42 in form of lyophilized peptide (≥ 95% purity by HPLC analysis) was dissolved in ultrapure water to obtain 1.33 mM and then diluted with Ca2+-free PBS to a final concentration of 100 µM. The solution was sonicated for 10 minutes prior to use. Aß$_{1-42}$ has isoelectric point about 5.5 (Moores *et al.,* 2011). The sequence of human Aß1-42 is shown in Figure 5.

H$_2$N-Asp-Ala-Glu-Phe-Arg-His-Asp-Ser-Gly-Tyr-Glu-Val-His-His-Gln-Lys-
Leu-Val-Phe-Phe-Ala-Glu-Asp-Val-Gly-Ser-Asn-Lys-Gly-Ala-Ile-Ile-Gly-
Leu-Met-Val-Gly-Gly-Val-Val-Ile-Ala-OH
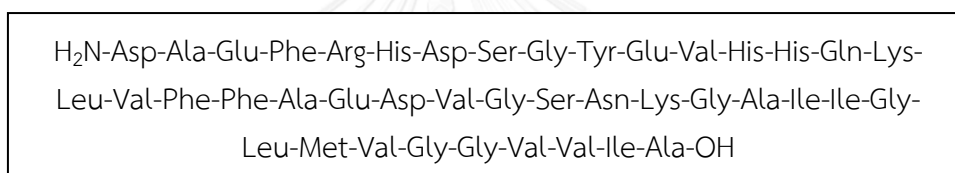
Figure 5. Sequence of human Aß$_{1-42}$ peptide

2.4.3 Effect of gold nanoparticles on inhibition of Aß$_{1-42}$ aggregation

In order to investigate the inhibitory effect of AuCt and AuPEI on aggregation of Aß protein, the pre-incubation of Aß$_{1-42}$ solution was done before mixing with AuNPs by adding 10 µM of Aß$_{1-42}$ solution in 96-well plate and letting peptide aggregation at the room temperature which took approximately 60 hours. AuCt or AuPEI at concentrations of 1, 2, 3, 4, 6 or 8 µM was added into 96-well plate containing aggregated Aß at 1:1 volume ratio of AuNPs to Aß$_{1-42}$. It was noted that AuPEI was filtrated through 3 kDa ultracentrifugal filter with 1000 x g spinning for 20 minutes and 10 x g spinning for 10 minutes before use. Then, freshly prepared ThT solution was added to make a final concentration of 20 µM. The final volume of the mixture was 200 µL per well. Aß solution without AuNPs was also incubated with ThT solution and served as a positive control. By applying orbital shaker to the sample

plate, the samples were continuously shaked at 1000 rpm speed. All samples were placed and incubated (0-96 hours) at room temperature until the fluorescence measurement. Fluorescence intensity of the sample is measured by using fluorescence microplate reader at an excitation wavelength of 445 nm and an emission wavelength of 482 nm. The fluorescence data was calculated as percentage of inhibition as follows:

$$\% \text{ inhibition } = 100 - \left[\frac{(F_I - F_B) \times 100}{(F_C - F_B)} \right] \tag{6}$$

where F_C is the fluorescence of the sample observed in Aβ peptide aggregation without AuNPs, F_I is the fluorescence of the sample observed in the presence of the AuNPs and F_B was the fluorescence of the blank (ThT solution and AuNPs). In addition, the effect of nanoparticle stabilizers, trisodium citrate and PEI solution on Aβ protein aggregation was also observed using the ThT binding assay as described previously. The experiment was performed in triplicate.

2.4.4 Effect of gold nanoparticles on inhibition of zinc-induced Aβ$_{1-42}$ aggregation

The effect of AuCt and AuPEI on inhibition of zinc-induced Aβ aggregation was investigated by ThT binding assay. In this study, zinc ion was used for rapidly inducing Aβ aggregation. The 10 µM zinc solution was prepared by dissolving zinc chloride (ZnCl$_2$) in ultrapure water. Again the Aβ aggregation was induced before testing with AuNPs. The procedure was the same as previous study except for an addition of 20 µl of 100 µM ZnCl$_2$ solution into the Aβ solution in 96-well plate. AuCt or AuPEI (1, 2, 3, 4, 6 or 8 µM) was mixed with aggregated Aβ in 96-well plate. Then, the sample was mixed with 20 µM ThT solution. The mixture was shaken and incubated at the room temperature. After period of time (0-96 hours), the sample was measured for the fluorescence intensity by using fluorescence microplate reader at the emission and excitation wavelengths of 445 nm and 482 nm, respectively. The fluorescence

data was calculated as percentage of inhibition following the equation as described previously. The effect of trisodium citrate and PEI solution on inhibition of zinc-induced Aß aggregation was also observed by the same method. All of the samples were measured in triplicate.

2.4.5 TEM analysis

Apart from ThT binding assay, negative stain electron microscope was used for examination of Aß aggregation. The staining dye was prepared by preparing 1% w/v phosphotungstic acid (PTA) in aqueous solution and adjusting to pH 7.4 with 1 M sodium hydroxide solution (NaOH). The test sample (10 μL) was dropped on the formvar-coated grid (300 mesh) for 5 minutes and staining the sample with filtrated 1% w/v PTA solution for 2 minutes. The excess solution was removed by touching the grid to filter paper. The grid was allowed to dry at room temperature and then visualized under TEM.
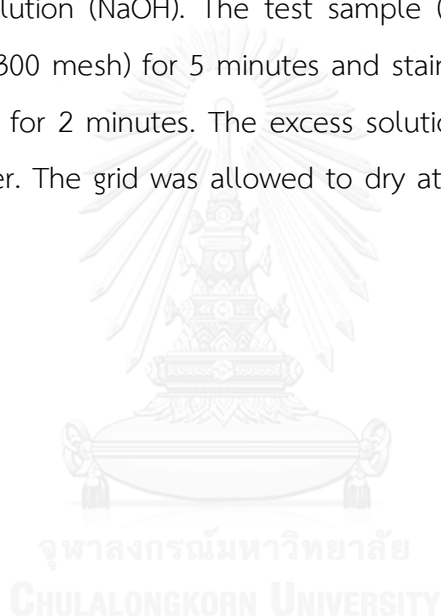
CHAPTER IV
RESULTS AND DISSCUSSION

1. Preparation of gold nanoparticles

Two types of AuNPs (200 ppm as 1 mM Au atom) were prepared by chemical reduction method as follow Kim *et al* and Kimling *et al* (Kim *et al.*, 2011; Kimling *et al.*, 2006). Trisodium citrate (Ct) and PEI were used as both reducing and stabilizing agents. The concentrations of trisodium citrate or PEI were optimized to obtain the suitable preparation. In addition, the stability test was performed by observing the changes of AuNPs at 4°C and room temperature (RT).

AuCt were prepared by using different molar ratios of Au to trisodium citrate, 1:4, 1:8 and 1:12, while the molar ratios of Au to PEI were 1:0.36, 1:0.72 and 1:1.08. The appearances of AuCt and AuPEI were dark red color in all preparation as illustrated in Figures 4A and 5A. After preparation, AuCt and AuPEI were kept in either 4°C or RT for 1 week, 1 month, 3 months and 6 months of storage. The change in appearance of AuNPs after time storage is shown in Figures 4 (B-E) and 5 (B-E). All of AuCt kept at RT showed some preciptation after 1 month storage. Similarly, the precipitation was also observed in AuCt (1:12) kept at 4°C but not AuCt (1:4) and AuCt (1:8). It looked like AuCt should be kept in the cool place in order to preserve the stability. The instability of AuCt (1:12) even stored in cool temperature might be due to high reactant concentration and inproper proportion between Au and trisodium citrate. However, AuCt (1:4) had some precipitation (and agglomeration) after 3 months of storage. Therefore, the suitable concentration ratio for Auct preparation would be 1:8 which was in agreement with the finding reported by Kimling and coworker (Kimling *et al.*, 2006).

For AuPEI, there were some formulations that appearances were unchanged within 3 months. The results here were similar to the previous studies (Kim *et al.*, 2011; Kuo *et al.*, 2005). The change in color to be darken red and some agglomeration were found in all AuPEI stored at RT while the change in color was found in AuPEI (1:0.36) stored at 4°C. The less stability of AuPEI (1:0.36) might come from the fact

that there were not enough PEI molecules for stabilizing Au atom. The results indicated that the proper concentration ratios of Au atom to PEI of 1:0.72 and 1:1.08 could produce the stable PEI-stabilized gold nanoparticles. However, AuPEI (1:0.72) and AuPIE (1:1.08) had some floating particle found after storage for 6 months (4°C).

Figure 6. The appearances of AuCt after preparation (A), after 1 week storage (B), after 1 month storage (C), after 3 months storage (D) and after 6 months storage (E), at 4℃ (left) and at room temperature (RT) (right) for B-E. Molar ratios of Au:Ct are 1:4 (1), 1:8 (2) and 1:12 (3).
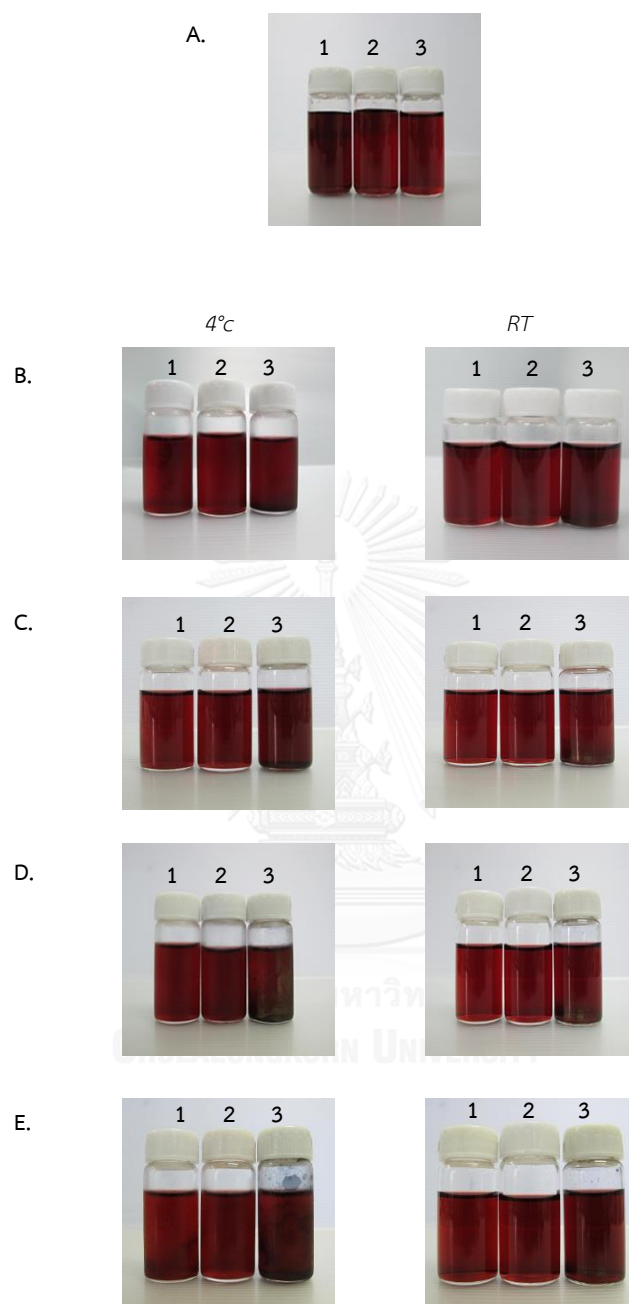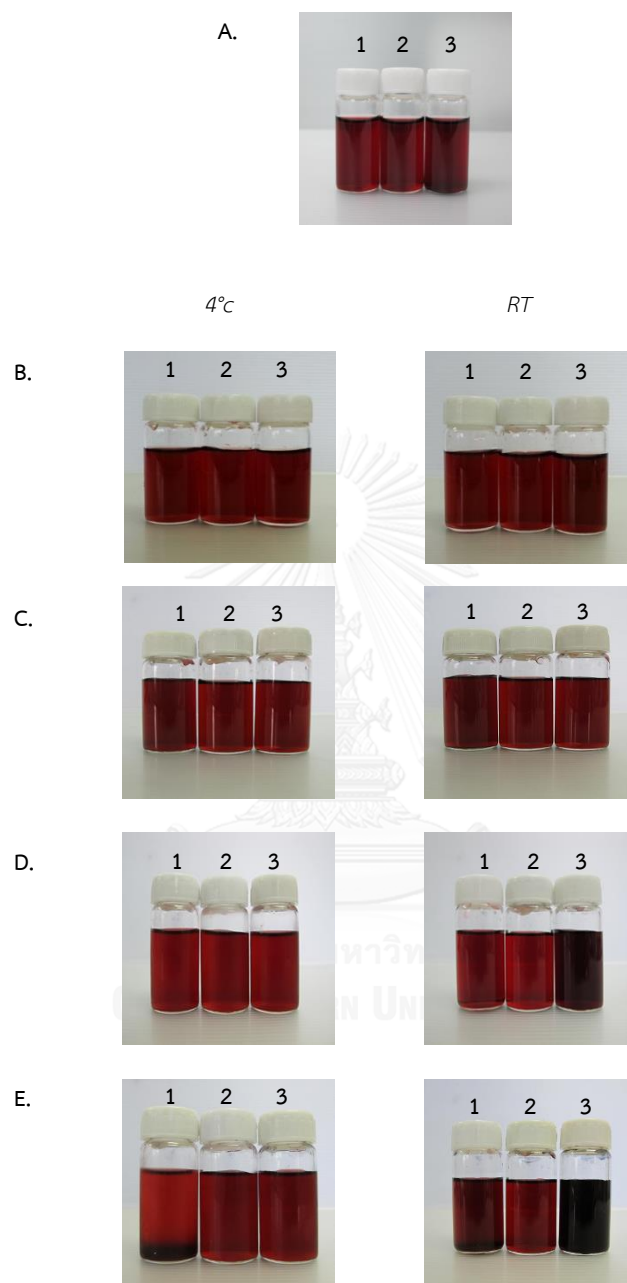
Figure 7. The appearances of AuPEI after preparation (A), after 1 week storage (B), after 1 month storage (C), after 3 months storage (D) and after 6 months storage (E), at 4°C (left) and at room temperature (RT) (right) for B-E. Molar ratios of Au:PEI are 1:0.36 (1), 1:0.72 (2) and 1:1.08 (3).

2. Characterization of gold nanoparticles

2.1 UV-vis spectroscopy

UV-vis spectroscopy is widely used for characterizing the optical properties and presented as the SPR band of metallic nanoparticles. Figures 8-13 show SPR bands of AuCt and AuPEI after preparation and after storage time at 4°C and RT. AuNPs generally absorb light in blue-green portion of spectrum and reflect red light with the peak absorbance wavelength of surface plasmon band (λmax) around 500-540 nm (Kimling et al., 2006). The absorbance of AuNPs can be varied from 0.1 to be 3.0 which is dependent on the concentration of AuNPs (Kimling *et al.*, 2006; Pimpang and Choopun, 2011). In this study, AuCt (1:4), AuCt (1:8) and AuCt (1:12) after preparation represented the absorbance peaks at 520, 522 and 523 nm while peaks of AuPEI (1:0.36), AuPEI (1:0.72) and AuPEI (1:1.08) after preparation centered at 524, 521 and 522 nm, in orderly, (Figures 8-13). The absorbances of AuCt and AuPEI after preparation were in the range of 1.5 – 2.5.

All AuCt stored at RT showed the absorbance peak shift to the higher wavelength after a month of storage by for approximately 5 nm for AuCt (1:8) and AuCt (1:12) and about 10 nm for AuCt (1:4). The absorbance peaks found were also broaden. These changes were occurred together with AuCt (1:12) even being kept in the cool place (4°C). The spectra of AuCt (1:4) and AuCt (1:8) stored at 4°C were barely changed after a month of storage. However, after 3 months, slight shift of peak position (~3 nm) was found in AuCt (1:8) and higher shift of peak position (~8 nm) was found in AuCt (1:4). For all AuPEI kept at RT, shift of peak position was observed after 3 months while width of peak was increased after a week of storage. The absorbance peaks of AuPEI (1:0.36), AuPEI (1:0.72) and AuPEI (1:1.08) were located at 529, 524 and 528 nm. For AuPEI (1:0.36) and AuPEI (1:1.08) keep at 4°C, the peak absorbances were shifted to about 5 nm higher in wavelengths after 3 months of storage while the peak position of AuPEI (1:0.72) was seemed unchanged.

The shift of absorbance peak indicated the occurring of larger particle or some agglomeration of nanoparticles while broadening of the peak associated to the

change in polydispersity of nanoparticles (Keene and Tyner, 2011; Kim *et al.*, 2008; Kuo *et al.*, 2005). The results of peak shift and peak broadening of AuNPs stored at RT were correspondent to the change in their appearance in that some dark particles were found after storage. From the results, AuCt (1:8) and AuPEI (1:0.72) seemed to be suitable preparations of negative-charged AuNPs and positively-charged AuNPs, respectively. The proper temperature for storage of AuNPs should be the lower temperature (i.e. 4°C).

Figure 8. UV absorption spectra of AuCt (1:4) stored at either 4°C (A) or RT (B) after preparation, 1-week, 1-month and 3-month storage.

Figure 9. UV absorption spectra of AuCt (1:8) stored at either 4°C (A) or RT (B) after preparation, 1-week, 1-month and 3-month storage.

Figure 10. UV absorption spectra of AuCt (1:12) stored at either 4°C (A) or RT (B) after preparation, 1-week, 1-month and 3-month storage.

Figure 11. UV absorption spectra of AuPEI (1:0.36) stored at either 4°C (A) or RT (B) preparation, 1-week, 1-month and 3-month storage.
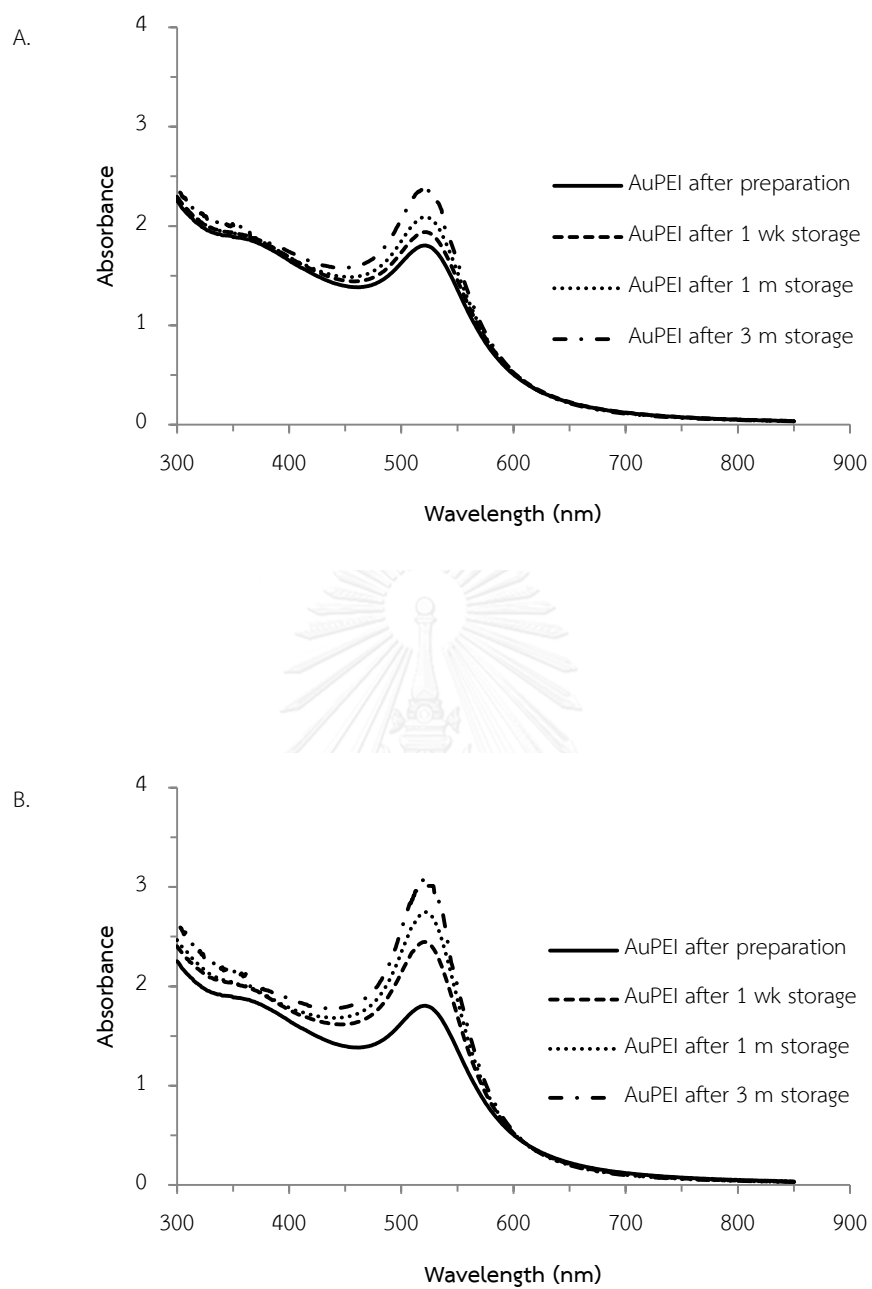
Figure 12. UV absorption spectra of AuPEI (1:0.72) stored at either 4°C (A) or RT (B) after preparation, 1-week, 1-month and 3-month storage.

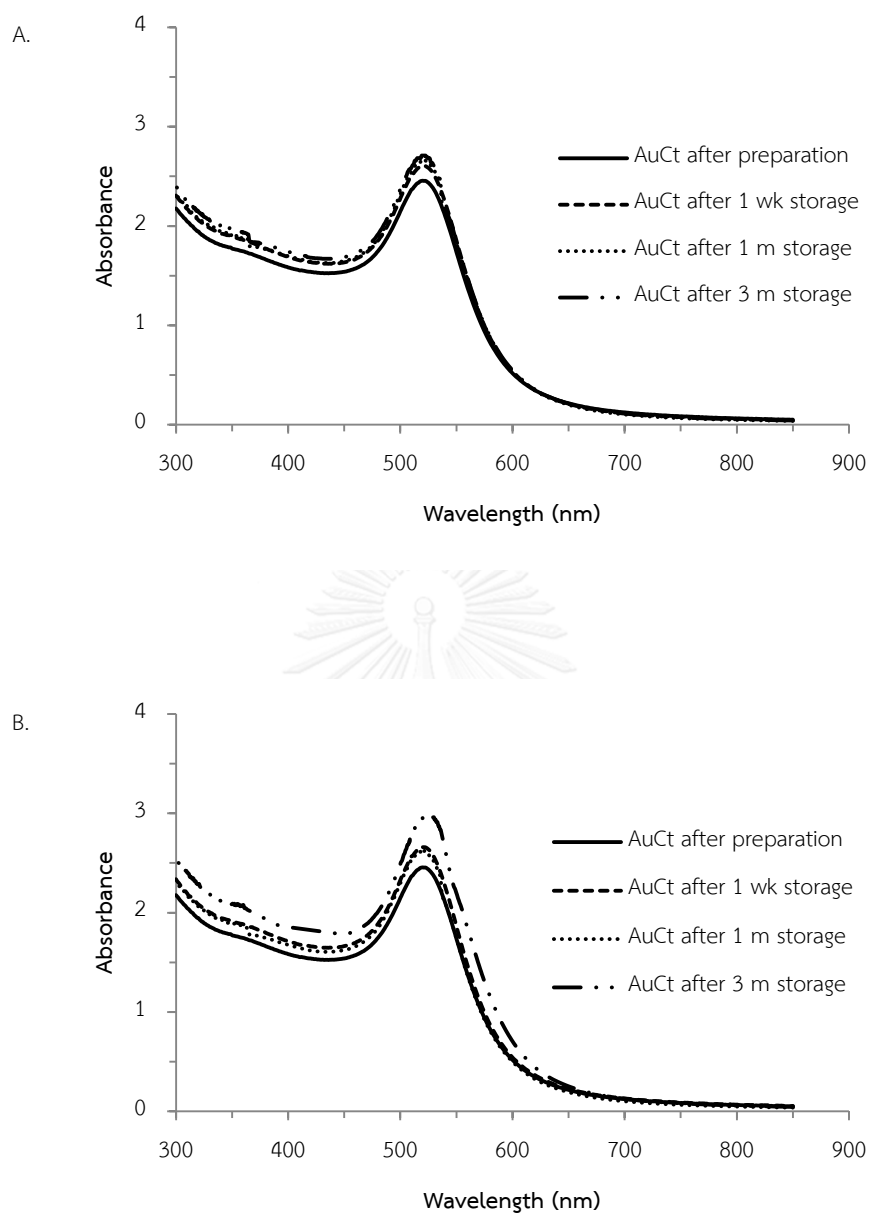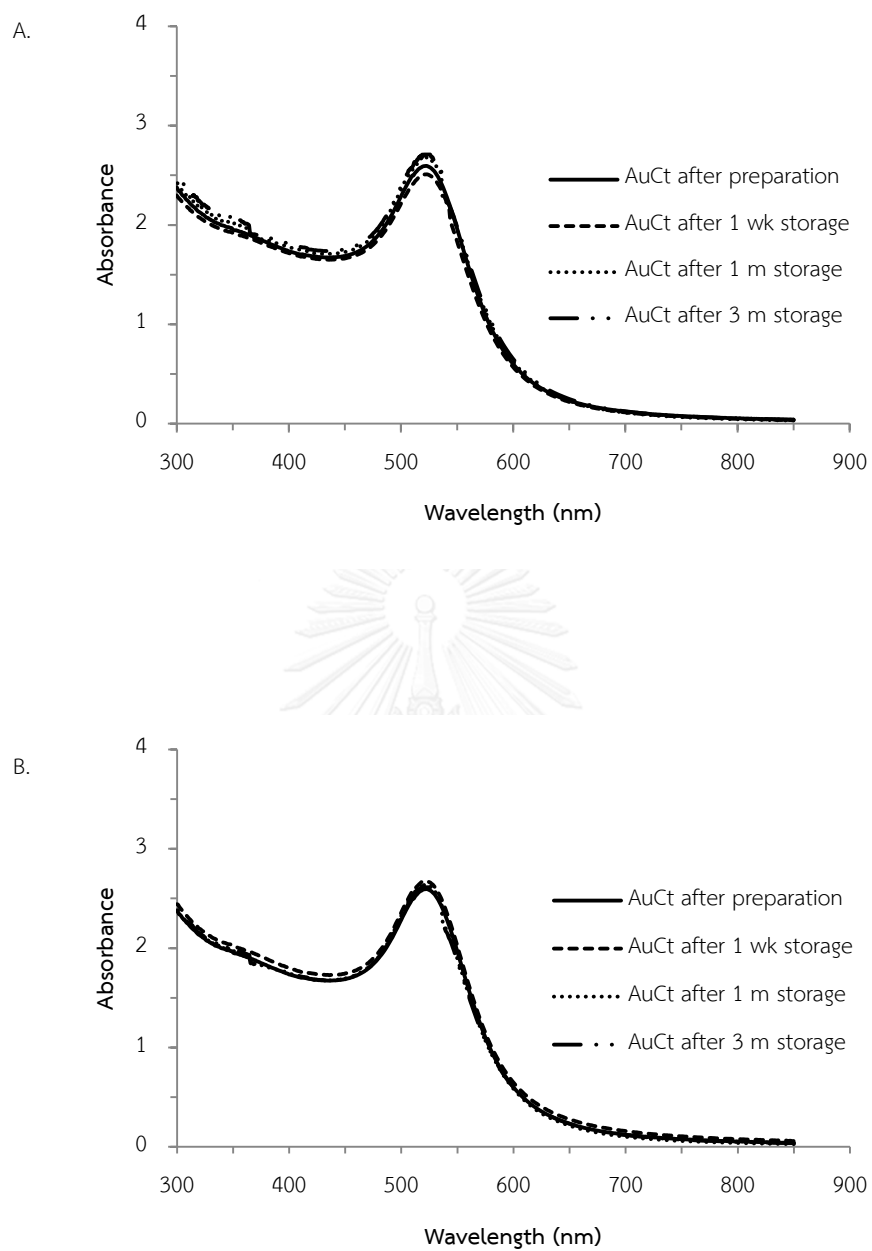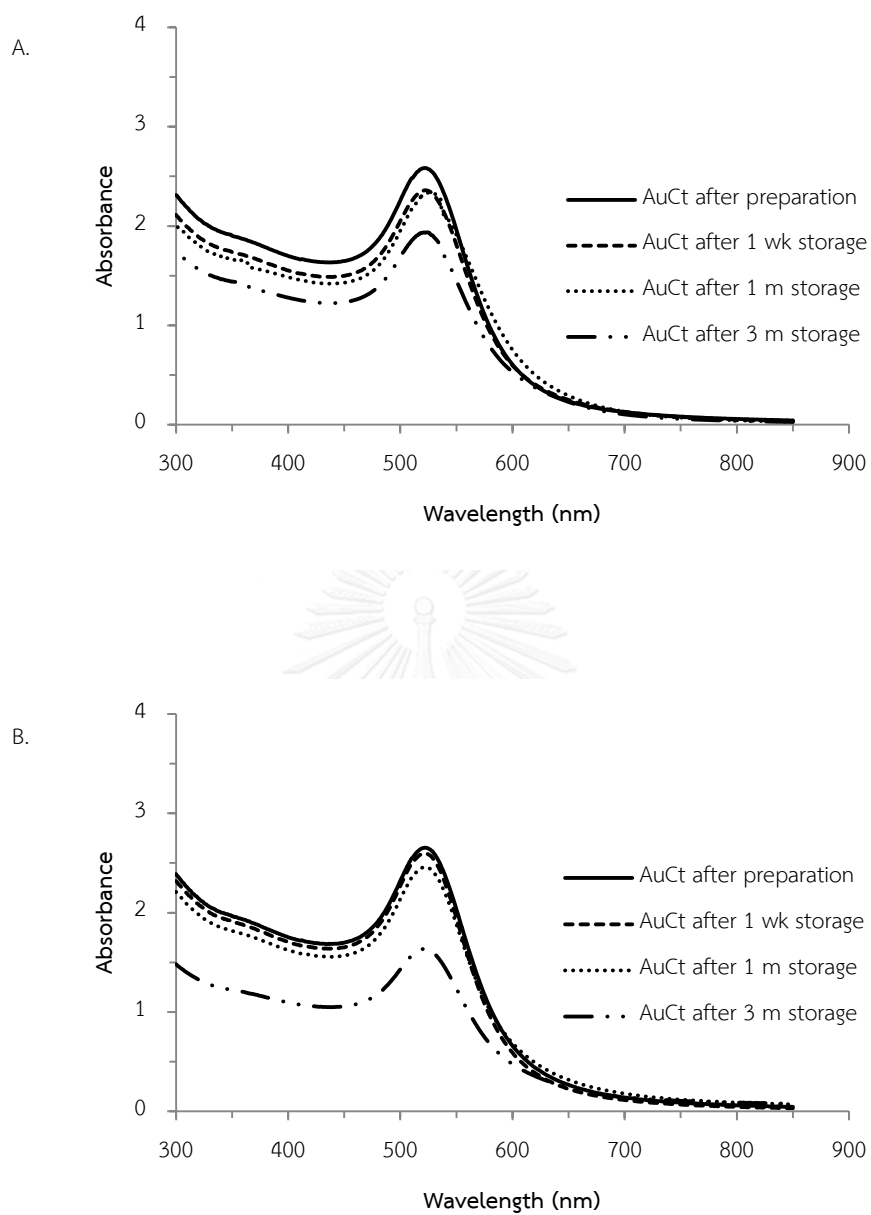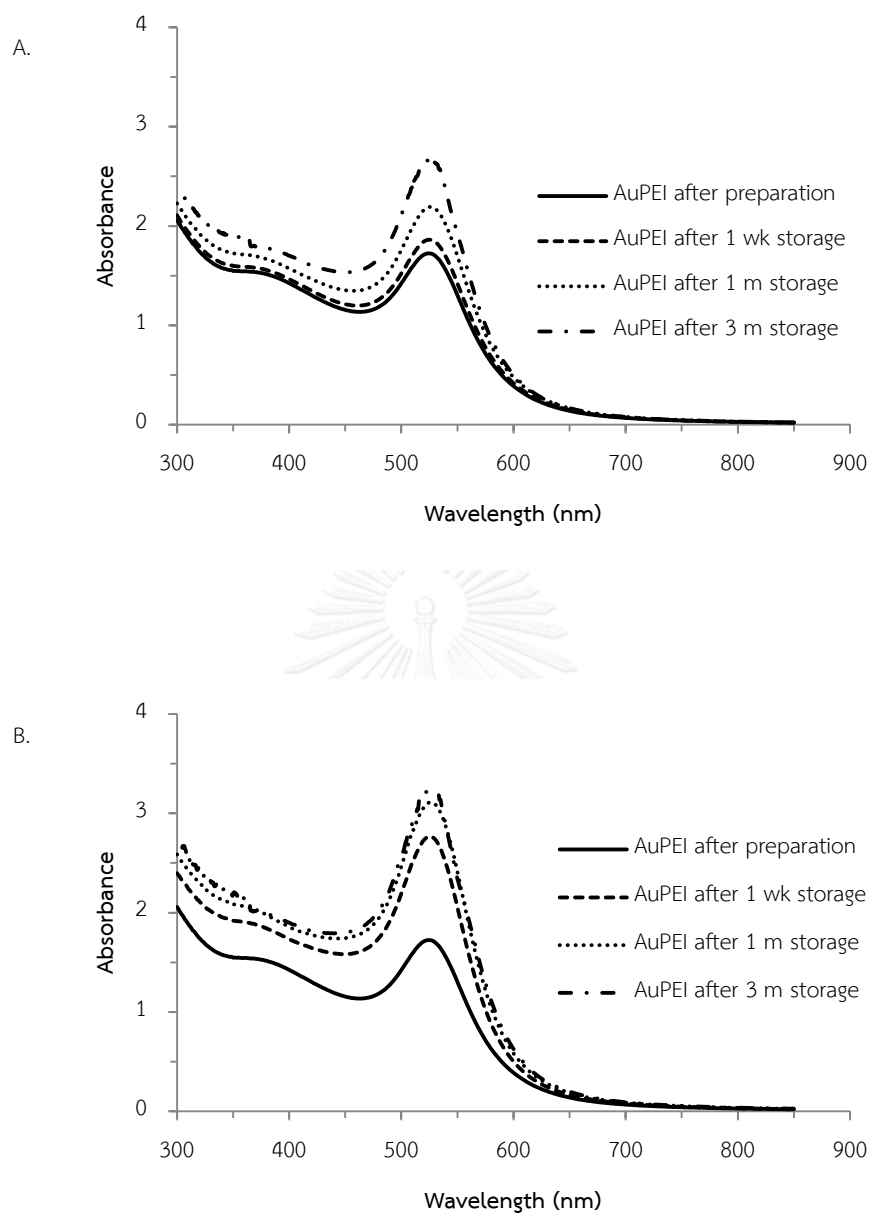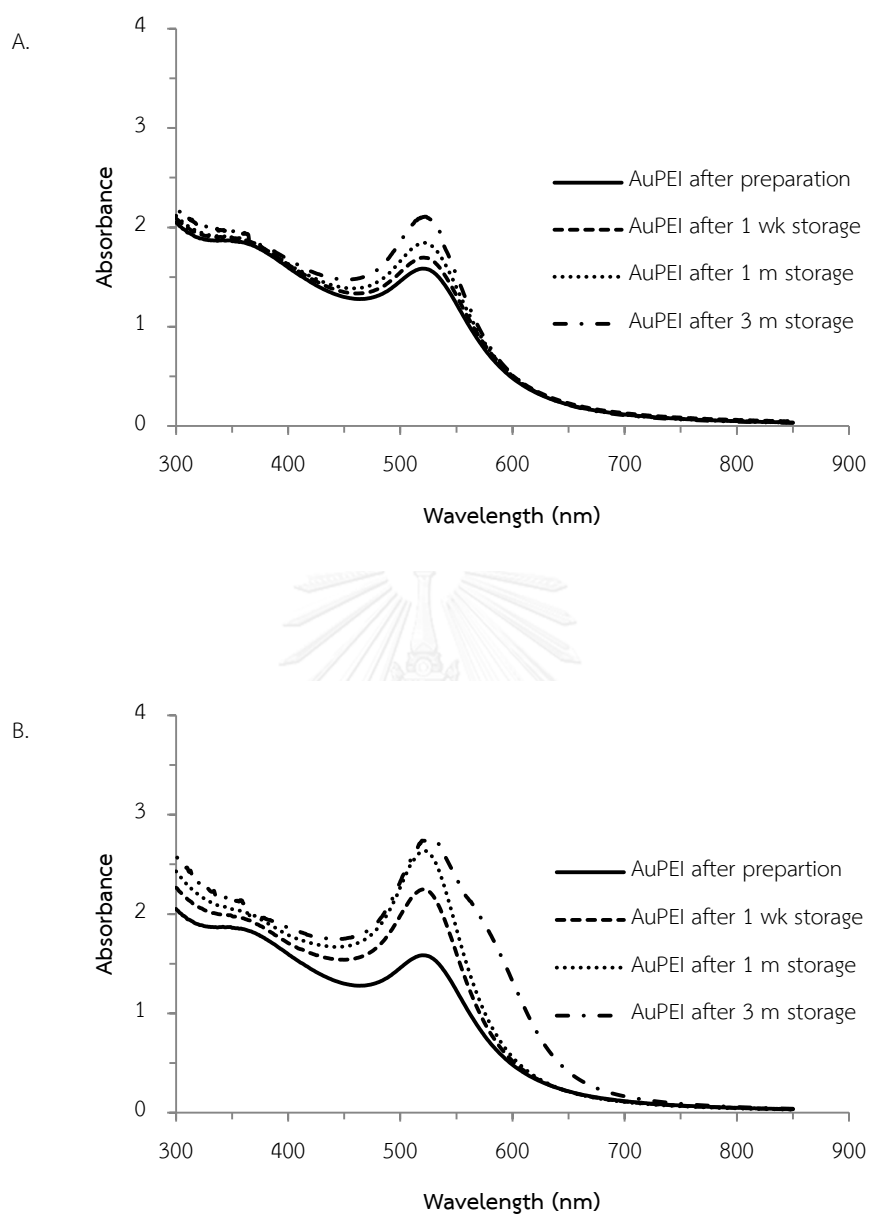**Figure 13.** UV absorption spectra of AuPEI (1:1.08) stored at either 4°C (A) or RT (B) after preparation, 1-week, 1-month and 3-month storage.

2.2 Morphology and particle size analysis

The TEM results revealed the spherical shape of both AuCt and AuPEI (Figures 14 and 15). Size distribution data of AuCt and AuPEI after preparation analyzed by TEM are shown in Figures 16 and 17. The highest variation in size distribution of 5.67 was found in AuPEI (1:0.36), whereas the other AuNPs showed the similar range of 0.53-1.89 for variation in sizes distribution (Table 1). From DLS analysis, the hydrodynamic sizes (mean ± SD) with polydispersity index or PdI (represented in bracket) of AuCt and AuPEI are shown in Table 1. The average sizes of AuCt were in a range of 18.37-23.04 nm and those of AuPEI were in a range of 17.15-28.47 nm. The hydrodynamic sizes of AuNPs were consecutively observed after time storage at different condition (4°C or RT). The DLS results indicated that there were some changes in particle sizes of AuNPs after being kept as illustrated in Figures 18 and 19. The particle sizes of AuCt stored at RT were higher than those stored at 4°C (Figure 18). In contrast, the variation in particle sizes of AuPEI after storage at different temperature were less and seemed slightly changed.

In addition, the particle size of AuNPS can be calculated from UV spectrum as illustrated in Eq (1) or Eq (2). In comparison, mean particle sizes of AuNPs obtained from UV-vis spectroscopy and DLS were considerably in the same range for AuCt and AuPEI (Table 1). Surprisingly, the particle sizes determined by the TEM analysis of AuCt and AuPEI became smaller (nearly 50% or more). Considerably, the result was not unexpected since the stabilizers of AuNPs, citrate and polyethyleneimine were hydrophilic in nature. The hydrophilic stabilizer can then form the layer surrounding the particles and interact with the water molecules in the dispersion medium (Gun'ko *et al.*, 2003; Haiss *et al.*, 2007). Conversely, the TEM technique allows only dehydrated form of a tested sample to be detected, hence the interaction with the water molecules or interparticle interaction were unable to be occurred. However, although the smaller sizes detected with the TEM results, this technique was the only one that indicated the morphology of the AuNPs. It was mentioned however that the size analysis of UV-vis spectroscopy and DLS techniques was dependent on the assumption of spherical shape and monodisperse non-interacting particles

(Khlebtsov and Khlebtsov, 2011). In addition, the DLS method provides better advantages than UV-vis spectroscopy in term of the polydispersity index (PdI) which possibly represents the distribution of particle size.

A.

B.

C.
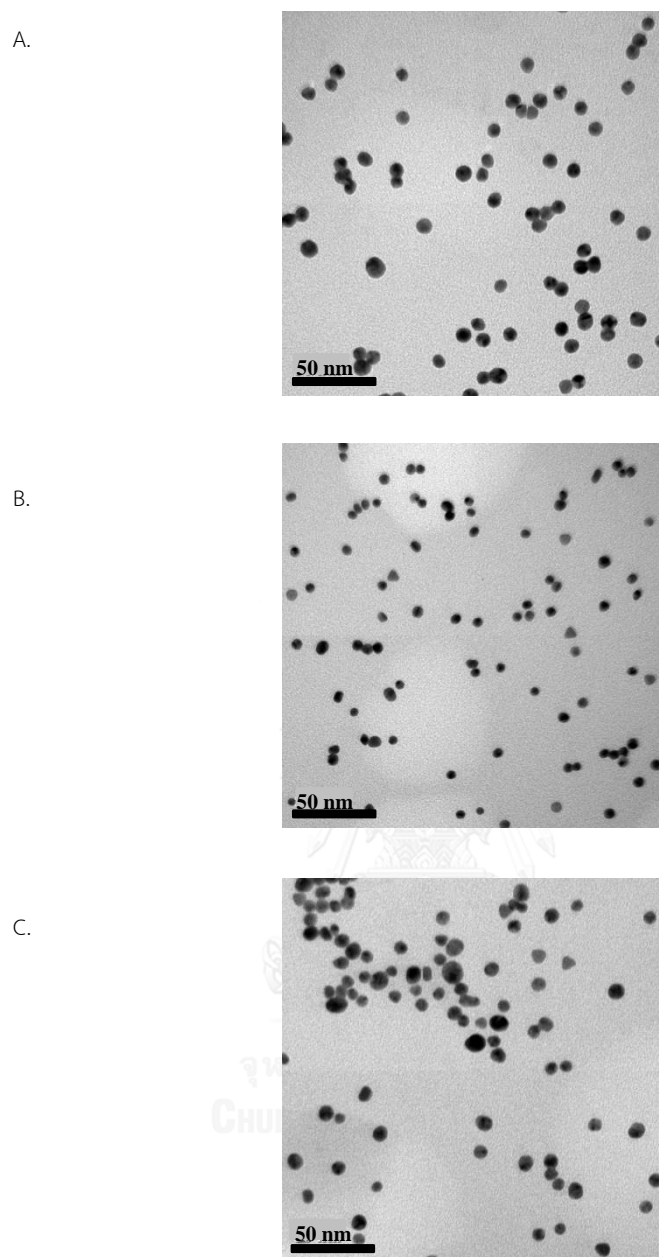
Figure 14. TEM images of AuCt (1:4) (A), AuCt (1:8) (B) and AuCt (1:12) (C) after preparation in which scale bar represents 50 nm.

A.

B.

C.
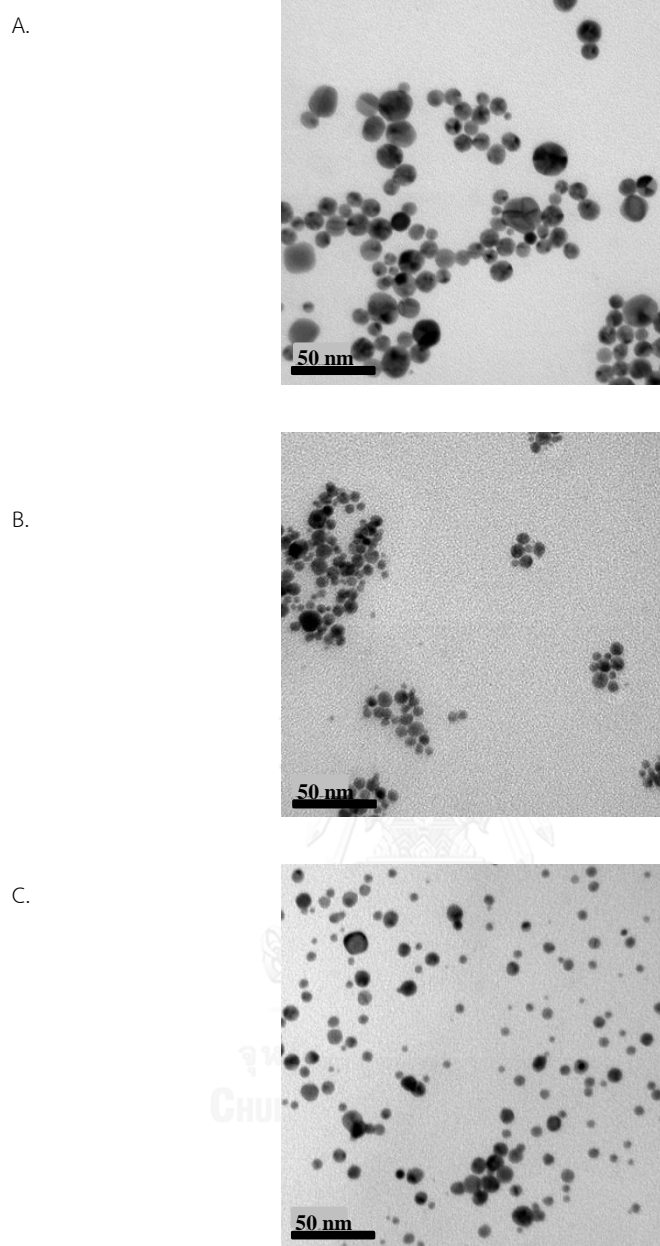
Figure 15. TEM images of AuPEI (1:0.36) (A), AuPEI (1:0.72) (B) and AuPEI (1:1.08) (C) after preparation in which scale bar represents 50 nm.
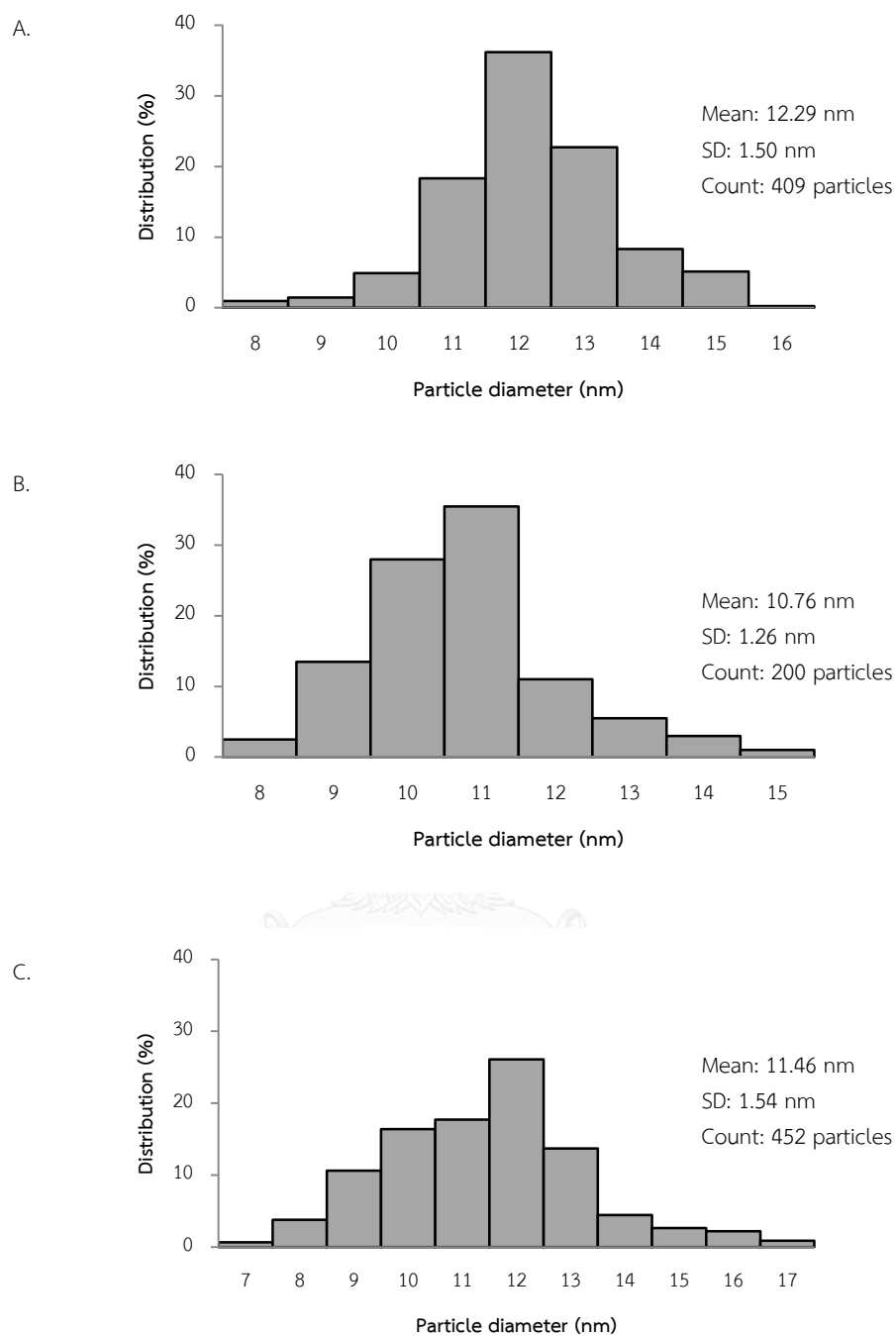
Figure 16. Particle size distribution of AuCt (1:4) (A), AuCt (1:8) (B) and AuCt (1:12) (C) after preparation determined by TEM.
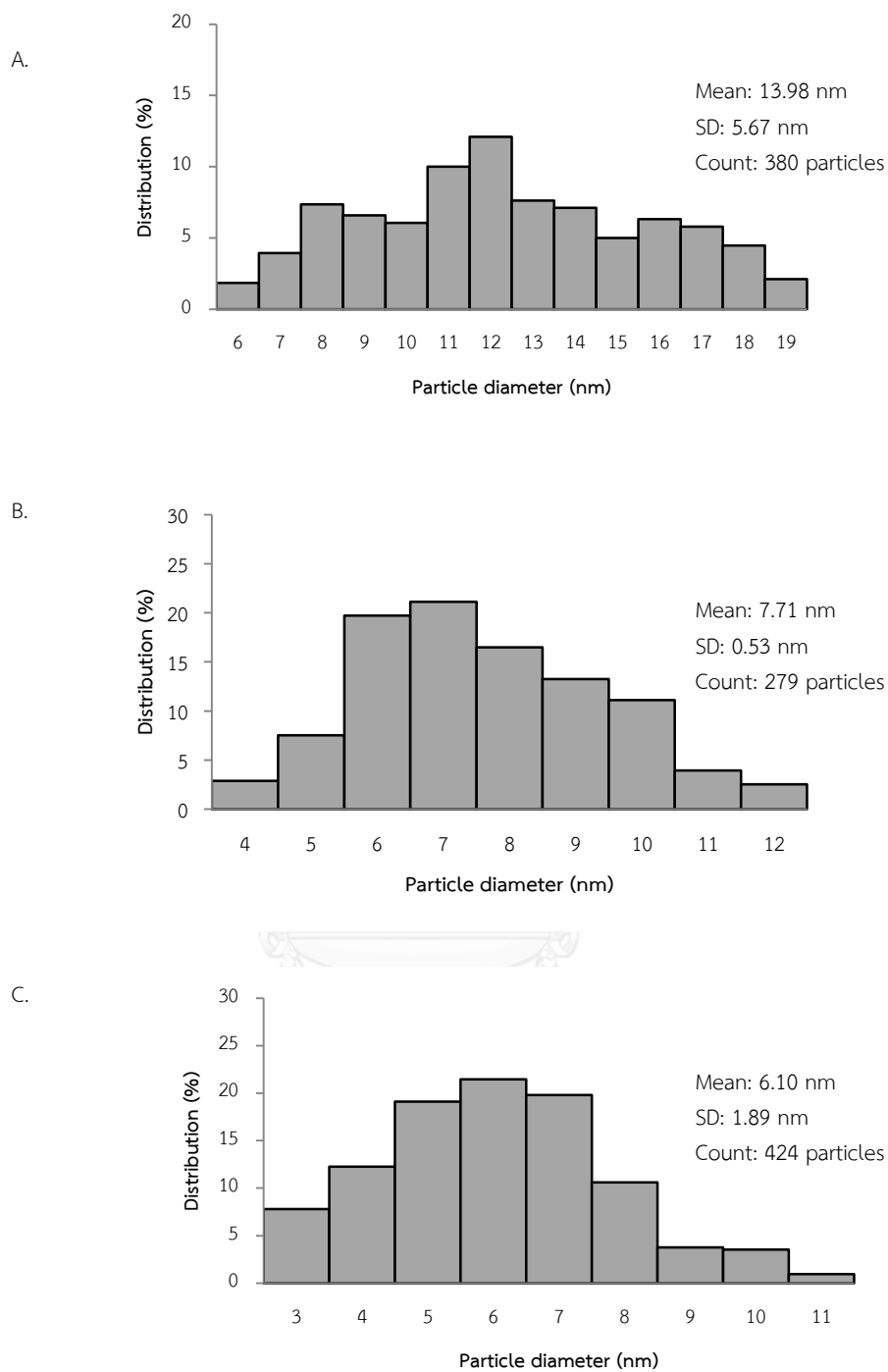
Figure 17. Particle size distribution of AuPEI (1:0.36) (A), AuPEI (1:0.72) (B) and AuPEI (1:1.08) (C) after preparation determined by TEM.
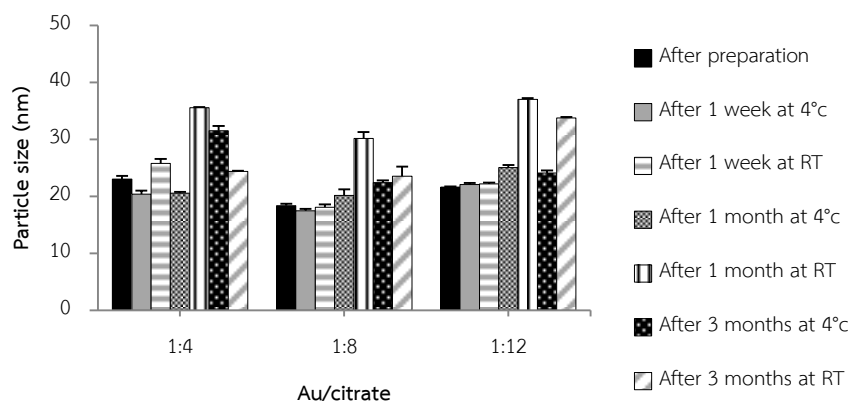
Figure 18. Hydrodynamic sizes of AuCt (1:4, 1:8, 1:12 Au:Ct ratio) stored at either 4°C or RT after preparation, 1-week, 1-month and 3-month storage determined by DLS.
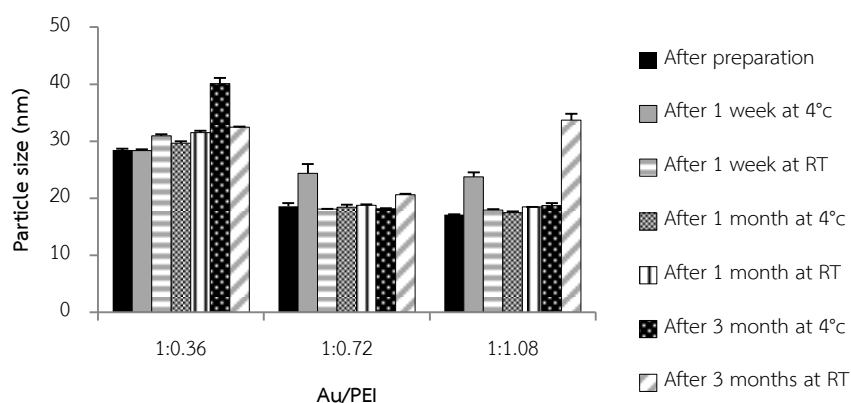
Figure 19. Hydrodynamic sizes of AuPEI (1:0.36, 1:0.72, 1:1.08 Au:PEI ratio) stored at either 4°C or RT after preparation, 1-week, 1-month and 3-month storage determined by DLS.

Table 1. Particle size analysis of AuCt and AuPEI after preparation.

AuNPs		Particle size (nm) measured by different methods		
		TEM	DLS (PdI)	UV
i) AuCt				
Au : Citrate	1 : 4	12.29 ± 1.50	23.04 ± 0.55 (0.38)	15.00
	1 : 8	10.76 ± 1.26	18.37 ± 0.34 (0.39)	20.57
	1 : 12	11.46 ± 1.54	21.63 ± 0.13 (0.35)	24.16
ii) AuPEI				
Au : PEI	1 : 0.36	13.98 ± 5.67	28.47 ± 0.22 (0.27)	27.43
	1 : 0.72	7.71 ± 0.53	18.59 ± 0.59 (0.27)	17.59
	1 : 1.08	6.10 ± 1.89	17.15 ± 0.02 (0.26)	20.57

2.3 Zeta potential

The surface properties of nanoparticle were studied by observing electrophoretic potential or zeta potential of nanoparticles using Zetasizer NanoZs. Figures 20 and 21 represent zeta potential of AuCt and AuPEI after preparation and after different time storage at either 4°C or RT. The surface charges of AuCt and AuPEI comes from the absorption of citrate or PEI as layers on the nanoparticle surface. AuCt and AuPEI are stabilized by the interparticle electrostatic interaction. Basically, nanoparticles with the zeta potential values of more than -30 mV or nanoparticles with positive charge of more than +30 mV are considered stable (Clogston and Patri, 2011).

Zeta potential values of AuCt (1:4, 1:8 and 1:12) after preparation were -38.70 ± 1.39 mV, -35.37 ± 2.56 mV and -39.23 ± 4.48 mV, respectively. Therefore, they all tended to be stable. However, zeta potential of AuCt stored at RT reduced after a month. AuCt were unstable after a month and some dark particles were observed. For AuCt stored at 4°C, only AuCt (1:8) had zeta potential value above -30 mV after 3 months of storage and they remained stable as seen from physical appearance. For AuPEI, zeta potentials of AuPEI (1:0.36), AuPEI (1:0.72) and AuPEI (1:1.08) after preparation were 32.83 ± 0.85 mV, 38.00 ± 1.68 mV and 23.53 ± 4.30 mV. So, the positive charges above +30 mV were found in AuPEI after preparation except AuPEI (1:1.08). There were a decrease in zeta potential values of AuPEI (1:0.72)

and AuPEI (1:1.08) over the time of storage at 4°C and RT. It was noticeably that some agglomeration was found only in AuPEI stored at RT after 3 months while AuPEI stored at 4°C had no sign of agglomeration. Both AuPEI (1:0.36) and AuPEI (1:0.72) stored at 4°C had zeta potential values around 20 mV after 3 months of storage; however, the higher variation in zeta potential of AuPEI (1:0.36) possibly indicating the trend of instability. Thus, AuPEI (1:0.72) was considered to be more stable. It is believed that the water molecules can be lost from nanoparticles and time and high temperature can accelerate the reaction. Hence, the chemical bonds between PEI-water and citrate-water might be excluded from the particles resulting in charged layers collapse and shrink and finally particle agglomeration (Li *et al.,* 2007). While AuCt were stabilized by electrostatic repulsive force, AuPEI were stabilized by both electrostatic repulsive force and steric interaction between polymer chains (Kuchibhatla *et al.,* 2005). Consequently, AuPEI seemed to be more stable than AuCt. It was in agreement with the results in this study in that AuPEI were more stable than AuCt. In summary, for stability test of AuNPs, AuCt and AuPEI were kept at different temperatures for several time periods in order to find the most stable formulations. The results indicated that stable AuNPs could be produced by controlling a molar ratio of Au atom to reactant to be 1:8 for AuCt and 1:0.72 for AuPEI. Owing to less change in particle size and lower PdI values of AuPEI after time storage, AuPEI seemed to be more stable and narrower in size distribution than AuCt. By keeping in the cool place (4°C), the stability of AuNPs could be extended.
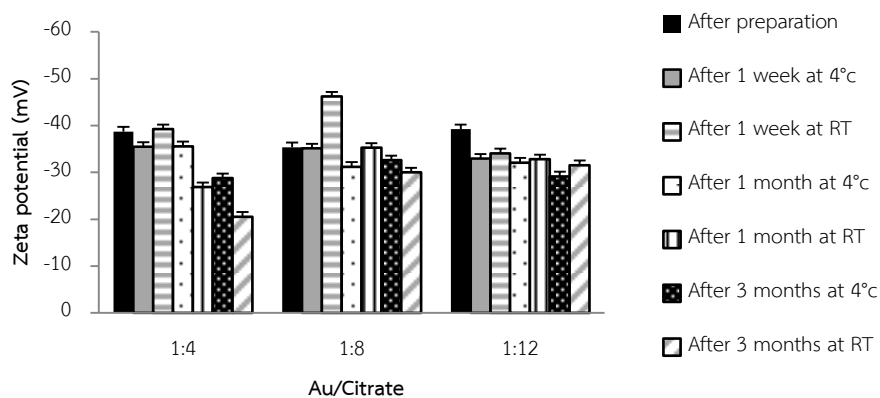
Figure 20. Zeta potential of AuCt stored at either 4°C or RT after preparation, 1-week, 1-month and 3-month storage.
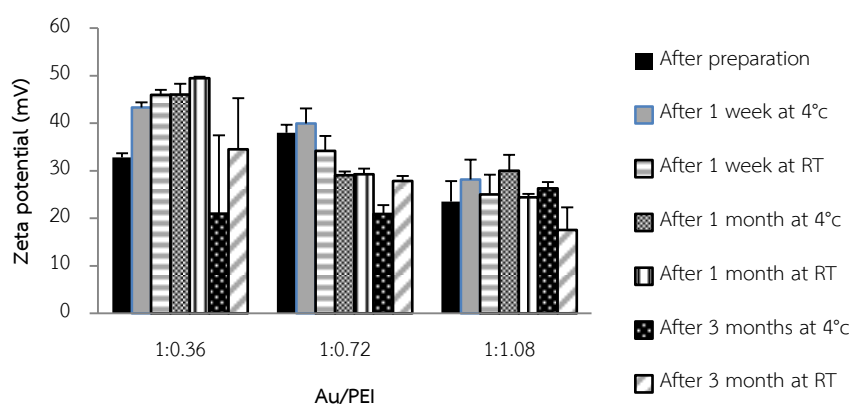
Figure 21. Zeta potential of AuPEI stored at either 4°C or RT after preparation, 1-week, 1-month and 3-month storage.

3. Thioflavin T binding assay

Aggregation of Aß1-42 peptide was carried out in PBS (pH 7.4) at room temperature. The time course of Aß1-42 peptide aggregation was investigated before testing with AuNPs in order to get the fully Aß aggregates consisting of ß-sheet structure which correlates with the extent of neurotoxicity (Simmons et al., 1994). By using thioflarin T (ThT) assay, the Aß aggregation (10 µM) without zinc and zinc-induced Aß aggregation (10 µM) kinetics were sigmoidal (Figure 22). ThT gives only a small signal when it is incubated with the freshly dissolved peptide. Upon incubation time, the signal increases substantially. The result was consistent to nucleation-dependent model which consists of lag (nucleation) phase, elongation (fibril growth) phase and plateau phase which Aß conformation changes from peptide to be oligomers and fibril aggregates (Biancalana and Koide, 2010; Khurana et al., 2005). After 60 hours of incubation, ThT fluorescences of both conditions reached the plateau which meant the maximum aggregation occurred. The formation of Aß peptide without zinc at the plateau should be mature fibril aggregate. The fibril structure of Aß contains rich ß-sheet pleated structure which has a binding affinity to ThT dye (Khurana et al., 2005). The plateau of zinc-induced Aß aggregation condition slightly delayed comparing to no zinc condition and lesser amount of ThT fluorescence intensity was observed. Noy et al and Tõugu et al have found that metal ions can change the conformation of Aß to be amorphous form that consists of less ß-sheet structure during the aggregation by binding rapidly to Aß peptide (Noy et al., 2008; Tõugu et al., 2009). Although, zinc can change the fibril formation of Aß but the toxicity of Aß still remains. Its toxicity is dependent on the concentration of zinc in which the excess of zinc at the molar ratio 1:1 (Aß : Zn2+) is enough to harm the cell in in vitro experiments (Cuajungco et al., 2000; Garai et al., 2007; Moreira et al., 2000). From the results, the fluorescence intensities of Aß aggregations have plateau around 60 hours. So, preformed-Aß aggregates in the absence or presence of zinc were performed by incubating Aß alone or incubating Aß with zinc, respectively, for 60 hours before testing with AuNPs.
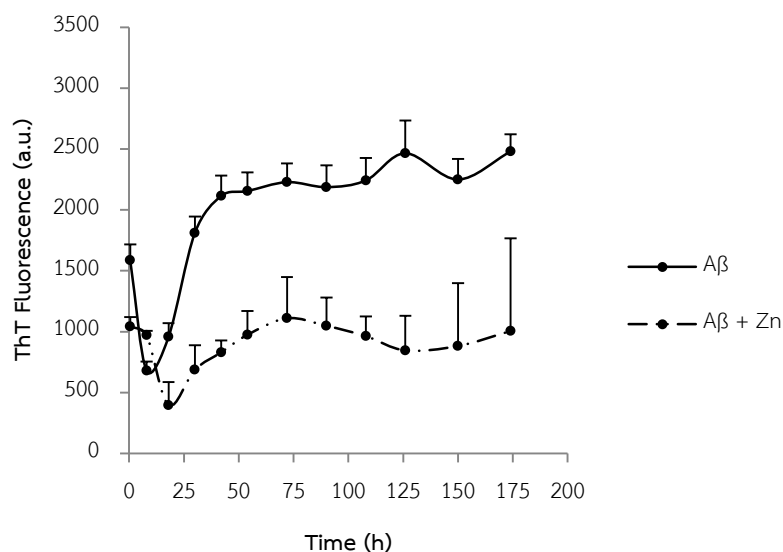
Figure 22. Kinetics of Aβ$_{1-42}$ aggregation in the absence and presence of zinc (at pH 7.4 and room temperature). Error bars indicate the standard deviation from triplicate measurements.

3.1 Effect of gold nanoparticles on inhibition of Aβ$_{1-42}$ aggregation

Figure 23 shows the fluorescence intensity of 60-h aggregated Aβ incubated with water (control) another 96 hours. The values were maintained for nearly 60 hours and seemed to decrease at the longer time. The reason for fluorescence intensity of the sample dropped down might be that the settling and packing of aggregated-Aβ at the long period of time cause a reduction in surface for ThT binding (Nilsson, 2004). For investigation of the effect of AuNPs on Aβ aggregation by ThT assay, either AuCt (1:8) or AuPEI (1:0.72) was mixed with aggregated-Aβ. The final concentrations of both AuNPs were varied from 1.0 to 8.0 μM. The fluorescence intensity was continuously monitored for 96 hours and then calculated as compared to the control (Eq-6) to obtain the percentage of inhibition. In addition, citrate solution and PEI solution were also mixed with aggregated-Aβ in order to observe the effect of AuNP stabilizers.

For AuCt incubated with aggregated-Aβ, the percentage of inhibition was dependent on AuCt concentration in which the higher inhibition, the increasing

concentration (Figure 24). However, the maximum inhibitory effect of AuCt (8 µM) on aggregated-Aß was less than 55% inhibition and seemed to decrease with time. Interestingly for AuPEI, all AuPEI could inhibit aggregated-Aß for more than 20% at the initial time of interaction and this effect increased to over 90% in the presence of 3, 4, 6 and 8 µM AuPEI with the continuing time (Figure 25). The plateau effect of 3, 4, 6 and 8 µM AuPEI was found after 24 hours of incubation. The inhibitory effect of 8 µM AuPEI was significantly different from those of 1 and 2 µM AuPEI ($p < 0.05$). However, the inhibition effect of AuCt 8 µM was not significantly different from those of 3, 4 and 6 µM AuPEI. In addition, citrate and PEI solutions were incubated with aggregated-Aß at the concentration used for AuNP synthesis. The results indicated that citrate (Figure 26) and PEI solutions (Figure 27) were able to inhibit over 60% of aggregated-Aß. and had the plateau around 12 hours after incubation. However, there were no significantly differences in the maximum percentage of inhibition when different concentrations of citrate solution or PEI solution were used. The inhibitory effect of both solutions tended to decrease with the incubation time.

According to the Aß conformation change upon aggregation from α-helix peptide to ß-sheet, two interactions involving in the Aß aggregation are hydrophobic and electrostatic interactions. The hydrophobic interactions create intramolecular α-helix formation while the electrostatic interactions create intermolecular ß-sheet formation. Therefore, disturbance with hydrophobic or electrostatic interaction can be cause of reduction and inhibition in Aß aggregation resulting in Aß conformational changes. The amino acid-based polymer nanoparticles (poly (*n*-acryloyl-L-phenylalanyl-L-phenylalanine methyl ester)) has been used as inhibitors in $Aß_{1-40}$ fibrillation in which dipeptide residues were designed to bind with hydrophobic core of Aß (Skaat *et al.,* 2012). Furthermore copolymeric (*N*-isopropylacrylamide : *N*-tert-butylacrylamide) particles with varying hydrophobicity were able to reverse and retard the fibril formation of recombinant Aß(M1-40) (Cabaleiro-Lago et al., 2008; Skaat et al., 2012). However, using hydrophobic interaction is not the only one strategy for inhibiting Aß aggregation but using electrostatic interaction is a considerable way for interupting Aß aggregation. Recently, there were reports about

the capability of charged particles that can inhibit or interfere Aß peptide aggregation (Giacomelli and Norde, 2005; Liao et al., 2012; Lim et al., 2011). Accordingly, in the present study, negatively charged gold nanoparticles (AuCt) and positively charged gold nanoparticles (AuPEI) also had inhibitory effect on aggregated-Aß resulting in ThT fluorescence intensity reduction. The less fluorescence intensity demonstrated the changes in quantity and morphology of Aß aggregates (Biancalana and Koide, 2010). In addition, these inhibitory effects were concentration-dependent and time-dependent. Both AuCt and AuPEI could interact with aggregated-Aß but AuPEI seemed to be more effective than AuCt. However, these results were inconsistent with the previous work which reported that negatively charged nanoparticles had inhibitory effect over positively charged nanoparticles (Liao et al., 2012; Lim et al., 2011). Hence, the key factor should be related to electrostatic interactions between the charged surfaces of nanoparticles and Aß. Also, the stage of Aß aggregation is an unavoidable factor. The previous research mostly examined the inhibitory effect of sample in the early stage of Aß aggregation consisting of Aß monomers or oligomers which are in contrast with the present study in which the effect on Aß aggregate consisting of full ß-sheets has been examined. (Moores et al., 2011) revealed about Aß electrostatic model in that Aß monomers and oligomers are composed of hydrophobic regions and strong positively charged at the end and the turn loop of peptide chain while stacked ß-sheets have two strong positively charged regions and two strong negatively charged regions (Moores et al., 2011). Based on this assumption, preformed-Aß aggregates contained ß-sheets are able to interact with both AuCt and AuPEI via electrostatic interaction. Interestingly, the study here has found that aggregated-Aß prefer interacting with positively charged AuPEI to negatively charged AuCt evidencing from higher inhibition seen in aggregated-Aß. However, how preformed-Aß aggregates prefer interacting with AuPEI is not well understood. It is possibly due to charged PEI polymers covering the nanoparticles making AuPEI more stable (polymeric stabilization) within the stack of Aß-aggregates.
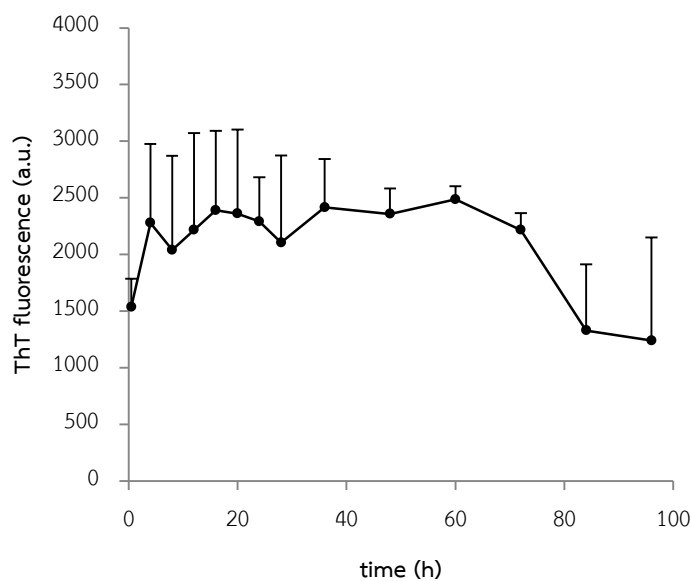
Figure 23. ThT fluorescence intensity of 60-h aggregated Aβ$_{1-42}$ (control) after incubation at RT. Error bars indicated the standard deviation from triplicate measurements.
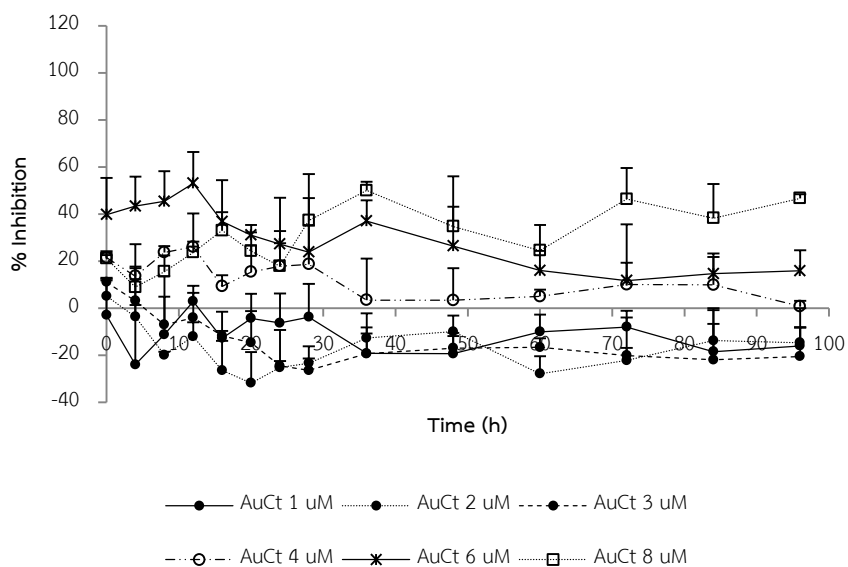
Figure 24. Inhibitory effect of AuCt on aggregation of aggregated-Aβ$_{1-42}$. Error bars indicated the standard deviation from triplicate measurements.
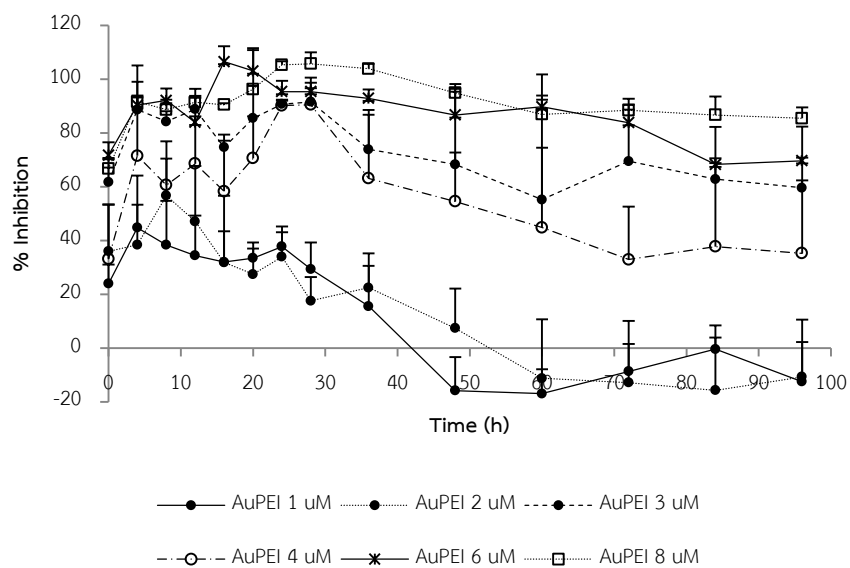
Figure 25. Inhibitory effect of AuPEI on aggregation of aggregated-Aβ1-42. Error bars indicated the standard deviation from triplicate measurements.
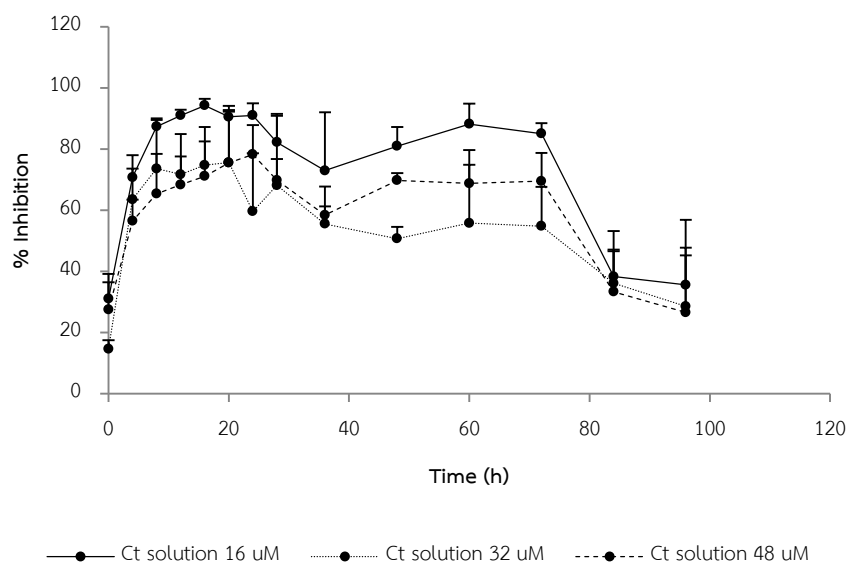
Figure 26. Inhibitory effect of Ct solution on aggregation of aggregated-Aβ$_{1-42}$. Error bars indicated the standard deviation from triplicate measurements.
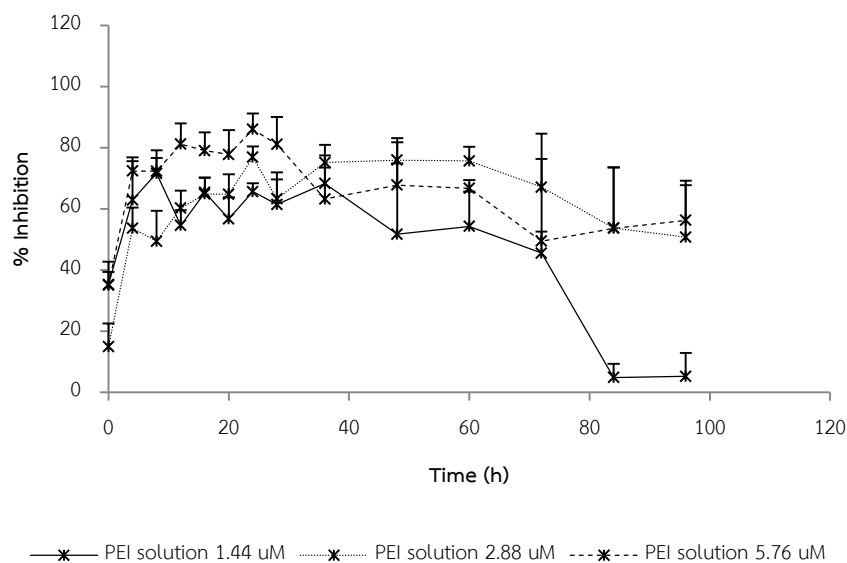
Figure 27. Inhibitory effect of PEI solution on aggregation of aggregated-Aß$_{1-42}$. Error bars indicated the standard deviation from triplicate measurements.

3.2 Effect of gold nanoparticles on inhibition of zinc-induced Aß$_{1-42}$ aggregation

The ability of AuCt, AuPEI, citrate solution and PEI solution to inhibit aggregation of preformed zinc-induced Aß aggregates was studied by ThT assay described earlier in the previous section. The concentrations of AuCt and AuPEI were varied from 1 µM to 8 µM and ultrapure water was used instead of AuNPs for a control. Fluorescence intensity of a control is illustrated in Figure 28. In co-incubation of AuCt with aggregated zinc-induced Aß, AuCt at concentrations of 1, 2 and 3 µM were unable to inhibit the aggregation whereas AuCt with concentrations of 4, 6 and 8 µM could inhibit aggregated zinc-induced Aß (Figure 29). AuCt (4, 6 and 8 µM) reached the plateau within 12 hours and inhibited aggregation at levels of 28.7%, 21.85% and 43.36%, respectively. The inhibitory effects were however not statically different and decreased with the incubation time. For co-incubation of AuPEI with aggregated zinc-induced Aß, only 3 µM, 4 µM, 6 µM and 8 µM AuPEI had inhibitory effect on the aggregates (Figure 30). The plateau time of inhibition of AuPEI was similar to the plateau time of AuCt. The inhibition of 70 - 90% was the capability that

AuPEI could interupt the zinc-induced Aß aggregation. Inhibition of zinc-induced Aß aggregates of AuPEI 3 µM, 4 µM, 6 µM and 8 µM were not statistically different, but they were statistically different from 1 µM and 2 µM AuPEI. In addition, both citrate solution and PEI solution also had the inhibitory effect on aggregated zinc-induced Aß as seen in Figures 31 and 32.

It is well known that excess zinc exposure is toxic to the neuron both in vitro and in vivo and can be the cause of neuron degeneration possibly through a free-radical based mechanism (Butterfield, 1997). Moreover, zinc can promote and accelerate altering the structure of Aß aggregates by binding at N-terminal ß-strand. Zinc ions can link His13 of one Aß molecule with His14 of another Aß molecule together resulting in alteration of Aß aggregates formation (Dong et al., 2006; Tõugu et al., 2009). Zinc does not only act as a glue and links Aß proteins together, it also acts as a catalyst for Aß aggregation by reducing the lag time of Aß aggregation (Noy et al., 2008). Although, the differences in lag time of Aß aggregation and zinc-induced Aß aggregation in the present study was not clear out but it can be assured that Aß proteins interact with zinc ions and form misfolding Aß aggregation as seen from the difference in ThT fluorescence intensities. There were the reports about the level of metal ions like zinc was increased in the brain of Alzheimer's disease (AD) patients (Religa et al., 2006). Therefore, the accumulation of Aß aggregates due to the metal ions is correlated with AD pathology supporting from in vivo experiments (Lee et al., 2002; Lovell et al., 1998). The lack of zinc transporter3 (ZnT3) in Tg2576 transgenic mice was the cause of Aß plaque reduction and less insoluble Aß, as compared with Tg2576 transgenic mice which had overexpression of synaptic zinc (Lee et al., 2002). By using micro-PIXE analysis, amount of zinc in AD patients was found elevated compared to the control subjects and the elevation can accelerate aggregation of Aß peptide (Lovell et al., 1998). Thus, disruption of Aß and metals complex with metal chelators is a therapeutic approach. Clioquinol (CQ) and its second generation derivatives (PBT2) were considered as metal chelators for reducing Aß plaque (Adlard et al., 2008; Huang et al., 1997). Other studies demonstrate that both compounds were able to dissolve zinc-induced Aß aggregates in vitro (Huang et al., 1997) but

PBT2 seemed to be more effective in improvement of cognitive performance than CQ in transgenic mouse models of AD (Adlard et al., 2008). However, using of metal chelators should be aware and reconsidered because metal chelators like CQ, EDTA and apo-MT can unexpectedly promote Aß fibrils instead of inhibiting Aß formation (Huang et al., 1997; Tõugu et al., 2009). Therefore, nanoparticles may be the new strategy for treatment of zinc-induced AD.

In the present experiment, negatively (AuCt) and positively (AuPEI) charged gold nanoparticles were studied for their effect on inhibition in zinc-induced Aß aggregation. The results revealed that AuPEI had more inhibitory effect (~90%) on aggregation than AuCt (~40% inhibition). The concentration of AuCt (> 3 µM) used for inhibiting zinc-induced Aß aggregates was higher than AuPEI (> 2 µM). The inhibitory effect of AuNPs on zinc-induced Aß aggregates was considered not only be dependent on the surface potential but also the concentrations of AuNPs.
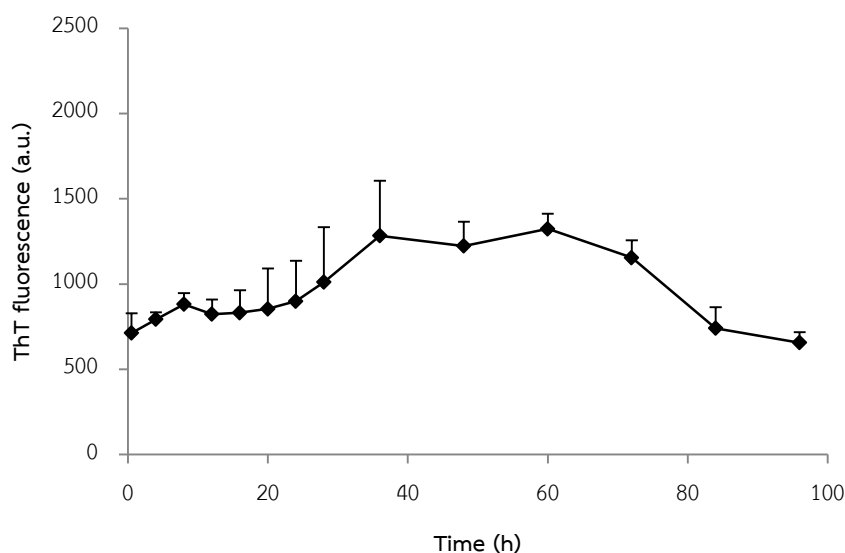
Figure 28. ThT fluorescence intensity of 60-h aggregated $Aß_{1-42}$ in the presence of zinc (control) after incubation at RT. Error bars indicated the standard deviation from triplicate measurements.
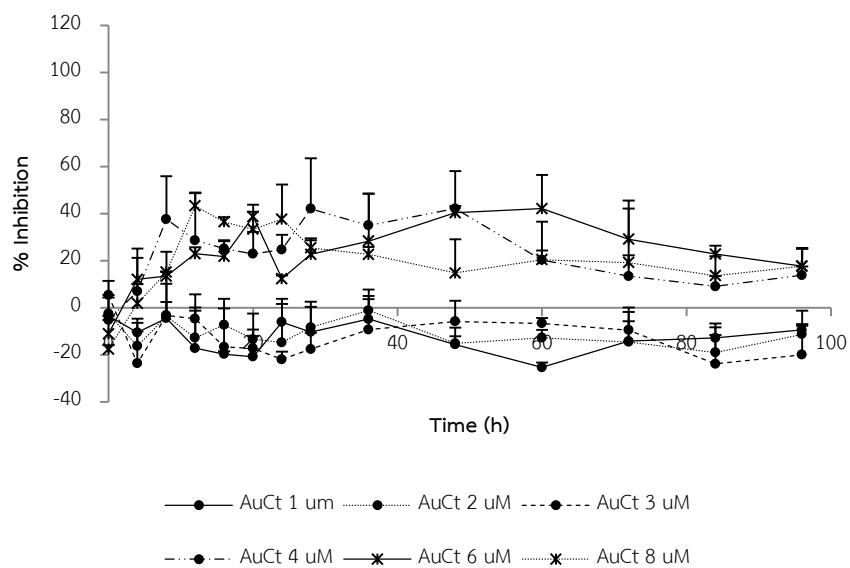
Figure 29. Inhibitory effect of AuCt on aggregation of aggregated zinc-induced Aβ$_{1-42}$. Error bars indicated the standard deviation from triplicate measurements.
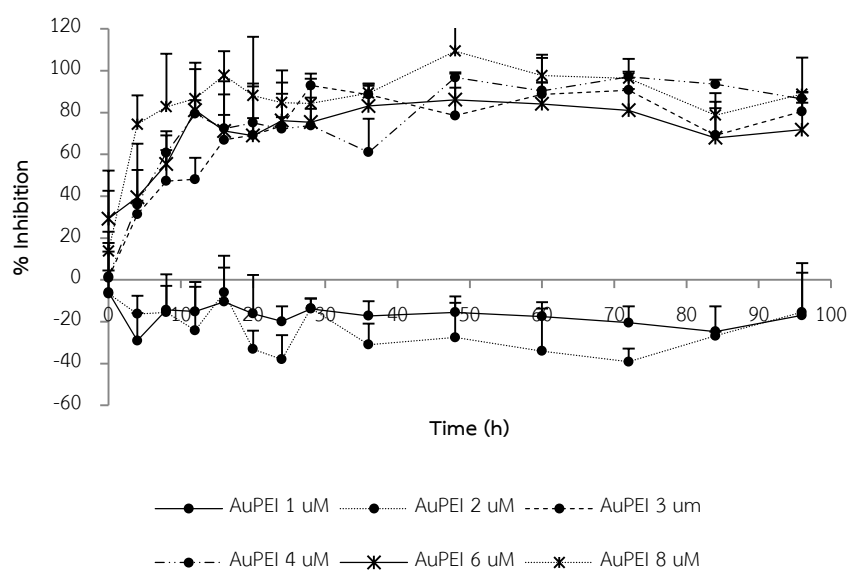
Figure 30. Inhibitory effect of AuPEI on aggregation of aggregated zinc-induced Aβ$_{1-42}$. Error bars indicated the standard deviation from triplicate measurements.
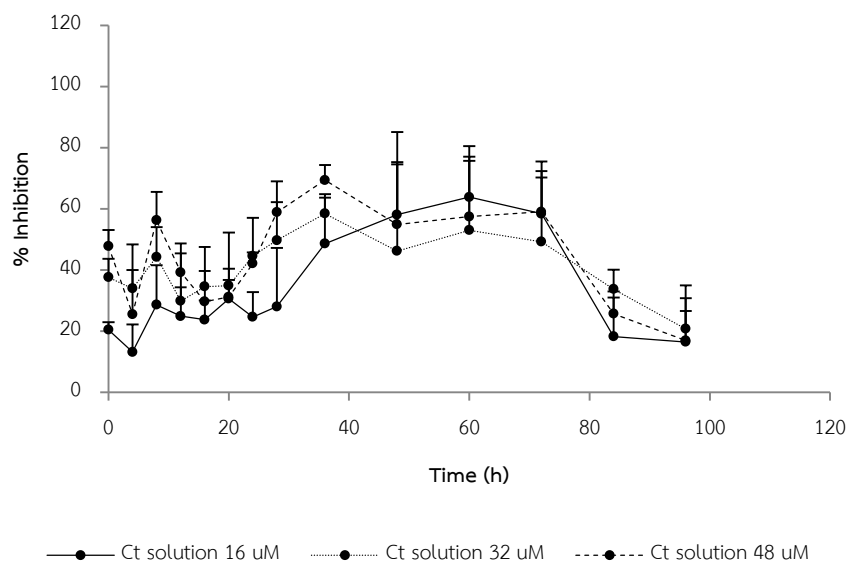
Figure 31. Inhibitory effect of Ct solution on aggregation of aggregated zinc-induced Aβ$_{1-42}$. Error bars indicated the standard deviation from triplicate measurements.
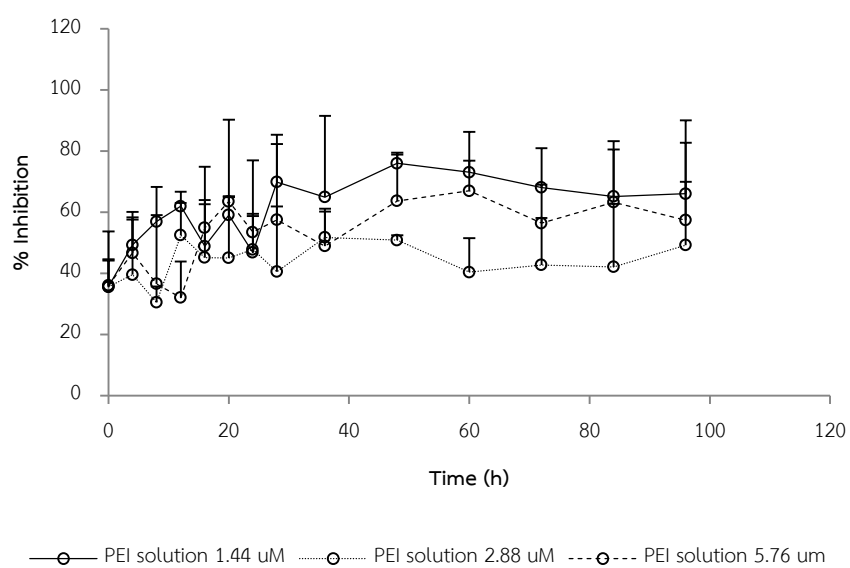
Figure 32. Inhibitory effect of PEI solution on aggregation of aggregated zinc-induced Aβ$_{1-42}$. Error bars indicated the standard deviation from triplicate measurements.

4.TEM analysis

For TEM observation, the morphologies of preformed-Aß aggregates and preformed zinc-induced Aß aggregates before and after incubation with AuNPs were visualized under negative strain condition. TEM analysis was performed as corresponding to the ThT assay in order to analyze the change in morphologies of preformed-Aß aggregates. In the absence of zinc, Aß aggregates produced by incubation Aß alone in buffer for 60 hours, formed long, smooth and unbranching fibrils as expected and illustrated in Figure 33. The result was consistent with other TEM observations (Ahmed *et al.*, 2010; Mold *et al.*, 2013). Co-incubation between preformed-Aß aggregates and AuNPs for another 24 hours showed some changes in the end-point products which depended on type and concentration of AuNPs. In the presence of AuCt, the fibrils became shorter and fragmental when they were incubated with 8 μM AuCt (Figure 34). However, the changes were hardly noticed in the fewer concentrations of AuCt. Some AuNPs attached and located close to the fibrils but not all of them. In the presence of AuPEI, the fibrils were attached and covered by AuPEI (Figure 35). With increasing AuPEI concentration, the long and smooth fibrils were barely observed. It was believed that fibrils might turn to be small fragmented fibrils and attached with AuPEI.

For preformed zinc-induced Aß aggregates, their morphology were amorphous aggregates without appearance of fibrils (Figure 36). The morphology found was consistent with previous reports (Bolognin *et al.*, 2011; Noy *et al.*, 2008). Preformed zinc-induced Aß aggregates were incubated with either AuCt or AuPEI in the same manner as those without zinc for another 24 hours prior to TEM observation. In the presence of AuCt, preformed zinc-induced Aß aggregates became dense and packed (Figure 37). However it was unexpected that Aß fibrils were also observed. When the concentrations of AuCt were increased to 8 μM, Aß aggregates shrank and became smaller aggregates, whereas, coexistence of Aß fibrils still remained. The fibrillation observed may be due to the AuCt suppress the effect of zinc ions on Aß. The same finding was reported in Aß aggregation with metal chelators in other experiment (Tõugu *et al.*, 2009). However, AuCt also suppress amorphous aggregation evidencing

from no further increasing in fluorescence intensity in ThT assay. In the presence of AuPEI, TEM images revealed that preformed zinc-induced Aß aggregates were attached and bonded with AuPEI as if AuPEI were the part of Aß aggregates. With increasing AuPEI concentration, preformed zinc-induced Aß aggregates became smaller aggregates with globular shape (Figure 38).

From the results, the morphologies of preformed-Aß aggregates and preformed zinc-induced Aß aggregates were fibrils and amorphous aggregates, respectively, after 60 hours of incubation. Incubation with AuNPs was the cause of Aß morphology changes which not only depended on the charge of AuNPs but also depended on the concentration of AuNPs.
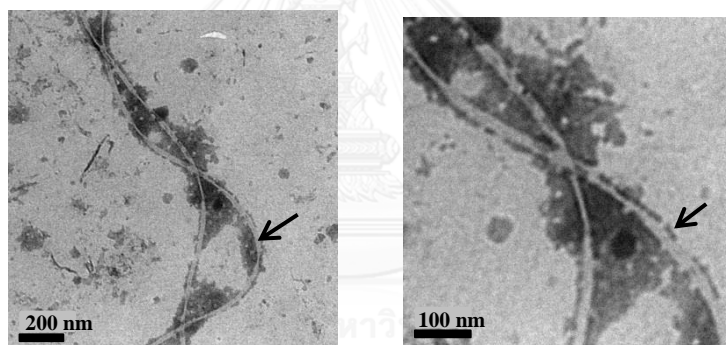
Figure 33. TEM images of Aß aggregates after 60 hours of incubation, scale bar of 200 nm (left) and 100 nm (right).
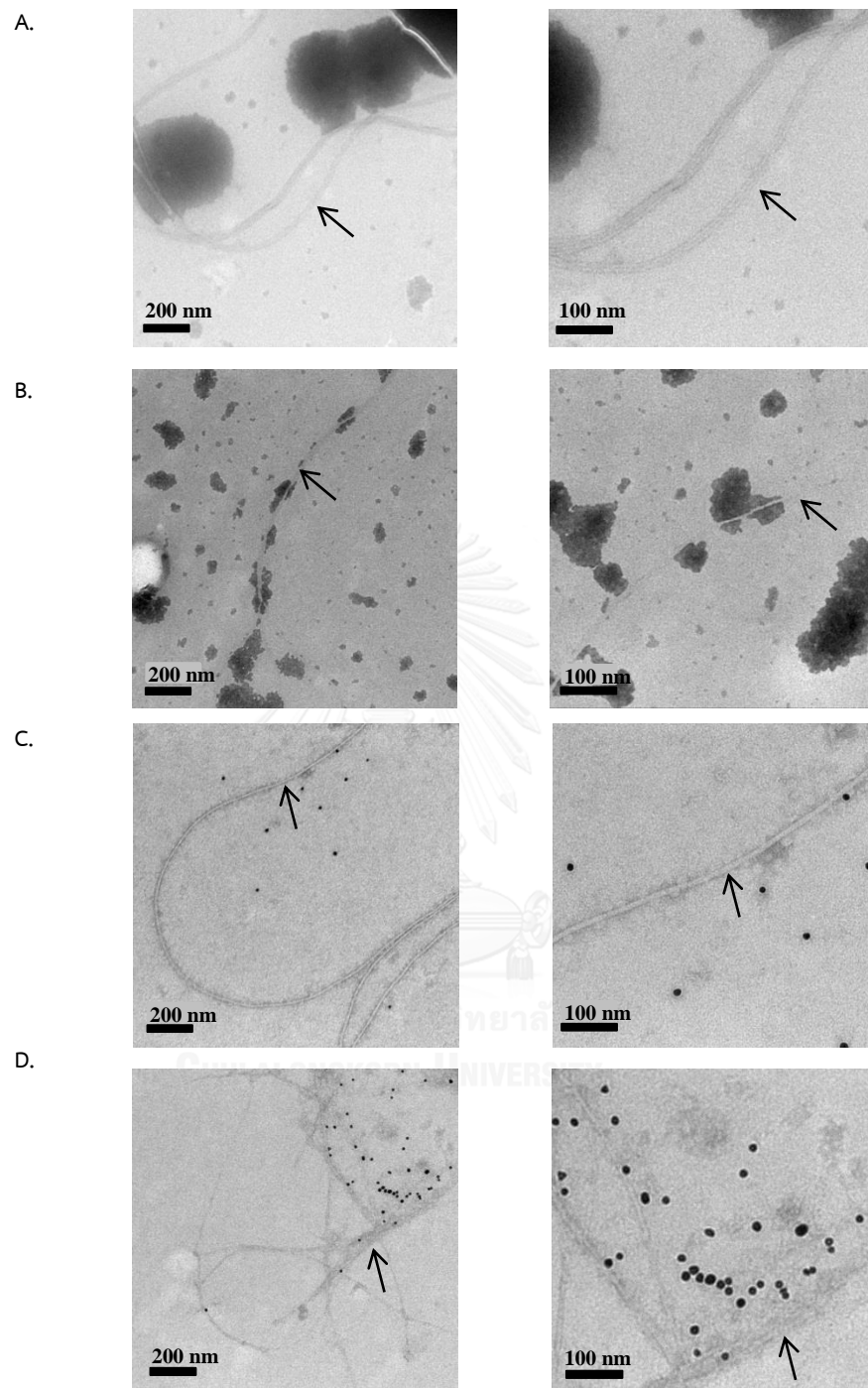
Figure 34. TEM images of 60-h aggregated Aβ incubated for another 24 hours in the absence of AuCt (A) and in the presence of AuCt 2 μM (B), AuCt 4 μM (C) and AuCt 8 μM (D), scale bar of 200 nm (left) and 100 nm (right).

A.

B.

C.

D.
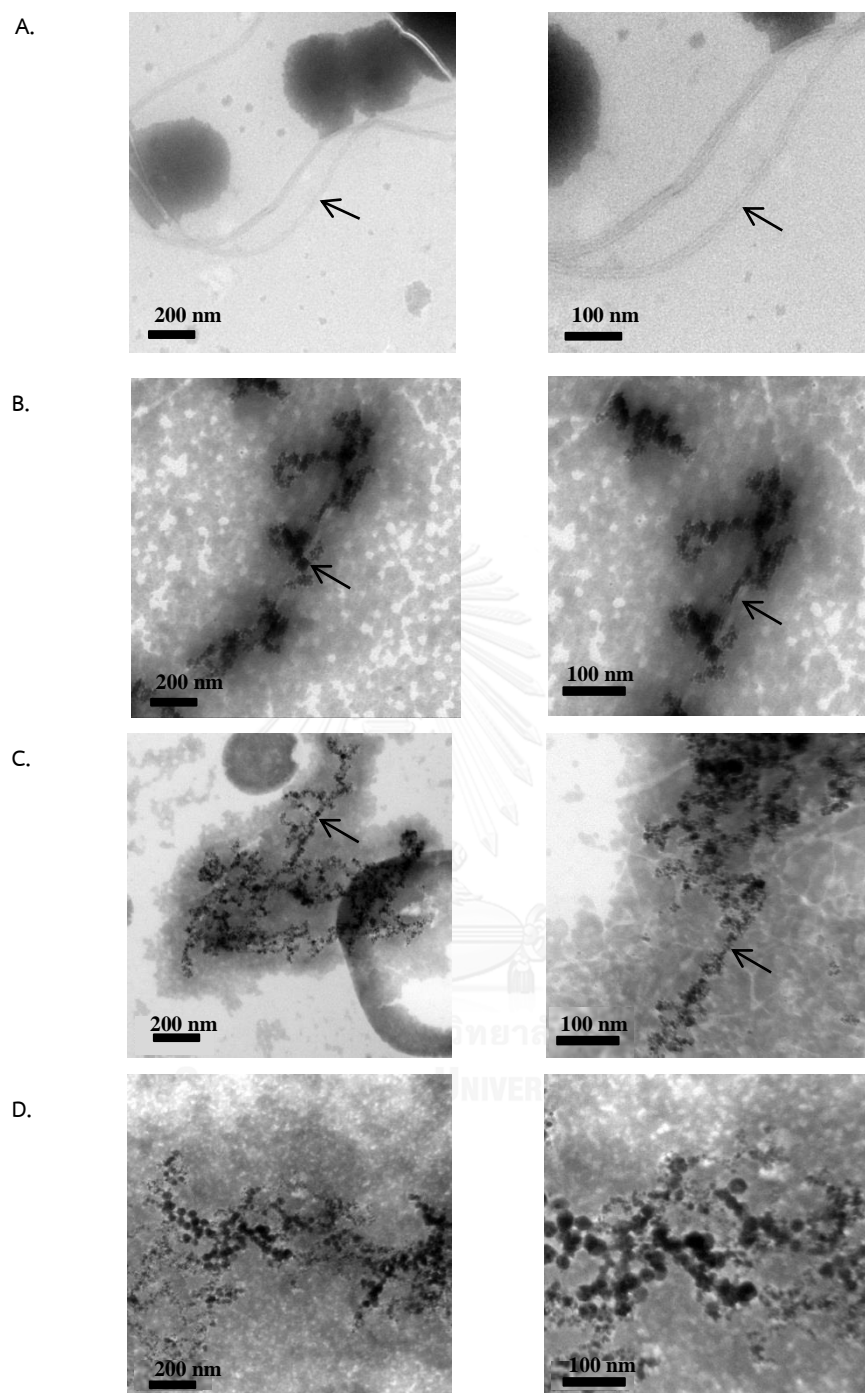
Figure 35. TEM images of 60-h aggregated Aß incubated for another 24 hours in the absence of AuPEI (A) and in the presence of AuPEI 2 μM (B), AuPEI 4 μM (C) and AuPEI 8 μM (D), scale bar of 200 nm (left) and 100 nm (right).
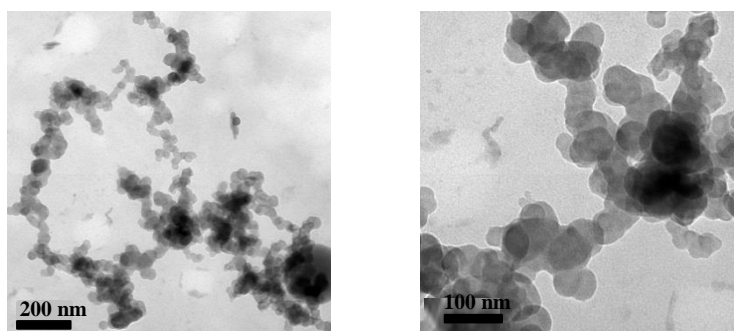
Figure 36. TEM images of zinc-induced Aß aggregates after 60 hours of incubation, scale bar of 200 nm (left) and 100 nm (right).

A.

B.

C.

D.
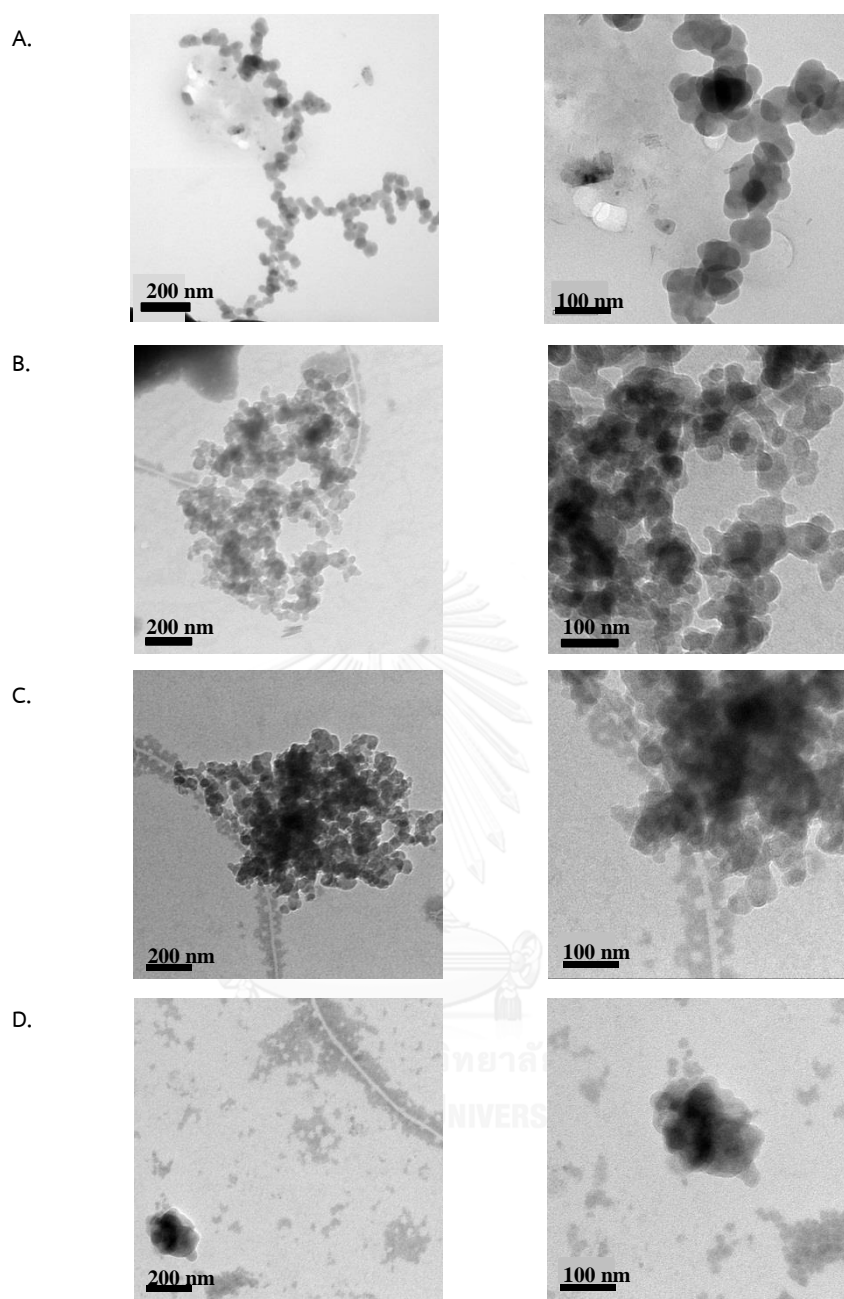
Figure 37. TEM images of 60-h aggregated zinc-induced Aβ incubated for another 24 hours in the absence of AuCt (A) and in the presence of AuCt 2 μM (B), AuCt 4 μM (C) and AuCt 8 μM (D), scale bar of 200 nm (left) and 100 nm (right).

A.

B.

C.

D.
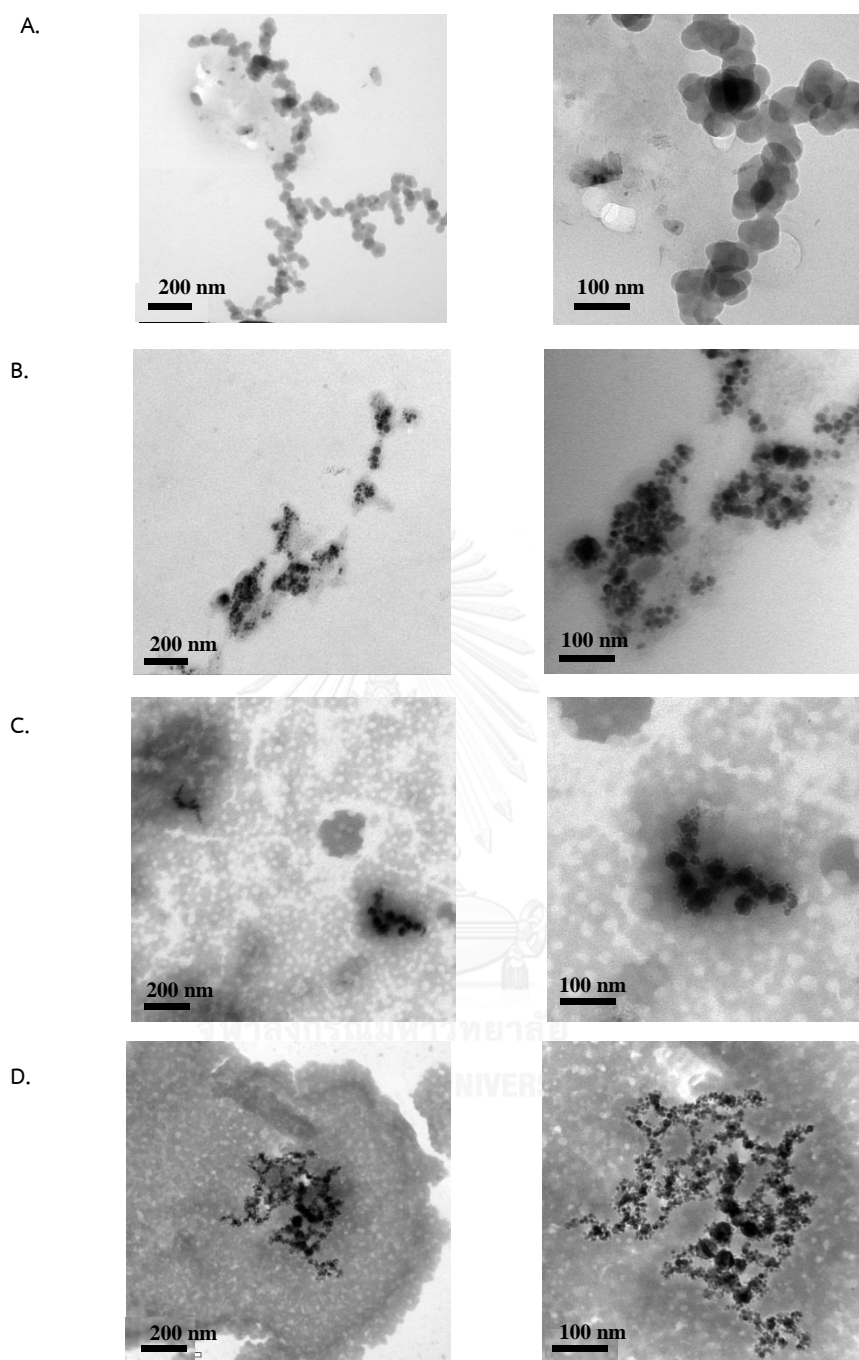
Figure 38. TEM images of 60-h aggregated zinc-induced Aβ incubated for another 24 hours in the absence of AuPEI (A) and in the presence of AuPEI 2 μM (B), AuPEI 4 μM (C) and AuPEI 8 μM (D), scale bar of 200 nm (left) and 100 nm (right).

CHAPTER V

CONCLUSION

AuNPs has been used in a variety of applications due to the unique properties such as controllable chemical composition, biocompatibility and optical properties. AuNPs also has nanosize and high surface area for interacting with biomolecules like Aß proteins. The misfolding of Aß proteins leads to Aß aggregate and insoluble deposits which are considered to involve in Alzheimer's disease.

In this research, AuNPs were synthesized, characterized and examined the inhibitory effect on $Aß_{1-42}$ aggregates and zinc-induced $Aß_{1-42}$ aggregates. Citrate stabilized AuNPs (AuCt) and PEI stabilized AuNPs (AuCt) were prepared at 1 mM (200 ppm) Au atom by using different molar ratios of Au to stabilizer. The optimum molar ratios for preparing AuCt and AuPEI were 1:8 and 1:0.72, respectively. AuCt (1:8) and AuPEI (1:0.72) were characterized by using TEM, DLS and UV-vis spectroscopy. By DLS analysis, AuCt and AuPEI showed the particles size of 18.37 ± 0.34 nm and 18.59 ± 0.59 nm, while zeta potentials were -35.37 ± 2.56 mV and 38.00 ± 1.68 mV, in orderly. The particle sizes of AuNPs obtained from DLS technique were considerably in the same range with the UV analysis. However, the particle sizes of AuCt and AuPEI became smaller when determined by TEM analysis. AuPEI seemed to be more stable than AuCt in that the particle size of AuCt was slightly increased after 1 month while particles size of AuPEI was barely changed within 3 months. Zeta potentials of AuCt and AuPEI were slightly reduced after time storage.

Aß self-assembly led to the formation of Aß aggregates which was in the fibril form as observed from TEM analysis. AuCt and AuPEI were found to inhibit, reduce and deform the Aß fibrils. From ThT assay, the inhibitory effect of AuNPs was dependent on nanoparticle concentrations. These results were in parallel with TEM analysis in that fragmented and ragged fibrils were observed in the presence of AuCt and AuPEI. In addition, AuPEI had the higher affinity to Aß aggregates than AuCt. As confirmed by TEM analysis which showed that Aß fibrils preferentially bond to AuPEI.

In the presence of zinc, Aß self-assembly created amorphous aggregates but not the fibrils. Addition of AuCt or AuPEI led to inhibition of zinc-induced Aß aggregates as demonstrated in ThT assay and TEM analysis. Likewise, the inhibitory effects of both AuNPs in ThT assay were concentration-dependent while AuPEI had the higher affinity to bind with zinc-induced Aß aggregates than AuCt. TEM images showed the smaller amorphous zinc-induced Aß aggregates in the presence of AuCt and AuPEI. Notably, some fibrils still remained along with smaller amorphous aggregates in the presence of AuCt. While the bonding between AuCt and amorphous aggregates were hardly observed, AuPEI was seen to attach and locate inside amorphous aggregates.

From the overall of study, the conclusion was that citrate-stabilized AuNPs and PEI-stabilized AuNPs promoted the inhibitory effect on $A\beta_{1-42}$ aggregates and zinc-induced $A\beta_{1-42}$ aggregates. The inhibitory effects of AuNPs were concentration-dependent and surface potential-dependent. Positively charged AuNPs (AuPEI) were considered to be greater inhibitor due to higher affinity to $A\beta_{1-42}$ aggregates and zinc-induced Aß aggregates than negatively charged AuNPs (AuCt). The inhibitory mechanism of AuNPs on $A\beta_{1-42}$ aggregates should be further clarified if AuNPs are considered to be developed for treatment of disease related to Aß aggregation.

REFERENCES

Adams, S. J., DeTure, M. A., McBride, M., Dickson, D. W. and Petrucelli, L. (2010). Three repeat isoforms of tau inhibit assembly of four repeat tau filaments. PLoS One, *5*(5), e10810.

Adlard, P. A., Cherny, R. A., Finkelstein, D. I., Gautier, E., Robb, E., Cortes, M., Volitakis, I., Liu, X., Smith, J. P. and Perez, K. (2008). Rapid restoration of cognition in Alzheimer's transgenic mice with 8-hydroxy quinoline analogs is associated with decreased interstitial Aß. Neuron, *59*(1), 43-55.

Ahmed, M., Davis, J., Aucoin, D., Sato, T., Ahuja, S., Aimoto, S., Elliott, J. I., Van Nostrand, W. E. and Smith, S. O. (2010). Structural conversion of neurotoxic amyloid-[beta] 1-42 oligomers to fibrils. Nature Structural and Molecular Biology, *17*(5), 561-567.

Amici, J., Sangermano, M., Celasco, E. and Yagci, Y. (2011). Photochemical synthesis of gold–polyethylenglycol core–shell nanoparticles. European Polymer Journal, *47*(6), 1250-1255.

Araya, E., Olmedo, I., Bastus, N. G., Guerrero, S., Puntes, V. F., Giralt, E. and Kogan, M. J. (2008). Gold nanoparticles and microwave irradiation inhibit beta-amyloid amyloidogenesis. Nanoscale Research Letters, *3*(11), 435-443.

Arriagada, P. V., Growdon, J. H., Hedley-Whyte, E. T. and Hyman, B. T. (1992). Neurofibrillary tangles but not senile plaques parallel duration and severity of Alzheimer's disease. Neurology, *42*(3), 631-631.

Bastus, N. G., Kogan, M. J., Amigo, R., Grillo-Bosch, D., Araya, E., Turiel, A., Labarta, A., Giralt, E. and Puntes, V. F. (2007). Gold nanoparticles for selective and remote heating of ß-amyloid protein aggregates. Materials Science and Engineering: C, *27*(5), 1236-1240.

Bhumkar, D. R., Joshi, H. M., Sastry, M. and Pokharkar, V. B. (2007). Chitosan reduced gold nanoparticles as novel carriers for transmucosal delivery of insulin. Pharmaceutical Research, *24*(8), 1415-1426.

Biancalana, M. and Koide, S. (2010). Molecular mechanism of Thioflavin-T binding to amyloid fibrils. Biochimica et Biophysica Acta (BBA)-Proteins and Proteomics, *1804*(7), 1405-1412.

Bolognin, S., Messori, L., Drago, D., Gabbiani, C., Cendron, L. and Zatta, P. (2011). Aluminum, copper, iron and zinc differentially alter amyloid-Aß 1–42 aggregation and toxicity. The International Journal of Biochemistry and Cell Biology, *43*(6), 877-885.

Butterfield, D. A. (1997). ß-Amyloid-associated free radical oxidative stress and neurotoxicity: implications for Alzheimer's disease. Chemical Research in Toxicology, *10*(5), 495-506.

Cabaleiro-Lago, C., Quinlan-Pluck, F., Lynch, I., Lindman, S., Minogue, A. M., Thulin, E., Walsh, D. M., Dawson, K. A. and Linse, S. (2008). Inhibition of amyloid ß protein fibrillation by polymeric nanoparticles. Journal of the American Chemical Society, *130*(46), 15437-15443.

Čaušević, M., Farooq, U., Lovestone, S. and Killick, R. (2010). ß-Amyloid precursor protein and tau protein levels are differently regulated in human cerebellum compared to brain regions vulnerable to Alzheimer's type neurodegeneration. Neuroscience Letters, *485*(3), 162-166.

Chithrani, B. D., Ghazani, A. A. and Chan, W. C. (2006). Determining the size and shape dependence of gold nanoparticle uptake into mammalian cells. Nano letters, *6*(4), 662-668.

Chueh, P. J., Liang, R.-Y., Lee, Y.-H., Zeng, Z.-M. and Chuang, S.-M. (2014). Differential cytotoxic effects of gold nanoparticles in different mammalian cell lines. Journal of hazardous materials, *264*, 303-312.

Clogston, J. D. and Patri, A. K. (2011). Zeta potential measurement. In S. E. McNeil (Ed.), Characterization of Nanoparticles Intended for Drug Delivery, pp. 63-70. New York: Humana Press.

Connor, E. E., Mwamuka, J., Gole, A., Murphy, C. J. and Wyatt, M. D. (2005). Gold nanoparticles are taken up by human cells but do not cause acute cytotoxicity. Small, *1*(3), 325-327.

Crews, L. and Masliah, E. (2010). Molecular mechanisms of neurodegeneration in Alzheimer's disease. Human Molecular Genetics, *19*(R1), R12-20.

Cuajungco, M. P., Goldstein, L. E., Nunomura, A., Smith, M. A., Lim, J. T., Atwood, C. S., Huang, X., Farrag, Y. W., Perry, G. and Bush, A. I. (2000). Evidence that the ß-

amyloid plaques of Alzheimer's disease represent the redox-silencing and entombment of Aß by zinc. Journal of Biological Chemistry, *275*(26), 19439-19442.

Dodart, J. C., Bales, K. R., Johnstone, E. M., Little, S. P. and Paul, S. M. (2002). Apolipoprotein E alters the processing of the beta-amyloid precursor protein in APP(V717F) transgenic mice. Brain Research, *955*(1-2), 191-199.

Dong, J., Shokes, J. E., Scott, R. A. and Lynn, D. G. (2006). Modulating amyloid self-assembly and fibril morphology with Zn (II). Journal of the American Chemical Society, *128*(11), 3540-3542.

Dong, S., Tang, C., Zhou, H. and Zhao, H. (2004). Photochemical synthesis of gold nanoparticles by the sunlight radiation using a seeding approach. Gold Bulletin, *37*(3-4), 187-195.

Evans, D. B., Rank, K. B., Bhattacharya, K., Thomsen, D. R., Gurney, M. E. and Sharma, S. K. (2000). Tau phosphorylation at serine 396 and serine 404 by human recombinant tau protein kinase II inhibits tau's ability to promote microtubule assembly. Journal of Biological Chemistry, *275*(32), 24977-24983.

First, M. B. (1994). Diagnostic and statistical manual of mental disorders. 4th ed. Washington, D.C. : American Psychiatric Association.

Fong, L. Y., Jiang, Y. and Farber, J. L. (2006). Zinc deficiency potentiates induction and progression of lingual and esophageal tumors in p53-deficient mice. Carcinogenesis, *27*(7), 1489-1496.

Forsell, C., Froelich, S., Axelman, K., Vestling, M., Cowburn, R. F., Lilius, L., Johnston, J. A., Engvall, B., Johansson, K. and Dahlkild, Å. (1997). A novel pathogenic mutation (Leu262Phe) found in the presenilin 1 gene in early-onset Alzheimer's disease. Neuroscience Letters, *234*(1), 3-6.

Gan, P. P., Ng, S. H., Huang, Y. and Li, S. F. Y. (2012). Green synthesis of gold nanoparticles using palm oil mill effluent (POME): A low-cost and eco-friendly viable approach. Bioresource Technology, *113*, 132-135.

Garai, K., Sahoo, B., Kaushalya, S., Desai, R. and Maiti, S. (2007). Zinc lowers amyloid-β toxicity by selectively precipitating aggregation intermediates. Biochemistry, *46*(37), 10655-10663.

Geldmacher, D. S. (2004). Donepezil (Aricept®) for treatment of Alzheimers disease and other dementing conditions. Expert Review of Neurotherapeutics, *4*(1), 5-16.

Georganopoulou, D. G., Chang, L., Nam, J.-M., Thaxton, C. S., Mufson, E. J., Klein, W. L. and Mirkin, C. A. (2005). Nanoparticle-based detection in cerebral spinal fluid of a soluble pathogenic biomarker for Alzheimer's disease. Proceedings of the National Academy of Sciences of the United States of America, *102*(7), 2273-2276.

Giacomelli, C. E. and Norde, W. (2005). Conformational changes of the amyloid β-peptide (1–40) adsorbed on solid surfaces. Macromolecular Bioscience, *5*(5), 401-407.

Götz, J., Chen, F., Barmettler, R. and Nitsch, R. M. (2001). Tau filament formation in transgenic mice expressing P301L tau. Journal of Biological Chemistry, *276*(1), 529-534.

Groenning, M. (2010). Binding mode of Thioflavin T and other molecular probes in the context of amyloid fibrils-current status. Journal of Chemical Biology, *3*(1), 1-18.

Guela, C., Wu, C.-K., Saroff, D., Lorenzo, A., Yuan, M. and Yankner, B. A. (1998). Aging renders the brain vulnerable to amyloid ß-protein neurotoxicity. Nature Medicine, *4*(7), 827-831.

Gun'ko, V. M., Klyueva, A. V., Levchuk, Y. N. and Leboda, R. (2003). Photon correlation spectroscopy investigations of proteins. Advances in Colloid and Interface Science, *105*(1), 201-328.

Gurland, B. J., Wilder, D. E., Lantigua, R., Stern, Y., Chen, J., Killeffer, E. H. and Mayeux, R. (1999). Rates of dementia in three ethnoracial groups. International Journal of Geriatric Psychiatry, *14*(6), 481-493.

Gutiérrez-Wing, C., Velázquez-Salazar, J. J. and José-Yacamán, M. (2012). Procedures for the Synthesis and Capping of Metal Nanoparticles. In M. Soloviev (Ed.), Nanoparticles in Biology and Medicine, Vol. 906, pp. 3-19: Humana Press.

Hackley, V. A. and Clogston, J. D. (2011). Measuring the hydrodynamic size of nanoparticles in aqueous media using batch-mode dynamic light scattering. In

S. E. McNeil (Ed.), Characterization of Nanoparticles Intended for Drug Delivery, pp. 35-52. New York: Humana Press.

Haiss, W., Thanh, N. T., Aveyard, J. and Fernig, D. G. (2007). Determination of size and concentration of gold nanoparticles from UV-vis spectra. Analytical Chemistry, 79(11), 4215-4221.

Han, S.-H., Chang, Y. J., Jung, E. S., Kim, J.-W., Na, D. L. and Mook-Jung, I. (2011). Effective screen for amyloid ß aggregation inhibitor using amyloid ß-conjugated gold nanoparticles. International Journal of Nanomedicine, 6, 1-12.

Harrison, W., Netsky, M. G. and Brown, M. D. (1968). Trace elements in human brain: copper, zinc, iron, and magnesium. Clinica Chimica Acta, 21(1), 55-60.

Hatters, D. M. and Griffin, M. D. (2011). Diagnostics for amyloid fibril formation: where to begin? Methods Mol Biol, 752, 121-136.

Huang, X., Atwood, C. S., Moir, R. D., Hartshorn, M. A., Vonsattel, J.-P., Tanzi, R. E. and Bush, A. I. (1997). Zinc-induced Alzheimer's Aß1–40 aggregation is mediated by conformational factors. Journal of Biological Chemistry, 272(42), 26464-26470.

Hunter, A. C. (2006). Molecular hurdles in polyfectin design and mechanistic background to polycation induced cytotoxicity. Advanced Drug Delivery Reviews, 58(14), 1523-1531.

Jolivalt, C., Leininger-Muller, B., Bertrand, P., Herber, R., Christen, Y. and Siest, G. (2000). Differential oxidation of apolipoprotein E isoforms and interaction with phospholipids. Free Radical Biology and Medicine, 28(1), 129-140.

Keene, A. M. and Tyner, K. M. (2011). Analytical characterization of gold nanoparticle primary particles, aggregates, agglomerates, and agglomerated aggregates. Journal of Nanoparticle Research, 13(8), 3465-3481.

Khanna, P., Gokhale, R., Subbarao, V., Vishwanath, A. K., Das, B. and Satyanarayana, C. (2005). PVA stabilized gold nanoparticles by use of unexplored albeit conventional reducing agent. Materials Chemistry and Physics, 92(1), 229-233.

Khlebtsov, B. and Khlebtsov, N. (2011). On the measurement of gold nanoparticle sizes by the dynamic light scattering method. Colloid Journal, 73(1), 118-127.

Khlebtsov, N. G. (2008). Determination of size and concentration of gold nanoparticles from extinction spectra. Analytical Chemistry, *80*(17), 6620-6625.

Khurana, R., Coleman, C., Ionescu-Zanetti, C., Carter, S. A., Krishna, V., Grover, R. K., Roy, R. and Singh, S. (2005). Mechanism of thioflavin T binding to amyloid fibrils. Journal of Structural Biology, *151*(3), 229-238.

Kim, E. J., Yeum, J. H., Ghim, H. D., Lee, S. G., Lee, G. H., Lee, H. J., Han, S. I. and Choi, J. H. (2011). Ultrasmall polyethyleneimine-gold nanoparticles with high stability. Polymer-Korea, *35*(2), 161-165.

Kim, K., Lee, H. B., Lee, J. W., Park, H. K. and Shin, K. S. (2008). Self-assembly of poly (ethylenimine)-capped Au nanoparticles at a toluene– water interface for efficient surface-enhanced Raman scattering. Langmuir, *24*(14), 7178-7183.

Kimling, J., Maier, M., Okenve, B., Kotaidis, V., Ballot, H. and Plech, A. (2006). Turkevich mehtod for gold nanoparticle synthesis revisited. The Journal of Physical Chemistry B, *110*(32), 15700-15707.

Klaver, C. C., Kliffen, M., van Duijn, C. M., Hofman, A., Cruts, M., Grobbee, D. E., van Broeckhoven, C. and de Jong, P. T. (1998). Genetic association of apolipoprotein E with age-related macular degeneration. The American Journal of Human Genetics, *63*(1), 200-206.

Knopman, D., DeKosky, S. T., Cummings, J., Chui, H., Corey–Bloom, J., Relkin, N., Small, G., Miller, B. and Stevens, J. (2001). Practice parameter: Diagnosis of dementia (an evidence-based review) Report of the Quality Standards Subcommittee of the American Academy of Neurology. Neurology, *56*(9), 1143-1153.

Kobayashi, S., Tateno, M., Park, T. W., Utsumi, K., Sohma, H., Ito, Y. M., Kokai, Y. and Saito, T. (2011). Apolipoprotein E4 frequencies in a Japanese population with Alzheimer's disease and dementia with Lewy bodies. PloS One, *6*(4), e18569.

Konoha, K., Sadakane, Y. and Kawahara, M. (2006). Zinc neurotoxicity and its role in neurodegenerative diseases. Journal of Health Science, *52*(1), 1-8.

Kuchibhatla, S. V., Karakoti, A. and Seal, S. (2005). Colloidal stability by surface modification. The Journal of The Minerals, Metals and Materials Society, *57*(12), 52-56.

Kumar, S. and Walter, J. (2011). Phosphorylation of amyloid beta (Abeta) peptides - a trigger for formation of toxic aggregates in Alzheimer's disease. Aging (Albany NY), *3*(8), 803-812.

Kuo, P.-L., Chen, C.-C. and Jao, M.-W. (2005). Effects of polymer micelles of alkylated polyethylenimines on generation of gold nanoparticles. The Journal of Physical Chemistry B, *109*(19), 9445-9450.

LaDu, M. J., Falduto, M. T., Manelli, A. M., Reardon, C. A., Getz, G. S. and Frail, D. E. (1994). Isoform-specific binding of apolipoprotein E to beta-amyloid. Journal of Biological Chemistry, *269*(38), 23403-23406.

Lautenschlager, N., Cupples, L., Rao, V., Auerbach, S., Becker, R., Burke, J., Chui, H., Duara, R., Foley, E. and Glatt, S. (1996). Risk of dementia among relatives of Alzheimer's disease patients in the MIRAGE study What is in store for the oldest old? Neurology, *46*(3), 641-650.

Lee, J.-Y., Cole, T. B., Palmiter, R. D., Suh, S. W. and Koh, J.-Y. (2002). Contribution by synaptic zinc to the gender-disparate plaque formation in human Swedish mutant APP transgenic mice. Proceedings of the National Academy of Sciences of the United States of America, *99*(11), 7705-7710.

Levine, H. (1993). Thioflavine T interaction with synthetic Alzheimer's disease β-amyloid peptides: Detection of amyloid aggregation in solution. Protein Science, *2*(3), 404-410.

Li, D., He, Q., Cui, Y., Wang, K., Zhang, X. and Li, J. (2007). Thermosensitive copolymer networks modify gold nanoparticles for nanocomposite entrapment. Chemistry-A European Journal, *13*(8), 2224-2229.

Li, P., Li, D., Zhang, L., Li, G. and Wang, E. (2008). Cationic lipid bilayer coated gold nanoparticles-mediated transfection of mammalian cells. Biomaterials, *29*(26), 3617-3624.

Liao, Y. H., Chang, Y. J., Yoshiike, Y., Chang, Y. C. and Chen, Y. R. (2012). Negatively charged gold nanoparticles inhibit Alzheimer's amyloid-β fibrillization, induce fibril dissociation, and mitigate neurotoxicity. Small, *8*(23), 3631-3639.

Lim, M., Soto-Ortega, D., Mahtab, R. and Moss, M. (2011). Gold nanospheres as inhibitors of amyloid-ß protein aggregation involved in Alzheimer's disease. Journal of the South Carolina Academy of Science, *9*(2), 14-17.

Lin, Y. T., Cheng, J. T., Liang, L. C., Ko, C. Y., Lo, Y. K. and Lu, P. J. (2007). The binding and phosphorylation of Thr231 is critical for Tau's hyperphosphorylation and functional regulation by glycogen synthase kinase 3beta. Journal of Neurochemistry, *103*(2), 802-813.

Lorenzo, A. and Yankner, B. A. (1994). Beta-amyloid neurotoxicity requires fibril formation and is inhibited by congo red. Proceedings of the National Academy of Sciences of the United States of America, *91*(25), 12243-12247.

Lovell, M., Robertson, J., Teesdale, W., Campbell, J. and Markesbery, W. (1998). Copper, iron and zinc in Alzheimer's disease senile plaques. Journal of the Neurological Sciences, *158*(1), 47-52.

Mahl, D., Diendorf, J., Meyer-Zaika, W. and Epple, M. (2011). Possibilities and limitations of different analytical methods for the size determination of a bimodal dispersion of metallic nanoparticles. Colloids and Surfaces A: Physicochemical and Engineering Aspects, *377*(1), 386-392.

Mahley, R. W. (1988). Apolipoprotein E: cholesterol transport protein with expanding role in cell biology. Science, *240*(4852), 622-630.

Malugin, A. and Ghandehari, H. (2010). Cellular uptake and toxicity of gold nanoparticles in prostate cancer cells: a comparative study of rods and spheres. Journal of Applied Toxicology, *30*(3), 212-217.

Maylor, E. A., Simpson, E. E., Secker, D. L., Meunier, N., Andriollo-Sanchez, M., Polito, A., Stewart-Knox, B., McConville, C., O'Connor, J. M. and Coudray, C. (2006). Effects of zinc supplementation on cognitive function in healthy middle-aged and older adults: the ZENITH study. British Journal of Nutrition, *96*(4), 752-760.

McGeer, P., Kamo, H., Harrop, R., McGeer, E., Martin, W., Pate, B. and Li, D. (1986). Comparison of PET, MRI, and CT with pathology in a proven case of Alzheimer's disease. Neurology, *36*(12), 1569-1569.

McNeill, G., Jia, X., Whalley, L., Fox, H., Corley, J., Gow, A., Brett, C., Starr, J. and Deary, I. (2011). Antioxidant and B vitamin intake in relation to cognitive function in

later life in the Lothian Birth Cohort 1936. <u>European Journal of Clinical Nutrition</u>, *65*(5), 619-626.

Minati, L., Edginton, T., Bruzzone, M. G. and Giaccone, G. (2009). Reviews: current concepts in alzheimer's disease: a multidisciplinary review. <u>American Journal of Alzheimer's Disease and Other Dementias</u>, *24*(2), 95-121.

Minati, L., Torrengo, S., Rossi, B., Serra, M. D., Antonini, V. and Speranza, G. (2011). Synthesis and characterization of Raman active gold nanoparticles. <u>Colloids and Surfaces A: Physicochemical and Engineering Aspects</u>, *386*(1), 92-97.

Mohamed, A. K. and Halim, A. (2012). The influence of size and exposure duration of gold nanoparticles on gold nanoparticles levels in several rat organs *in vivo*. <u>Journal of Cell Science & Therapy</u>, *3*(4), 1000129.

Mold, M., Ouro-Gnao, L., Wieckowski, B. M. and Exley, C. (2013). Copper prevents amyloid-beta 1-42 from forming amyloid fibrils under near-physiological conditions *in vitro*. <u>Scientific reports</u>, *3*. doi:10.1038/srep01256

Moores, B., Drolle, E., Attwood, S. J., Simons, J. and Leonenko, Z. (2011). Effect of surfaces on amyloid fibril formation. <u>PLoS One</u>, *6*(10). doi:10.1371/journal.pone.0025954

Moreira, P., Pereira, C., Santos, M. S. and Oliveira, C. (2000). Effect of zinc ions on the cytotoxicity induced by the amyloid ß-peptide. <u>Antioxidants and Redox Signaling</u>, *2*(2), 317-325.

Motawaj, M., Burban, A., Davenas, E. and Arrang, J.-M. (2011). Activation of brain histaminergic neurotransmission: A mechanism for cognitive effects of memantine in Alzheimer's disease. <u>Journal of Pharmacology and Experimental Therapeutics</u>, *336*(2), 479-487.

Murphy, C. J., Gole, A. M., Stone, J. W., Sisco, P. N., Alkilany, A. M., Goldsmith, E. C. and Baxter, S. C. (2008). Gold Nanoparticles in Biology: Beyond Toxicity to Cellular Imaging. <u>Accounts of Chemical Research</u>, *41*(12), 1721-1730.

Murphy, C. J., Sau, T. K., Gole, A. M., Orendorff, C. J., Gao, J., Gou, L., Hunyadi, S. E. and Li, T. (2005). Anisotropic Metal Nanoparticles: Synthesis, Assembly, and Optical Applications. <u>The Journal of Physical Chemistry B</u>, *109*(29), 13857-13870.

Nathan, B., Bellosta, S., Sanan, D., Weisgraber, K., Mahley, R. and Pitas, R. (1994). Differential effects of apolipoproteins E3 and E4 on neuronal growth *in vitro*. Science, *264*(5160), 850-852.

Nazem, A. and Mansoori, G. A. (2011). Nanotechnology for Alzheimer's disease detection and treatment. Insciences Journal, *1*(4), 169-193.

Neely, A., Perry, C., Varisli, B., Singh, A. K., Arbneshi, T., Senapati, D., Kalluri, J. R. and Ray, P. C. (2009). Ultrasensitive and highly selective detection of Alzheimer's disease biomarker using two-photon Rayleigh scattering properties of gold nanoparticle. American Chemical Society Nanotechnology, *3*(9), 2834-2840.

Nidhin, M., Indumathy, R., Sreeram, K. and Nair, B. U. (2008). Synthesis of iron oxide nanoparticles of narrow size distribution on polysaccharide templates. Bulletin of Materials Science, *31*(1), 93-96.

Nochlin, D., Bird, T. D., Nemens, E. J., Ball, M. J. and Sumi, S. M. (1998). Amyloid angiopathy in a volga german family with Alzheimer's disease and a presenilin-2 mutation (N141I). Annals of Neurology, *43*(1), 131-135.

Noy, D., Solomonov, I., Sinkevich, O., Arad, T., Kjaer, K. and Sagi, I. (2008). Zinc-amyloid β interactions on a millisecond time-scale stabilize non-fibrillar Alzheimer-related species. Journal of the American Chemical Society, *130*(4), 1376-1383.

Oteliza, P. L., Olin, K. L. and Fraga, C. G. (1995). Zinc deficiency causes oxidative damage to proteins, lipids and DNA in rat testes[1,2,3]. 823-829.

Perala, S. R. K. and Kumar, S. (2013). On the mechanism of metal nanoparticle synthesis in the Brust–Schiffrin method. Langmuir, *29*(31), 9863-9873.

Philip, D. (2008). Synthesis and spectroscopic characterization of gold nanoparticles. Spectrochimica Acta Part A: Molecular and Biomolecular Spectroscopy, *71*(1), 80-85.

Pimpang, P. and Choopun, S. (2011). Monodispersity and stability of gold nanoparticles stabilized by using polyvinyl alcohol. Chiang Mai Journal Science, *38*, 31-38.

Popovtzer, R., Agrawal, A., Kotov, N. A., Popovtzer, A., Balter, J., Carey, T. E. and Kopelman, R. (2008). Targeted gold nanoparticles enable molecular CT imaging of cancer. Nano Letters, *8*(12), 4593-4596.

Qiu, Y., Liu, Y., Wang, L., Xu, L., Bai, R., Ji, Y., Wu, X., Zhao, Y., Li, Y. and Chen, C. (2010). Surface chemistry and aspect ratio mediated cellular uptake of Au nanorods. Biomaterials, *31*(30), 7606-7619.

Religa, D., Strozyk, D., Cherny, R., Volitakis, I., Haroutunian, V., Winblad, B., Naslund, J. and Bush, A. (2006). Elevated cortical zinc in Alzheimer's disease. Neurology, *67*(1), 69-75.

Sagare, A. P., Bell, R. D., Srivastava, A., Sengillo, J. D., Singh, I., Nishida, Y., Chow, N. and Zlokovic, B. V. (2013). A lipoprotein receptor cluster IV mutant preferentially binds amyloid-β and regulates its clearance from the mouse brain. Journal of Biological Chemistry, *288*(21), 15154-15166.

Sakono, M., Zako, T. and Maeda, M. (2011). Naked-eye detection of amyloid aggregates using gold nanoparticles modified with amyloid beta antibody. Analytical Sciences: the International Journal of the Japan Society for Analytical Chemistry, *28*(1), 73-73.

Simmons, L. K., May, P. C., Tomaselli, K. J., Rydel, R. E., Fuson, K. S., Brigham, E. F., Wright, S., Lieberburg, I., Becker, G. W. and Brems, D. N. (1994). Secondary structure of amyloid beta peptide correlates with neurotoxic activity *in vitro*. Molecular Pharmacology, *45*(3), 373-379.

Skaat, H., Chen, R., Grinberg, I. and Margel, S. (2012). Engineered polymer nanoparticles containing hydrophobic dipeptide for inhibition of amyloid-β fibrillation. Biomacromolecules, *13*(9), 2662-2670.

Soenen, S. J., Manshian, B., Montenegro, J. M., Amin, F., Meermann, B., Thiron, T., Cornelissen, M., Vanhaecke, F., Doak, S. and Parak, W. J. (2012). Cytotoxic effects of gold nanoparticles: a multiparametric study. ACS nano, *6*(7), 5767-5783.

Sonavane, G., Tomoda, K. and Makino, K. (2008). Biodistribution of colloidal gold nanoparticles after intravenous administration: effect of particle size. Colloids and Surfaces B: Biointerfaces, *66*(2), 274-280.

St George-Hyslop, P. H., Tanzi, R. E., Polinsky, R. J., Haines, J. L., Nee, L., Watkins, P. C., Myers, R. H., Feldman, R. G., Pollen, D. and Drachman, D. (1987). The genetic defect causing familial Alzheimer's disease maps on chromosome 21. Science, *235*(4791), 885-890.

Takahashi, M., Iseki, E. and Kosaka, K. (2000). Cdk5 and munc-18/p67 co-localization in early stage neurofibrillary tangles-bearing neurons in Alzheimer type dementia brains. Journal of the Neurological sciences, *172*(1), 63-69.

Thies, W. and Bleiler, L. (2011). 2011 Alzheimer's disease facts and figures. Alzheimer's and Dementia: the Journal of the Alzheimer's Association, *7*(2), 208-244.

Thomas, M. and Klibanov, A. M. (2003). Conjugation to gold nanoparticles enhances polyethylenimine's transfer of plasmid DNA into mammalian cells. Proceedings of the National Academy of Sciences of the United States of America, *100*(16), 9138-9143.

Tomiyama, T., Kaneko, H., Kataoka, K.-i., Asano, S. and Endo, N. (1997). Rifampicin inhibits the toxicity of pre-aggregated amyloid peptides by binding to peptide fibrils and preventing amyloid-cell interaction. Biochemical Journal, *322*, 859-865.

Tõugu, V., Karafin, A., Zovo, K., Chung, R. S., Howells, C., West, A. K. and Palumaa, P. (2009). Zn (II)-and Cu (II)-induced non-fibrillar aggregates of amyloid-β (1–42) peptide are transformed to amyloid fibrils, both spontaneously and under the influence of metal chelators. Journal of Neurochemistry, *110*(6), 1784-1795.

Triulzi, R. C., Dai, Q., Zou, J., Leblanc, R. M., Gu, Q., Orbulescu, J. and Huo, Q. (2008). Photothermal ablation of amyloid aggregates by gold nanoparticles. Colloids and Surfaces B: Biointerfaces, *63*(2), 200-208.

Urban, A. S., Pfeiffer, T., Fedoruk, M., Lutich, A. A. and Feldmann, J. (2011). Single-step injection of gold nanoparticles through phospholipid membranes. American Chemical Society Nanotechnology, *5*(5), 3585-3590.

Van Doren, E. A., De Temmerman, P.-J. R., Francisco, M. A. D. and Mast, J. (2011). Determination of the volume-specific surface area by using transmission electron tomography for characterization and definition of nanomaterials. Journal of Nanobiotechnology, *9*(1), 17.

Verdile, G., Fuller, S., Atwood, C. S., Laws, S. M., Gandy, S. E. and Martins, R. N. (2004). The role of beta amyloid in Alzheimer's disease: still a cause of everything or the only one who got caught? Pharmacological Research, *50*(4), 397-409.

Vijayakumar, S. and Ganesan, S. (2013). Size-dependent in vitro cytotoxicity assay of gold nanoparticles. Toxicological & Environmental Chemistry, *95*(2), 277-287.

Wang, C.-Y., Wang, T., Zheng, W., Zhao, B.-L., Danscher, G., Chen, Y.-H. and Wang, Z.-Y. (2010). Zinc overload enhances APP cleavage and Aß deposition in the Alzheimer mouse brain. PloS one, *5*(12), e15349.

Wisniewski, T., Lalowski, M., Golabek, A., Frangione, B. and Vogel, T. (1995). Is Alzheimer's disease an apolipoprotein E amyloidosis? The Lancet, *345*(8955), 956-958.

Yankner, B. A., Caceres, A. and Duffy, L. K. (1990). Nerve growth factor potentiates the neurotoxicity of beta amyloid. Proceedings of the National Academy of Sciences of the United States of America, *87*(22), 9020-9023.

Young-Pearse, T. L., Bai, J., Chang, R., Zheng, J. B., LoTurco, J. J. and Selkoe, D. J. (2007). A critical function for ß-amyloid precursor protein in neuronal migration revealed by in utero RNA interference. The Journal of Neuroscience, *27*(52), 14459-14469.

Zhang, Y., McLaughlin, R., Goodyer, C. and LeBlanc, A. (2002). Selective cytotoxicity of intracellular amyloid ß peptide1–42 through p53 and Bax in cultured primary human neurons. The Journal of Cell Biology, *156*(3), 519-529.

APPENDICES

APPENDIX A

Particle size analysis

Table 2. Particle size of AuCt after preparation.

Time storage	Molar ratio of Au:citrate	Diameter (nm)	Polydispersity index
After preparation	1:4	23.04 ± 0.55	0.38
	1:8	18.37 ± 0.34	0.39
	1:12	21.63 ± 0.13	0.35

Table 3. Particle size of AuCt after storage at 4°C.

Time storage	Molar ratio of Au:citrate	Diameter (nm)	Polydispersity index
1 week	1:4	20.40 ± 0.60	0.35
	1:8	17.46 ± 0.33	0.35
	1:12	22.09 ± 0.28	0.42
1 month	1:4	20.57 ± 0.22	0.37
	1:8	20.20 ± 1.07	0.41
	1:12	25.05 ± 0.49	0.44
3 months	1:4	31.51 ± 0.88	0.59
	1:8	22.42 ± 0.42	0.41
	1:12	24.13 ± 0.45	0.44

Table 4. Particle size of AuCt after storage at room temperature.

Time storage	Molar ratio of Au:citrate	Diameter (nm)	Polydispersity index
1 week	1:4	25.77 ± 0.80	0.46
	1:8	18.10 ± 0.52	0.35
	1:12	22.21 ± 0.19	0.32
1 month	1:4	35.57 ± 0.09	0.31
	1:8	30.16 ± 1.16	0.59
	1:12	37.04 ± 0.21	0.36
3 months	1:4	24.42 ± 0.11	0.37
	1:8	23.53 ± 1.68	0.42
	1:12	33.79 ± 0.18	0.46

Table 5. Particle size of AuPEI after preparation.

Time storage	Molar ratio of Au:PEI	Diameter (nm)	Polydispersity index
After preparation	1:0.36	28.47 ± 0.22	0.27
	1:0.72	18.59 ± 0.59	0.27
	1:1.08	17.15 ± 0.02	0.26

Table 6. Particle size of AuPEI after storage at 4°C.

Time storage	Molar ratio of Au:PEI	Diameter (nm)	Polydispersity index
1 week	1:0.36	28.34 ± 0.25	0.261
	1:0.72	24.37 ± 1.61	0.35
	1:1.08	23.78 ± 0.76	0.50
1 month	1:0.36	29.65 ± 0.34	0.25
	1:0.72	18.40 ± 0.47	0.18
	1:1.08	17.49 ± 0.23	0.23
3 months	1:0.36	40.07 ± 1.03	0.35
	1:0.72	18.15 ± 0.08	0.12
	1:1.08	18.68 ± 0.46	0.22

Table 7. Particle size of AuPEI after storage at room temperature.

Time storage	Molar ratio of Au:PEI	Diameter (nm)	Polydispersity index
1 week	1:0.36	30.92 ± 0.30	0.22
	1:0.72	18.09 ± 0.07	0.13
	1:1.08	17.93 ± 0.18	0.20
1 month	1:0.36	31.52 ± 0.33	0.22
	1:0.72	18.75 ± 0.20	0.11
	1:1.08	18.47 ± 0.03	0.12
3 months	1:0.36	32.44 ± 0.12	0.23
	1:0.72	20.63 ± 0.15	0.11
	1:1.08	33.67 ± 1.15	0.36

APPENDIX B

Zeta potential

Table 8. Zeta potential of AuCt after preparation.

Time storage	Molar ratio of Au:citrate	Zeta-potential (mV)
After preparation	1:4	-38.70 ± 1.39
	1:8	-35.37 ± 2.56
	1:12	-39.23 ± 4.48

Table 9. Zeta potential of AuCt after storage at 4°C.

Time storage	Molar ratio of Au:citrate	Zeta-potential (mV)
1 week	1:4	-35.47 ± 1.60
	1:8	-35.13 ± 5.27
	1:12	-32.93 ± 3.02
1 month	1:4	-35.57 ± 1.53
	1:8	-31.20 ± 5.40
	1:12	-32.10 ± 0.53
3 months	1:4	-28.77 ± 3.19
	1:8	-32.60 ± 2.11
	1:12	-29.13 ± 2.08

Table 10. Particle size of AuPEI after storage at room temperature.

Time storage	Molar ratio of Au:citrate	Zeta-potential (mV)
1 week	1:4	-39.23 ± 0.83
	1:8	-46.20 ± 2.18
	1:12	-34.07 ± 5.95
1 month	1:4	-26.87 ± 2.45
	1:8	-35.27 ± 2.14
	1:12	-32.80 ± 0.96
3 months	1:4	-20.53 ± 0.40
	1:8	-30.00 ± 1.39
	1:12	-31.53 ± 0.67

Table 11. Zeta potential of AuPEI after preparation.

Time storage	Molar ratio of Au:PEI	Zeta-potential (mV)
After preparation	1:0.36	32.83 ± 0.85
	1:0.72	38.00 ± 1.68
	1:1.08	23.53 ± 4.30

Table 12. Zeta potential of AuPEI after storage at 4ºC.

Time storage	Molar ratio of Au:PEI	Zeta-potential (mV)
1 week	1:0.36	43.33 ± 1.36
	1:0.72	39.93 ± 1.85
	1:1.08	28.20 ± 5.71
1 month	1:0.36	46.00 ± 2.27
	1:0.72	29.03 ± 0.84
	1:1.08	29.97 ± 3.37
3 months	1:0.36	20.97 ± 16.50
	1:0.72	20.90 ± 1.91
	1:1.08	26.27 ± 1.33

Table 13. Particle size of AuPEI after storage at room temperature.

Time storage	Molar ratio of Au:PEI	Zeta-potential (mV)
1 week	1:0.36	45.97 ± 1.05
	1:0.72	34.13 ± 3.19
	1:1.08	25.03 ± 4.15
1 month	1:0.36	49.47 ± 0.32
	1:0.72	29.27 ± 1.18
	1:1.08	24.40 ± 0.75
3 months	1:0.36	34.47 ± 10.80
	1:0.72	27.83 ± 1.10
	1:1.08	17.50 ± 4.80

VITA

Miss Chutima Kongsuwan was born on March 4, 1983 in Bangkok, Thailand. She graduated with a Bachelor Degree in Pharmaceutical Sciences in 2006 form the Faculty of Pharmacy, Silpakorn University, Thailand.